STUDIES OF INTERACTIONS BETWEEN PEPTIDES/PROTEINS AND LIPID BILAYERS USING SUM FREQUENCY GENERATION VIBRATIONAL SPECTROSCOPY

by

Khoi Tan Nguyen

A dissertation submitted in partial fulfillment
of the requirements for the degree of
Doctor of Philosophy
(Chemistry)
in The University of Michigan
2010

Doctoral Committee:

Professor Zhan Chen, Chair
Professor Raoul Kopelman
Professor Ayyalusamy Ramamoorthy
Assistant Professor Chuanwu Xi

To Mom and Dad

ACKNOWLEDGEMENTS

My acknowledgements must begin with my advisor, Prof. Zhan Chen, who gave me the complete freedom to tackle challenging projects and supported me both scientifically and emotionally all along. His ability to ask penetrating questions and extract the essential elements of a problem from his exceptional mind proved invaluable for solving many of the obstacles we faced throughout all these years. He often jokingly expressed his pride in being able to prove me wrong; and I will definitely miss these moments: the moments when I got so embarrassed at being wrong and tried harder, just to get things right. I will miss the moments when we both could not sleep and discussed some problems through emails until dawn. I was specially blessed having the opportunity to work with many wonderful individuals in the Chenlab, including Dr. Shuji Ye (who now holds a professor position at the University of Science and Technology of China) for his generous help when I started doing SFG, Mr. Qing Shi who was an exchange doctorate student from Tianjin University (China) for teaching me ping pong and all of his invaluable encouragements.

I also want to express my thankfulness to the Hoppers, who generously supported me in all aspects during my two years in Houston. More importantly, I cannot thank enough the Dos and my little sister, Morgan, for giving me so much care, and for being extremely supportive in everything I do.

My very special acknowledgement goes to Anh Vo who has been my loyal friend for almost 20 years. Had it not been for Anh Vo, I would not have survived the long nights in which I worked almost until dawn. He was also part of the reason why I decided to go on to graduate school in the first place. I would also like to send my sincere appreciation to my physical chemistry professor at New Mexico Tech, professor Lawrence Werbelow, who persuaded me to go to graduate school and did a great job helping me realize the true meaning of doing science.

I dedicate this thesis to my parents Lan Vo, Tan Nguyen and my sister Uyen who sacrificed her master degree in architecture at the prestigious National University of Singapore so that I could stay with SFG. I am grateful to my family. My brother Minh has always provided a lot of fun whenever we have gotten together. I thank my parents, for the countless things they unconditionally have provided over the years, including my little life which has been filled with so many opportunities.

Last but not least, I thank Ms. Kayla Ahrens for her precious emotional support during the past three months.

The research in this dissertation was supported by the National Institute of Health and Office of Naval Research.

.

TABLE OF CONTENTS

LIST OF FIGURES

LIST OF TABLES

ABSTRACT

The orientation of peptides and proteins on surfaces can have drastic implications on the function of these interfacial molecules. Interfacial proteins and peptides can play crucial roles in biological applications and processes such as antimicrobial selectivity, membrane protein activity, biocompatibility, and biosensing performance. The α-helical and β-sheet structures are the most widely encountered secondary structures in peptides and proteins. The orientation of interfacial α-helical and β-sheet structure can be determined using a combination of linear and second order nonlinear optical vibrational spectroscopies, namely Attenuated Total Reflectance Fourier Transformation Infrared Spectroscopy (ATR-FTIR) and Sum Frequency Generation (SFG) vibrational spectroscopy. Here in this dissertation, orientation determination methods of the interfacial α-helical, 3-10 helical and β-sheet structures, using the combined ATR-FTIR and SFG spectroscopic techniques, have been systematically developed. SFG was used to probe multiple amide I vibrational modes, which are related to their respective molecular hyperpolarizability tensor components through the orientation of the studied secondary structures. By implementing the bond additivity model along with group theory, the molecular hyperpolarizability tensor was determined for the SFG active vibrational modes of the secondary structures from the calculated IR transition dipole moment and the Raman polarizability tensor. The SFG susceptibility ratio of the signals collected in different polarization combinations, together with polarized ATR-FTIR amide I signals,

can be used to determine the orientation angles of the interfacial secondary structures being studied. As an illustration of the methodology, the orientations of magainin 2 (an α-helical peptide), Cytochrome b5 (an α-helical structure containing protein), tachyplesin I (a β-sheet peptide), at various interfaces were determined.

CHAPTER 1

SFG AS A POWERFUL TECHNIQUE IN STUDIES OF SURFACE CHEMISTRY

1.1 Motivation

Animal cell membranes are flexible lipid bilayers that are important in many biological functions of cells. They play the role of interfacial media between the interior of cells and their surroundings; therefore, the processes which govern all interactions between cells and their environment happen right at these biological interfaces. More specifically, cell membranes are interfacial media at which cellular processes or functions such as intra- and inter- cellular communication, protein translocation, signal transduction, apoptosis, oxidation or antimicrobial activities occur. The communication between cells or organelles within the cells occurs through the signaling molecules (such as G-protein, GABA, ion channel proteins, etc) or interfacial interactions in the cellular media. The major aim of this dissertation is to establish methods to characterize the interactions between the biological molecules and the cellular interfacial media, or cell membranes. Even though such research is the focus of the dissertation, the characterization methodology developed in this thesis can have much wider applications. It can be extended to the studies of bio-molecules on many surfaces and interfaces, including interfaces involving artificial biomedical materials, bio-sensing probes, and anti-fouling materials used in marine environments.

Bio-molecules in nature, e.g., proteins, can have drastically varied structures, ranging from a simple structure containing a single α-helix to an extremely complex one containing multiple secondary structures. Researchers in many different fields such as biophysics, biochemistry, and molecular biology have been working hard to unveil the interaction mechanisms of various bio-molecules at bio-interfaces at the molecular level. Many different techniques ranging from experimental methods such as Raman scattering,[1-3] infrared absorption,[4-11] oriented circular dichroism,[12] confocal laser scanning microscopy,[13] fluorescence spectroscopy,[14, 15] differential scanning calorimetry,[16] atomic force microscopy,[17-19] X-ray diffraction,[20] nuclear magnetic resonance[21, 22] to molecular dynamics simulation[23] have been applied in such research.

Over the last two decades, sum frequency generation (SFG) vibrational spectroscopy has been developed into a powerful and highly versatile spectroscopic tool for surface and interfacial studies. Our research group has contributed substantially to the development of SFG to probe the amide I vibration modes of proteins and peptides and use such signals to obtain structural information of these bio-molecules on surfaces/at interfaces.[24-29] This thesis research is focused on the application of SFG to determine secondary structures such as helices and β-sheets of interfacial proteins and peptides.

1.2 Introduction of nonlinear optical processes

The nonlinear optical response of a system generally describes the deviation of the system from responding linearly to the incident excitation field. The need of using higher order nonlinear terms to describe the system is illustrated in Figure 1.1, in which the quadratic term describing a harmonic oscillation is far from enough to model the real

response of the system. When the potential energy is transformed into the time domain, it is evident that the harmonic oscillator model and the real potential energy at any point in time are much different to each other, especially as time evolves.

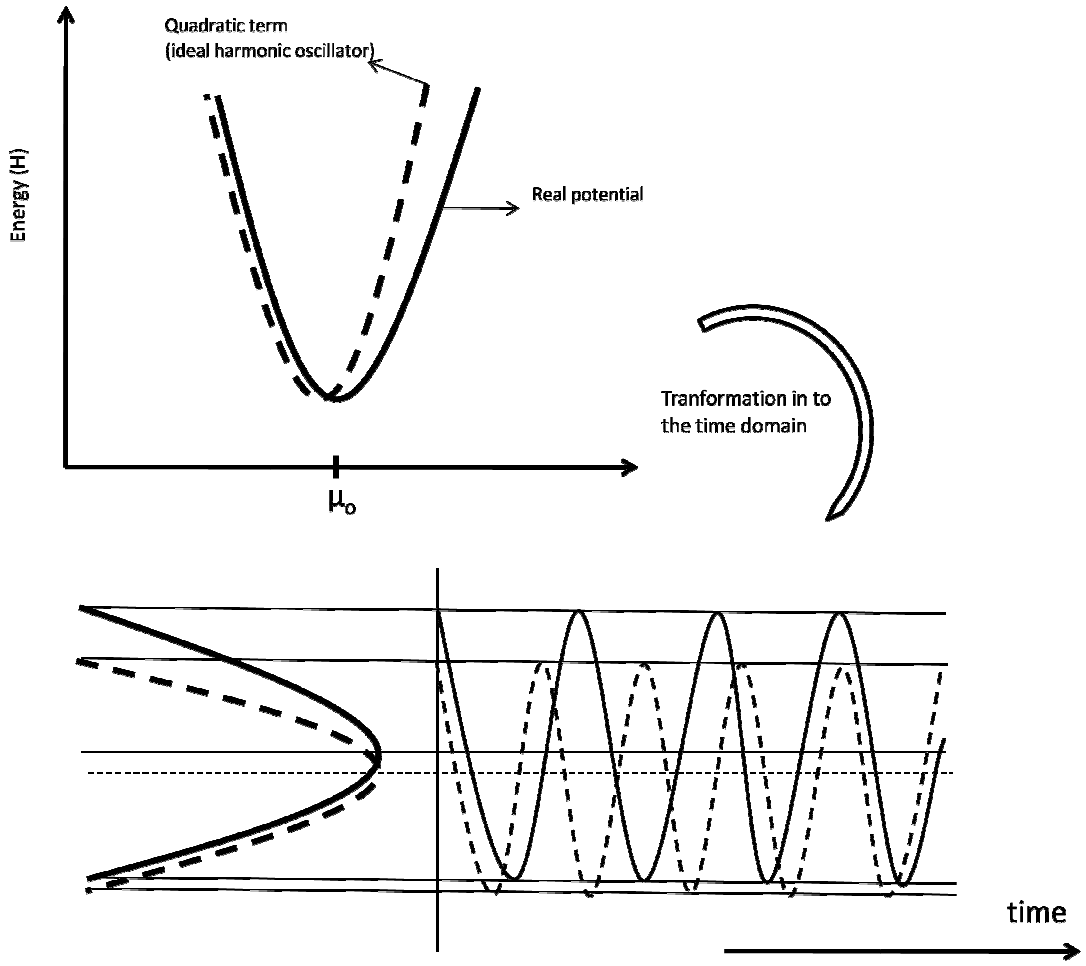

Figure 1.1: The real potential versus the potential described by the harmonic oscillator.

In nonlinear optical spectroscopy, input beams at one or more optical frequencies interact through the nonlinear polarization in a crystal or any material to generate signal beams at new frequencies. In each case, the generated frequency components are constrained by certain relationships, depending on which non-linear optical process is

concerned. The polarization induced in a medium can be expanded as a Taylor series in the applied electric field

$$P_i = \varepsilon_o(\chi_{ij}^{(1)} E_j + \chi_{ijk}^{(2)} E_j E_k + \chi_{ijkl}^{(3)} E_j E_k E_l \dots) \quad \textbf{(1.1)}$$

where the first term in the series $\varepsilon_o(\chi_{ij}^{(1)} E_j)$ represents the linear effects typically described in terms of the dielectric constant or the index of the refraction. The next term generates the second-order nonlinear optical effects, which we discuss primarily in this dissertation. The third-order term produces higher nonlinear optical effects (e.g., four-wave mixing). The commonly studied second-order nonlinear optical effects include Second Harmonic Generation (SHG), Sum Frequency Generation (SFG), Difference Frequency Generation (DFG) and optical parametric amplification (OPA). These processes are summarized in Table 1.1. In this thesis research, we will use the SFG as a spectroscopic technique, which will be discussed further below.

In general, these nonlinear optical processes are extremely inefficient when the phase-matching condition is not satisfied. For example, the phase-matching problem arises because dispersion in the medium causes a phase velocity mismatch between the nonlinear polarization of equation (1.1) and the wave it radiates, causing their relative phases to walk quickly away from each other and limiting the coherent length in the material to a distance typically between a few microns and a few hundred microns. Therefore, the phase matching conditions are extremely important especially in the cases when the conversion efficiency is of high priority. In particular, OPA and DFG are important processes in creating the tunable IR beam in our SFG setups; therefore, the phase matching conditions should be strictly met in these conversions. However, in the cases in which these nonlinear optical processes are used as spectroscopic techniques to

study surfaces/interfaces, it is only extremely important to ensure that right at the surface/interface being investigated, the two input beams are spatially overlapped and must have a desired phase relationship to each other.

2^{nd} order nonlinear optical process	Input beams	Output beams
SHG	ω_1	(ω_2), $\omega_2 = 2\omega_1$
SFG	ω_1, ω_2	(ω_3), $\omega_3 = \omega_2 + \omega_1$
DFG	ω_1, ω_2	(ω_2), $\omega_3 = \omega_2 - \omega_1$
OPA	$\omega_{pump}, \omega_{signal}$	$(\omega_{idler}, \omega_{signal})$, $\omega_{idler} = \omega_{pump} - \omega_{signal}$

Table 1.1: Summary of second order nonlinear optical processes.

Sum frequency generation (SFG) process has been widely studied. When two beams are overlapped spatially and temporally, they interact with a sample and SFG signals are produced and may be able to be detected. Our laboratory has been using the reflection geometry which minimizes the SFG contribution from the bulk. Using this geometry, the sum-frequency efficiency can be obtained from the solution of the wave equation.[30] With the proper boundary conditions, the sum frequency (SF) intensity is given by:[31]

$$I(\omega) = \frac{8\pi^3 \omega_s^2 sec^2\theta_\omega}{\hbar c^3 \sqrt{\varepsilon_1(\omega)\varepsilon_1(\omega_1)\varepsilon_1(\omega_2)}} \left| e^{\dagger}(\omega).\chi_s^{(2)} : E(\omega_1)E(\omega_2) \right|^2 I_1(\omega_1) I_2(\omega_2) \qquad \textbf{(1.2)}$$

where $\chi_s^{(2)}$ represents the second order surface nonlinear susceptibility of the medium (or sample) defined by $P_s^{(2)} = \varepsilon_o \chi_s^{(2)} : E(\omega_1)E(\omega_2)$; and $E(\omega_i) \equiv F(\omega_i)\hat{e}(\omega_i)$, with $F(\omega_i)$ being the transmission Fresnel factor and $\hat{e}(\omega_i)$ being the unit polarization vector of

$E(\omega_i)$. θ_ω is the angle between the SF output beam and the surface normal, $\varepsilon(\omega_i)$ is the electric constant at the specified frequency, and $I_i(\omega_i)$ is the input beam intensity at ω_i.

The SFG susceptibility $\chi_s^{(2)}$ of a material is a third rank tensor. It is a macroscopic quantity of a medium, e.g., an ensemble of a certain type of chromophore. This macroscopic quantity is related to the molecular nonlinear polarizability tensor, $\beta^{(2)}$, of the chromophore through the three rotational angles.[31-36]

$$\chi_{IJK}^{(2)} = \sum_{i'j'k'=x'y'z'} N_S \langle R_{Ii'} R_{Jj'} R_{Kk'} \rangle \beta_{i'j'k'}^{(2)} \quad \textbf{(1.3)}$$

The molecular nonlinear polarizability tensor, $\beta^{(2)}$, in the above equation (1.3) can be described by the sum-over-state expression, which is widely used to treat SFG processes at the molecular level. The description of $\beta^{(2)}$ is important in the derivation of the SFG signal deconvolution function used in our data analysis.[31, 32, 37] The generic form of the sum-over-state expression for $\beta^{(2)}$ takes the form of

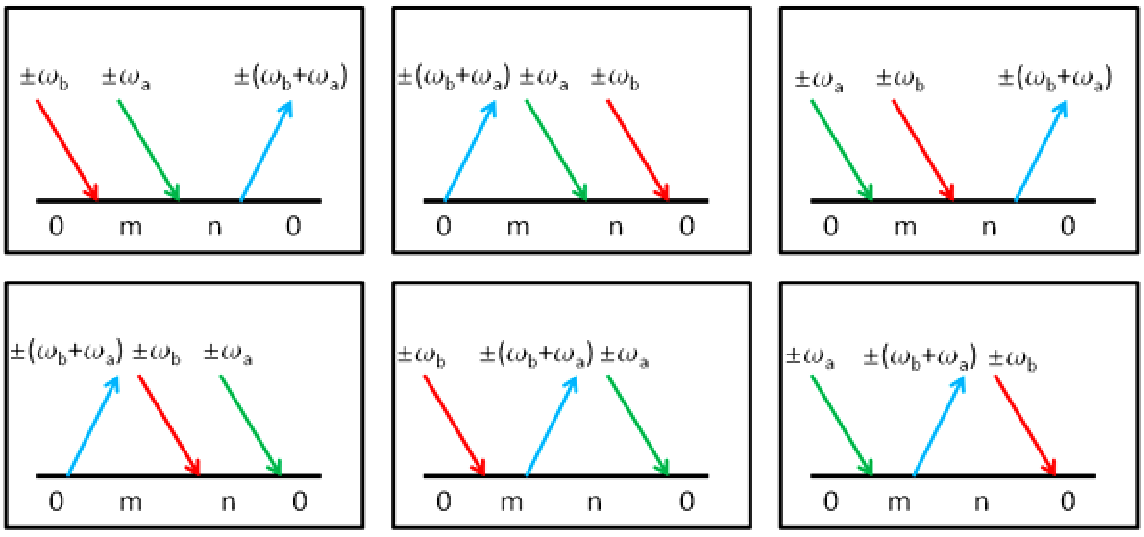

Figure 1.2: Schematic diagrams (a Feynman-like diagram) of SFG and DFG processes.

$$\beta^{ijk}(-\omega_{sum};\omega_a,\omega_b) = \frac{-1}{4\hbar^2}\sum_{n,m}\left\{\mu^i_{0m}\mu^k_{mn}\mu^j_{n0}\left[\frac{1}{(\omega_m+\omega_{sum}+i\Gamma_m)(\omega_n+\omega_a+i\Gamma_n)}+\right.\right.$$

$$\left.\frac{1}{(\omega_m-\omega_{sum}-i\Gamma_m)(\omega_n-\omega_a-i\Gamma_n)}\right]+$$

$$\mu^k_{0m}\mu^i_{mn}\mu^j_{n0}\left[\frac{1}{(\omega_m-\omega_a-i\Gamma_m)(\omega_n-\omega_{sum}-i\Gamma_n)}+\frac{1}{(\omega_m+\omega_a+i\Gamma_m)(\omega_n+\omega_{sum}+i\Gamma_n)}\right]+$$

$$\mu^i_{0m}\mu^j_{mn}\mu^k_{n0}\left[\frac{1}{(\omega_m+\omega_{sum}+i\Gamma_m)(\omega_n+\omega_b+i\Gamma_n)}+\frac{1}{(\omega_m-\omega_{sum}-i\Gamma_m)(\omega_n-\omega_b-i\Gamma_n)}\right]+$$

$$\mu^k_{0m}\mu^j_{mn}\mu^i_{n0}\left[\frac{1}{(\omega_m-\omega_b-i\Gamma_m)(\omega_n-\omega_{sum}-i\Gamma_n)}+\frac{1}{(\omega_m+\omega_b+i\Gamma_m)(\omega_n+\omega_{sum}+i\Gamma_n)}\right]+$$

$$\mu^j_{0m}\mu^k_{mn}\mu^i_{n0}\left[\frac{1}{(\omega_m-\omega_b-i\Gamma_m)(\omega_n+\omega_a+i\Gamma_n)}+\frac{1}{(\omega_m+\omega_b+i\Gamma_m)(\omega_n-\omega_a-i\Gamma_n)}\right]+$$

$$\left.\mu^j_{0m}\mu^i_{mn}\mu^k_{n0}\left[\frac{1}{(\omega_m-a-i\Gamma_m)(\omega_n+\omega_b+i\Gamma_n)}+\frac{1}{(\omega_m+\omega_a+i\Gamma_m)(\omega_n-\omega_b-i\Gamma_n)}\right]\right\} \qquad \textbf{(1.4)}$$

For the vibrational SFG spectroscopy discussed in this dissertation, in which one of the two input beams is in the infrared frequency region, the transition resonance occurs with the incident infrared beam (ω_b). Equation (1.4) takes into account both the diagonal (states $m = n$) and off-diagonal (states $m \neq n$) contributions. Within the Born-Oppenheimer (adiabatic) approximation, the diagonal contribution is dominant and we can neglect the off-diagonal contributions; upon algebraic simplifications, equation (1.4) becomes

$$\beta^{ijk}\left(-\omega_{sum};\omega_a,\omega_{b_*}\right)_n = \frac{-\mu^k_{n0}(\alpha^{ij}_{0n})_{AR}}{2\hbar(\omega_n-\omega_b-i\Gamma_n)} \qquad \textbf{(1.5)}$$

where Γ_n is the half-width of the the transition being described. The equation (1.5) above utilizes the spectral line-shape of a vibrational resonance. In this equation (1.5), one can see that when ω_b approaches a vibrational transition frequency ω_n, the SFG signal should be resonantly enhanced. μ and α are IR transition dipole moment and Raman polarizability tensor for this vibrational transition. As a side note, the Oppenheimer

(adiabatic) approximation can be assumed when the quantum states have much more energy than the photon's.

As mentioned earlier, the SFG susceptibility $\chi_s^{(2)}$observed in the lab is related to molecular hyperpolarizability tensor through three rotational angles. Since in many cases the hyperpolarizability of a vibrational transition of a functional group can be known, measured SFG results are then capable of providing orientational information of such functional groups. According to equation (1.3), the expression of $\chi_s^{(2)}$contains the three orientation angles from the Euler transformation.[32, 38]

$R = (R_3(\psi)R_2(\theta)R_1(\varphi))^T =$

$$\left[\begin{pmatrix} \cos(\psi) & \sin(\psi) & 0 \\ -\sin(\psi) & \cos(\psi) & 0 \\ 0 & 0 & 1 \end{pmatrix}\begin{pmatrix} \cos(\theta) & 0 & -\sin(\theta) \\ 0 & 1 & 0 \\ \sin(\theta) & 0 & \cos(\theta) \end{pmatrix}\begin{pmatrix} \cos(\varphi) & \sin(\varphi) & 0 \\ -\sin(\varphi) & \cos(\varphi) & 0 \\ 0 & 0 & 1 \end{pmatrix}\right]^T =$$

$$\begin{pmatrix} \cos(\psi)\cos(\theta)\cos(\varphi) - \sin(\psi)\sin(\varphi) & -\sin(\psi)\cos(\theta)\cos(\varphi) - \cos(\psi)\sin(\varphi) & \sin(\theta)\cos(\varphi) \\ \cos(\psi)\cos(\theta)\sin(\varphi) + \sin(\psi)\cos(\varphi) & -\sin(\psi)\cos(\theta)\cos(\varphi) - \cos(\psi)\cos(\varphi) & \sin(\theta)\sin(\varphi) \\ -\cos(\psi)\sin(\theta) & \sin(\psi)\sin(\theta) & \cos(\theta) \end{pmatrix}$$

(1.6)

where φ, θ, and ψ represent the in-plane rotation, the tilt angle and the twist angle, respectively.

Even though the $\chi_s^{(2)}$tensor has 27 elements, only some of the elements remain non-zero, depending on the symmetry of the medium under study. For example, for a uniaxial system, there are only 13 non-zero terms[38]: $\chi_{zzz}, \chi_{zxx} = \chi_{zyy}, \chi_{xzx} = \chi_{yzy}, \chi_{xxz} = \chi_{yyz}, \chi_{xyz} = -\chi_{yxz}, \chi_{xzy} = -\chi_{yzx}\ and\ \chi_{zxy} = -\chi_{zyx}$. If these non-zero elements can be measured in the laboratory, combined with the molecular SFG

hyperpolarizability tensor which can be obtained experimentally or computationally, the three orientation angles can be deduced.

SFG is a three-wave mixing process in which the polarization of the input and output beams can be adjusted. Different polarization combination of the input and output beams will disable or enable some $\chi_s^{(2)}$tensor components, allowing certain components to be observable in their corresponding polarization combinations only. After the consideration of the Fresnel factors which are specifically dependent on the optical geometry being used in the measurement, a relationship between the $\chi_s^{(2)}$ tensor components and the SFG signal probed in different polarization combinations can be established. The measured $\chi_s^{(2)}$tensor components from SFG signals collected using different polarization combinations can then be used to determine orientations of interfacial molecules. A more detailed discussion on this topic will be presented in the data analysis section later in this dissertation.

1.3 Surface specificity of SFG

SFG is one of the surface techniques that do not require ultra high vacuum to operate, which makes SFG an invaluable technique for studies on biological systems in which water presence is unavoidable. The surface specificity of SFG stems from its selection rules. SFG is the lowest even order nonlinear optical process and it is described by the lowest even order term in the Taylor series (equation 1.1). For even order nonlinear optical processes, $\chi_+^{(n=even)} = -\chi_-^{(n=even)}$. For centrosymmetric media, the inversion symmetry will retain the sign of $\chi_{IJK}^{(2)}$ upon the spatial inversion of the tensor, that is: $\chi_+^{(n=even)} = \chi_-^{(n=even)}$. Most bulk materials are centrosymmetric media.

Therefore, the SFG contribution of surfaces/interfaces will dominate over the SFG contribution from the bulk which is essentially zero under the electric dipole approximation. The introduction of an interface apart from the bulk will create an asymmetric plane that gives rise to SFG activity of oriented interfacial molecules. There are indeed special cases that SFG signals can be dominated from the contributions of the bulk; however, studies of such systems are not within the scope of this dissertation.

1.4 Applications of SFG vibrational spectroscopy

Recent advances in vibrational spectroscopic techniques such as Attenuated Total Reflectance Fourier Transformation Infrared (ATR-FTIR) spectroscopy, Raman scattering, vibrational Circular Dichroism (CD) and the newest born, SFG, have enabled both the chemical and structural characterization of biological macromolecules due to their unique molecular vibrational finger prints.[1-11, 24, 26, 29, 39-80] Among these techniques, SFG is a second-order nonlinear optical spectroscopic method which is able to measure more structural parameters than typical linear vibrational spectroscopic techniques such as ATR-FTIR, Raman scattering or CD because more beams are involved in the experiment. Even though these typical linear spectroscopic techniques can provide a wealth of information regarding the interfacial structures of macromolecules, they also have their own limitations: they are not intrinsically surface-sensitive and sometimes not enough information regarding orientation and other structural parameters can be obtained.

Being a combination process of IR absorption and anti-Stokes Raman scattering, SFG inherits most (if not all) the advantages that ATR-FTIR and Raman possess. Such advantages include the capability to perform chemical identification of samples, the

viability to perform experiment *in situ,* the relatively simple sample preparation requirement, the rapid data collection speed (in the time scale of minutes per spectrum as opposed to hours using other techniques), and being non-destructive to biological samples. SFG also has its own advantages over the linear optical vibrational spectroscopic techniques: it is intrinsically surface sensitive that excludes SFG contribution from the bulk; and it requires an extremely small amount of sample due to its superb detection sensitivity. With the combination of these advantages, SFG has been developed to be an excellent technique to study the structure of interfacial proteins at solid/protein solution interfaces with the bulk concentration of the protein solution in the nanomolar range.[24-26, 81]

Usually SFG signals are generated from an infinitely sharp interface. For an adsorbed protein layer, which is much thicker than an infinitely sharp interface, we have demonstrated using a thin film model that SFG signals can be treated as generated from the entire protein molecule (or the entire adsorbed protein layer) for interfacial protein structure determination.[82]

1.5 Instrumentation

1.5.1 SFG laser system

In our SFG laser system, the sum frequency generation signals from the samples are collected by overlapping temporally and spatially a visible beam and a tunable infrared beam on a sample surface or at a sample interface. The visible beam at 532 nm is generated by frequency-doubling the fundamental (1064 nm) 20 picosecond pulses output from an EKSPLA Nd:YAG laser. The infrared beam is tunable from 2.5 to 10μm, (1000 to 4000 cm^{-1}). It is generated from an optical parametric generation/amplification

and difference frequency generation system (from ESKPLA) by adjusting the rotation angles of the temperature stabilized LBO and $AgGaS_2$ crystals. Both beams are focused on the sample with diameters of approximately 0.5 mm.

Two photodiodes are used to monitor the input visible beam and infrared beam powers. These are used for normalization purposes to eliminate artifacts in the SFG signal caused by the wavelength dependency of the LBO and $AgGaS_2$ crystals in producing the tunable infrared beam, or the fluctuation of the visible beam. The SFG signal from surfaces/interfaces is collected by a photomultiplier tube and processed with a gated integrator. Surface vibrational spectra are obtained by measuring the SFG signal as a function of the input infrared frequency. SFG spectra with different polarization combinations including ssp (s-polarized sum frequency output, s-polarized visible input, and p-polarized infrared input), ppp, pss, spp and sps can be collected to probe orientation of surface chemical groups.

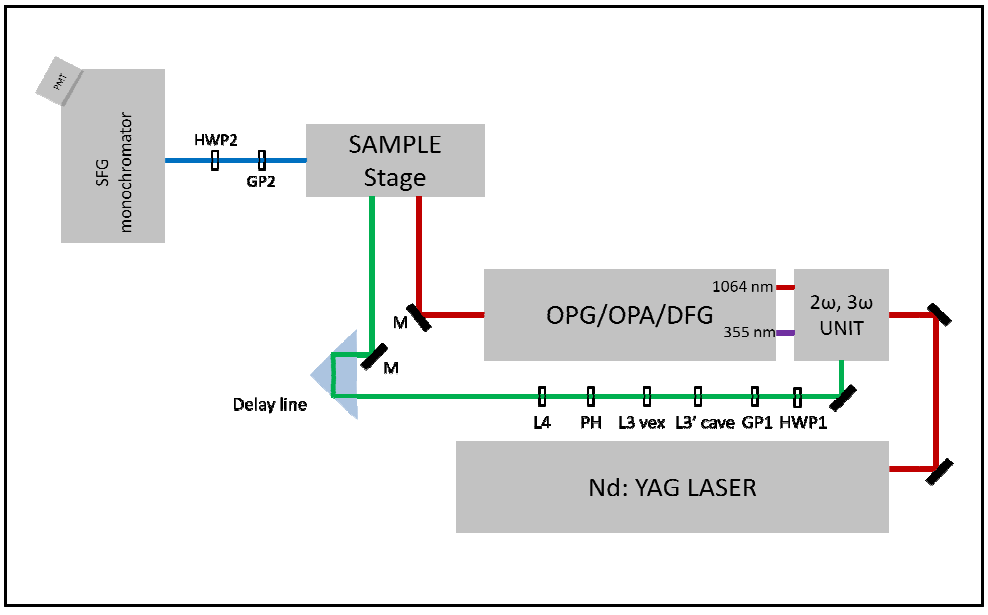

Figure 1.3: Schematic block diagram of the SFG setup in the Zhan Chen laboratory.

1.5.2 Optical setup in SFG signal collection.

1.5.2.A Sample on window substrates.

Window substrates have essentially two parallel surfaces, one of which is deposited with a sample. These substrates can be made from different materials such as fused silica or CaF_2, depending on the particular purpose they are used for. CaF_2 is transparent in mid-IR range, therefore, can be used for studies of amide I vibrations, C-F or C-D stretches. Whilst fused silica is preferred for C-H stretches studies due to its durability, it is not transparent in the amide I, C-F or C-D stretching frequency regions. The experimental geometry using window substrates (window geometry) can be used in two different ways: "face up" or "face down", indicating the side containing the sample to be on the top surface or the bottom surface, respectively. The graphical illustrations of these geometries can be found in figure 1.4.

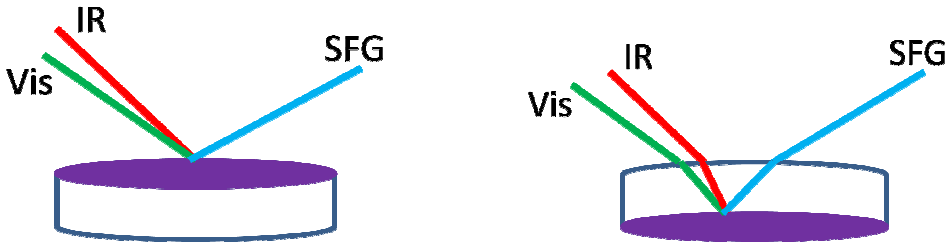

Figure 1.4: Face up and face down window geometries.

1.5.2.B Sample on prism substrates.

Right prisms made of fused silica or CaF_2 can be used for the so called "near total reflection geometry,"[75] in which the visible beam and the SF beam are totally reflected.

This geometry gives us much stronger SFG signal than the window geometry, which can be quantitatively explained by the calculation of the Fresnel coefficients, which will be discussed in detail in chapter 2.

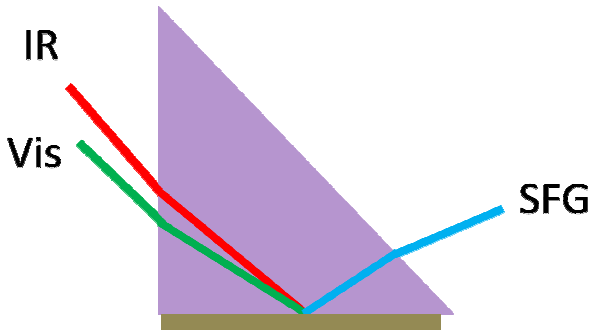

Figure 1.5: Near total reflection prism geometry.

1.6 Biological systems studied in this dissertation

The biological molecules studied in this dissertation are primarily proteins and peptides. The interfacial environments encountered in this dissertation research are substrate supported lipid bilayers, which model either mammalian or bacterial cell membranes. There has been extensive research on the properties of this type of model membranes by various groups.[52, 60, 63, 83, 84] Such studies focused on the lipid hydrophobic chain orientations, the transition temperature of the lipid bilayers in the pure or mixture form as well as the effects of cholesterol on the bilayers' physical properties. In addition, the interactions between biomolecules and lipid bilayers can also be characterized by monitoring the responses of the bilayers after these interactions occur. [55]

Proteins and peptides have different secondary structures such as α-helices, 3-10 helices, random coils, β-sheets, turns, etc, compromised by amino acids. Using vibrational spectroscopic techniques such as ATR-FTIR and Raman, orientation information on these secondary structures can be obtained either from their side chain

methyl/methylene C-H stretches[85] or the amide I (mainly C=O stretching) vibrational modes. In addition, there have been many excellent studies on the orientation determination of interfacial α-helical/β-sheet structures using other techniques such as X-ray diffraction and solid state NMR. Our research group focuses on the development of SFG into a powerful technique to determine the orientation of secondary structures using the amide I mode. We have made substantial progress in such research after the year of 2003, when we demonstrated the feasibility to detect the SFG amide I signal of interfacial proteins/peptides for the first time. Since then, we have developed SFG data analysis methods to deduce interfacial alpha helical structure orientation and used the methods to study various peptides and proteins, including melittin, G-protein, cecropin P1, alamethicin, magainin 2, pardaxin, and cytochomes. In addition to determine the average orientation of interfacial peptides and proteins, we also expanded the analyses to deduce multiple orientations that the helical structures may adopt at an interface. We introduced the maximum entropy approach as well in such studies. [86]

Even though the data analysis using SFG amide I signal for orientation determination of secondary structures is rather complex, the signal/noise ratio of SFG amide I signals is excellent, yielding more accurate results than those obtained from conventional spectroscopic techniques such as ATR-FTIR (which suffers from the overlap between the amide I signal and water bending signal),[44] or Raman (which suffers from the fluorescence background and lower signal intensity). SFG studies on biological systems, therefore, can be performed with conditions that no preceding technique has access to. This thesis research focused on the development of orientation determination

methodology of various secondary structures of interfacial peptides and proteins using SFG amide I signals.

1.7 Summary of the dissertation research

Chapter 2 of this dissertation introduces a new approach that refines the orientation determination methodology for interfacial alpha helical structures using SFG previously developed by our research group.[26, 29] While the previous methodology takes advantage of the experimental measurements of an indefinitely long α-helix to calculate the SFG hyperpolarizability tensor of the α-helical structure being studied, the new approach introduced in chapter 2 calculates these quantities, which, in principle, is able to provide better accuracy in the determination of the alpha helical structure orientation. In this calculation method, we implemented the bond additivity model, along with the group theory to compute the molecular Raman polarizability tensors and the IR transition dipole moments of alpha helical structure. This approach is then extended to the orientation analysis of 3-10 helical structures.

Chapter 3 of this dissertation applies the results deduced in chapter 2 to analyze the orientation of an antimicrobial peptide, magainin 2, in a model bacterial membrane. The average orientation of magainin 2 molecules adsorbed onto a mammalian model membrane was also studied. This is the first time a quantitative orientation determination of magainin 2 in a model cell membrane is reported. The orientation of magainin 2 molecules inserted into a model bacterial membrane agrees well with the MD simulation results in the literature.[87] The non-disruptive behavior of the peptide against mammalian cell membranes was verified by its orientation after adsorbing onto a model mammalian

model cell membrane, a POPC/POPC lipid bilayer (POPC- 1-Palmitoyl-2-Oleoyl-sn-Glycero-3-Phosphocholine).

Chapter 4 of this dissertation applies the results presented in chapter 2 to analyze the orientation of a more complex bio-molecule, a protein called Cytochrome b5, in lipid bilayers. This is a collaborative project with Dr Ronald Soong at Ramamoorthy's group at the University of Michigan. In this study, the orientation of the alpha-helical membrane anchor domain in the lipid bilayer's hydrophobic region was determined using SFG. Such results are well correlated to those from NMR studies. In addition, a thorough SFG study on the role of the linker connecting the water soluble domain and the membrane anchor in Cytochrome b5 was conducted. A temperature dependent SFG study on the insertion of the membrane anchoring domain into the lipid bilayer was also performed.

Chapter 5 of this dissertation develops the orientation analysis methodology of interfacial anti-parallel β-sheet structures. The average orientation of this structure, which includes the tilt and the twist angles, can be determined by combining the amide I SFG achiral and chiral signals along with polarized ATR-FTIR amide I signals. Experimentally, the orientation of a β-sheet antimicrobial peptide, tachyplesin I, when it adsorbed onto a polystyrene polymer surface, was determined explicitly. In addition, the orientation of this peptide upon its interaction with a DPPG/dDPPG lipid bilayer was determined using the discussed method (DPPG - 1,2-Dipalmitoyl-sn-Glycero-3-[Phospho-rac-(1-glycerol)] and dDPPG - 1,2-Dipalmitoyl-D62-sn-Glycero-3-[Phospho-rac-(1-glycerol)]). This work was carried out with Mr. John King, a rotation graduate student in our group.

Chapter 6 concludes the scope of the presented research work in this dissertation. Future directions and applications of the work will also be included.

1.8 Supplemented concepts extensively used in this dissertation

1.8.1. Introduction of the bond additivity model

The bond additivity model can be used to calculate IR transition dipole moments and Raman polarizability tensors of a vibrational mode of a molecule or a functional group according to their symmetry properties. The calculation uses the IR transition dipole moments and Raman polarizability tensors of the individual molecule or functional groups. In this model, the Raman polarizability tensors and the IR transition dipole moments of the individual vibrations couple with each other, forming a normal mode coordinate under a specific molecular symmetry point group.[88] For example, α-helical and 3-10 helical structures can be treated as having C_{3v} symmetry point group, while the anti-parallel β-sheet structures belong to D_2 symmetry point group.

The IR transition dipole moment and the Raman polarizability derivative of the individual vibrations can be obtained from *ab initio* calculations or by experimental means (using polarized IR absorption or Raman Scattering spectroscopies).[89, 90] SFG can be regarded as a combination of IR absorption and Raman scattering. Therefore, SFG hyperpolarizability can be calculated from the product of the Raman polarizability tensor and the IR transition dipole moment. Typically, the calculation of an IR transition dipole moment can be performed at a high accuracy (e.g., using *ab initio*). On the other hand, the calculation of a Raman polarizability tensor may not be accurate because of the virtual states in the Raman process should be included in the calculation. Therefore, we used the experimental reported outcomes for both the IR transition dipole moment and

the Raman polarizability tensor of an individual peptide amide I unit to calculate the IR transition dipole moment and the Raman polarizability tensor of a secondary structure. The theory of integrating the IR transition dipole moment and the Raman polarizability tensor of individual vibrations, first proposed by Higgs,[8] has been widely applied in the interpretation of IR and Raman spectra. More details of this method will be discussed in further detail in chapter 2.

1.8.2 Symmetry point groups of helical and β-sheet structures

The α- and 3-10 helical structures can be analyzed using C_{3v} symmetry. For a C_{3v} mode, there are three irreducible representations, A_1, A_2, and E. An SFG mode is only active when this mode is both IR and Raman active. The A_2 mode of a C_{3v} symmetry point group is not Raman active; therefore it is not SFG active. A C_{3v} character table is shown below, with the A_2 irreducible representation being neglected, because it is not SFG active.

C_{3v}	E	$2C_3\ (z)$	$3\sigma_v$	Linear (IR)	Quadratic (Raman)
A_1	1	1	1	z	$z^2, x^2+y^2, \pm i(xy-yx)$
$E_1 = \epsilon_1 \pm \epsilon_1^*$	2	-1	0	$x, y = (x+iy) \pm (x-iy)$	$(xz, zx; yz, zy) = (xz+iyz, zx+izy) \pm (xz-iyz, zx-izy)$

Table 1.2: The character table of the C_{3v} point group.

In the above table (1.2), column 1 lists the irreducible representations of the point group. In spectroscopy, they represent the vibrational modes of the oscillators. The directions of the changes in the IR transition dipole moment and the Raman polarizability tensor are shown in the fifth and sixth columns, respectively. From Table 1.2, one is able

to recognize the vibrational mode (at the molecular level) that each component of the IR transition dipole moment vector and the Raman polarizability tensor represents. For example, the A_1 mode is supposed to be the symmetric mode in which the change in the IR transition dipole moment occurs in the z direction and its magnitude is described by the z component of the transition dipole moment vector.

Anti-parallel β-sheet structures are characterized to have D_2 symmetry whose character table is shown below.

	E	$C_2\,(z)$	$C_2\,(y)$	$C_2(x)$	Linear	Quadratic
A	1	1	1	1		x^2, y^2, z^2
B_1	1	-1	1	1	z	xy
B_2	1	1	-1	1	y	xz
B_3	1	1	1	-1	x	yz

Table 1.3: The character table of the D_2 point group.

As one can see from this character table (1.3), the three modes B_1, B_2 and B_3 are IR active (the linear terms), while all the four modes (A, B_1, B_2, B_3) are Raman active (the quadratic terms). We can also tell the relative directions of the IR transition dipole moment vectors and Raman polarizability tensor components according to the character table.

1.8.3 s and p polarized light

To separate the vibrational modes in optical spectroscopy, the excitation source (e.g., a laser beam) is often polarized, meaning the excitation is restricted to a certain

direction only. In most cases, linear polarized beams are used in ATR-FTIR and SFG experiments. The linear polarizations, s and p, are used to characterize the polarizations of the linear beams. For SFG studies on a surface or an interface, usually we define the sample plane (or sample surface/interface) as xy plane, and the surface normal is z direction. In this case, the s polarization describes the electric field of a beam lies in the yx plane, whilst the p polarization described the electric field lies in the xz plane, as shown in Figure 1.6.

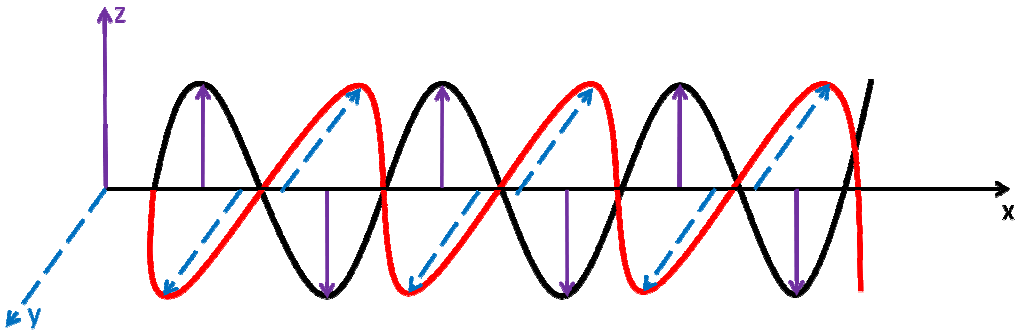

Figure 1.6: s and p polarized light. Red: s polarized electric field, black: p polarized electric field.

By taking advantage of polarized light in optical vibrational spectroscopy, we can separate the vibrational modes of the molecules under study, allowing for different independent measurements. For example, in ATR-FTIR spectroscopy, s and p polarized IR beams can be used to separate the x, y and z components of the transition dipole moment. In SFG, several polarization combinations of the input IR and visible beams as well as the output SF beam can be used to separately probe different SFG hyperpolarizability susceptibility components.

1.8.4 Fresnel coefficients

When light hits an interface between two media of different refractive indices, the fraction of light that transmits and reflects can be calculated accordingly. This fraction depends on the refractive indices of the two media, the incident angles of the light, and its polarization. For the prism geometry used in the SFG experiments throughout this dissertation, the combined Fresnel coefficient for each polarization combination was calculated and factored into the data analysis. For instance, the input IR and visible beams have to be transmitted through the air/substrate interface, then through the substrate/sample interface in order to reach the sample. We probe the SFG signal which is transmitted through the sample/substrate interface, then the substrate/air interface. The fraction of s and p polarized light that reflects and transmits through an interface can be calculated using the following formulas:

$$R_s = \left(\frac{n_1 \cos\theta_i - n_2 cos\theta_t}{n_1 \cos\theta_i + n_2 cos\theta_t}\right)^2, \qquad T_s = 1 - R_s \tag{1.7}$$

$$R_p = \left(\frac{n_1 \cos\theta_t - n_2 cos\theta_i}{n_1 \cos\theta_t + n_2 cos\theta_i}\right)^2, \qquad T_p = 1 - R_p \tag{1.8}$$

1.9 References

(1) Overman, A.S., Tsuboi, M., Thomas G.J. Jr *J. Mol. Biol.* **1996,** *259,* 331-336.

(2) Tsuboi, M., Benevides, J. M., Bondre, P. and Thomas, G. J., Jr. *Biochemistry* **2005,** *44,* 3091-3100.

(3) Wilser, W. T., Fitchen, D. B. *J. Chem. Phys.* **1975,** *62,* 720-724.

(4) Axelsen, P.H, Kaufman, B.K., McElhaney, R.N., Lewis, R.N. *Biophys. J.* **1995,** *69,* 2770-2781.

(5) Axelsen, P.H. and Citra, M. J. *Prog. Biophys. Molec. Biol.* **1996,** *66,* 227-253.

(6) Bechinger, B., Ruysschaert, J.-M., Goormaghtigh E. *Biophys. J.* **1999,** *76,* 552-563.

(7) Fraser, R.D.B. *J. Chem. Phys.* **1953,** *21,* 1511-1515.

(8) Higgs, P.W. *Proc. R. Soc. Lond. A* **1953,** *220,* 472-485.

(9) Marsh, D. *Methods Enzymol.* **1999,** *294,* 59-92.

(10) Tsuboi, M. *J. Polymer Sci.* **1962,** *59,* 139-153.

(11) Reisdorf, W. Jr, Krimm, S. *Biophys. J.* **1995,** *69,* 271-273.

(12) Ludtke, S., He, K., Heller, W., Harroun, T., Yang, L., Huang, H. *Biochemistry* **1996,** *35,* 13723-13728.

(13) Imura, Y., Nishida, M., Matsuzaki, K. *Biochimica et Biophysica Acta* **2007,** *1768,* 2578-2585.

(14) Luo, G., Wang, M., Konigsberg, W. H., Xie, X. S. *Proc. Nat. Acad. Sci. USA* **2007,** *104,* 12610-12615.

(15) Gerczei, T., Shah, B. N., Manzo, A. J., Walter, N. G., Correll, C. C. *J. Mol. Biol.* **2009,** *390,* 991-1006.

(16) Hallock, J.K., Lee, D. K., Ramamoorthy, A. *Biophys. J.* **2003,** *84,* 3052-3060.

(17) Alessandrini, A. and Facci, P. *Meas. Sci. Technol.* **2005,** *16,* R65-R92.

(18) Haas, H., Steitz, R., Fasano, A., Liuzzi, G. M., Polverini, E., Cavatorta, P., Riccio, P. *Langmuir* **2007,** *23,* 8491-8496.

(19) Kucerka, N., Nieh, M. P., Pencer, J., Harroun, T., Katsaras, J. *Curr. Opin. Coll. Int. Sci.* **2007,** *12,* 17-22.

(20) Ludtke, S., He, K., Huang, H. *Biochemistry* **1995,** *35,* 16764-16769.

(21) Andronesi, O.C., Becker, S., Seidel, K., Heise, H., Young, H. S., Baldus, M. *J. Am. Chem. Soc.* **2005,** *127,* 12965-12974.

(22) Durr, U.H.N., Yamamoto, K., Im, S., Waskell, L., Ramamoorthy, A. *J. Am. Chem. Soc.* **2007,** *129,* 6670-6671.

(23) Boczko, E.M., Brooks III, C. L. *Science* **1995,** *269,* 393-396.

(24) Chen, X., Boughton, A.P., Tesmer, J.J.G., Chen, Z. *J. Am. Chem. Soc.* **2007,** *129,* 12658-12659.

(25) Chen, X., Clarke, M.L., Wang, J., Chen, Z. *Intern. J. Mod. Phys. B* **2005,** *19,* 691-713.

(26) Chen, X., Wang, J., Boughton, A. P., Kristalyn, C. B., Chen, Z. *J. Am. Chem. Soc.* **2007,** *129,* 1420-1427.

(27) Chen, X., Wang, J., Sniadecki, J.J., Even, M.A., Chen, Z. *Langmuir* **2005,** *21,* 2262-2264.

(28) Wang, J., Even, M.A., Chen, X., Schmaier, A.H., Waite, J. H., Chen, Z. *J. Am. Chem. Soc.* **2003,** *125,* 9914-9915.

(29) Wang, J., Lee, S. H., Chen, Z. *J. Phys. Chem. B* **2008,** *112,* 2281-2290.

(30) Raschke, M.B., Shen, Y. R. **2005,** 184-189.

(31) Shen, Y. R. *The Principles of Nonlinear Optics;* John Wiley & Sons: New York,

1984.

(32) Moad, A. J., Simpson, G. J. *J. Phys. Chem. B* **2004,** *108,* 3548-3562.

(33) Heinz, T. F., Tom, H. W. K., Shen, Y. R. *Phys. Rev. A* **1983,** *28,* 1883-1885.

(34) Heinz, T. F. *In Nonlinear Surface Electromagnetic Phenomena;* North-Holland:

New York,1991; 29,352.

(35) Mazely, T. L., Hetherington, W. M., III. *J. Chem. Phys.* **1987,** *86,* 3640-3647.

(36) Simpson, G., Perry J.M., Ashmore-Good, C.L. *Phys. Rev. B* **2002,** *66,* 165437.

(37) Ward, J.F. *Rev. Mod. Phys.* **1965,** *37,* 1-18.

(38) Hirose, C., Akamatsu, N., Domen, K. *Appl. Spectrosc.* **1992,** *46,* 1051-1072.

(39) Bradbury, E. M., Brown, L., Downie, A. R., Elliot, A., Fraser, R. D. B., Hanby, W. E. *J. Mol. Biol.* **1962,** *5,* 230-247.

(40) Lee, S.-H., Krimm, S. *Biopolymers* **1998,** *46,* 283-317.

(41) Marsh, D. *Biophys. J.* **1998,** *75,* 354-358.

(42) Marsh, D., Müller, M., Schmitt, F.-J. *Biophys J.* **2000,** *78,* 2499-2510.

(43) Miyazawa, T., Blout, E. R. *J. Am. Chem. Soc.* **1961,** *83,* 712-719.

(44) Tamm, L. K., Tatulian, S. A. *Q. ReV. Biophys.* **1997,** *30,* 365-429.

(45) Chen, L.X., Strauss, H.L., Snyder, R.G. *Biophys. J.* **1993,** *64,* 1533-1541.

(46) Dwivedi, A.M., Krimm, S., Malcolm, B.R. *Biopolymers* **1984,** *23,* 2025-2065.

(47) Fanconi, B. *Biopolymers* **1973,** *12,* 2759-2776.

(48) Fanconi, B., Tomlinson, B., Nafie, L.A., Small, W., Peticolas, W.L. *J. Chem. Phys.* **1969,** *51,* 3993-4005.

(49) Koenig,J.L., Sutton, P.L. *Biopolymers* **1969,** *8,* 167-171.

(50) Lee, S.-H., Krimm, S. *J. Raman Spectrosc.* **1998,** *29,* 73-80.

(51) Tsuboi, M., Ikeda, T., Ueda, T. *Journal of Raman Spectrosc.* **1991,** *22,* 619-626.

(52) Anglin, T.C., Conboy, J.C. *Biophys. J.* **2008,** *95,* 186-193.

(53) Anderson, N.A., Richter, L. J., Stephenson, J. C., Briggman, K. A. *Langmuir* **2006,** *22,* 8333-8336.

(54) Anglin, T.C., Liu, J., Conboy, J. C. *Biophys.J.* **2007,** *92,* L1-L3.

(55) Chen, X., Wang, J., Kristalyn, C. B., Chen, Z. *Biophys. J* **2007,** *93,* 866-875.

(56) Doyle, A.W.; Fick, J.; Himmelhaus, M.;Eck, W.; Graziani, I.; Prudovsky, I.; Grunze, M.;Maciag, T.; Neivandt, D. J. *Langmuir* **2004,** *20,* 8961-8965.

(57) Harper, K.L., Allen, H. C. *Langmuir* **2007,** *23,* 8925-8931.

(58) Kim, J., Cremer, P. S. *Chem. Phys. Chem.* **2001,** *2,* 543.

(59) Levy, D., Briggman, K. A. *Langmuir* **2007,** *23,* 7155-7161.

(60) Liu, J., J. C. Conboy *Langmuir* **2005,** *21,* 9091-9097.

(61) Liu, J., Conboy, J. C. *Biophys. J.* **2005,** *89,* 2522-2532.

(62) Liu, J., Conboy, J. C. *J. Am. Chem. Soc.* **2004,** *126,* 8376-8377.

(63) Liu, J., Conboy, J. C. *J.Phys.Chem.C* **2007,** *111,* 8988-8999.

(64) Lobau, J., Sass, M., Pohle, W., Selle, C., Koch, M. H. J., Wolfrum, K. *J.Mol.Struct.* **1999,** *481,* 407-411.

(65) Ma, G., Allen, H. C. *Langmuir* **2006,** *22,* 5341-5349.

(66) Ma, G., Allen, H. C. *Langmuir* **2007,** *23,* 589-597.

(67) Nickolov, Z.S., Britt, D. W., Miller, J. D. *J.Phys.Chem.* **2006,** *110,* 15506-15513.

(68) Oh-e, M.,Yokoyama, H.,Yorozuya, S., Akagi, K., Belkin, M. A., Shen, Y. R. *Phys.Rev.Lett.* **2004,** *93,* 267402-1-267402-4.

(69) Petralli-Mallow, T.P., Briggman, K. A., Richter, L. J., Stephenson, J. C., Plant, A. L. *Proc.SPIE* **1999,** *3858,* 25-31.

(70) Sovago, M., Wurpel, G. W. H., Smits, M., Muller, M., Bonn, M. *J.Am.Chem.Soc.* **2007,** *129,* 11079-11084.

(71) Watry, M.R., Tarbuck, T. L., Richmond, G. I. *J.Phys.Chem.* **2003,** *107,* 512-518.

(72) White, R.J., Zhang, B., Daniel, S., Tang, J. M., Ervin, E. M., Cremer, P. S., White, H. S. *Langmuir* **2006,** *22,* 10777-10783.

(73) Wang, J., Buck, S. M., Chen, Z. *Analyst* **2003,** *128,* 773-778.

(74) Wang, J., Clarke, M. I., Zhang, Y. B., Chen, X., Chen, Z. *Langmuir* **2003,** *19,* 7862-7866.

(75) Wang, J., Even, M. A., Chen, X., Schmaier, A. H., Waite, J. H., Chen, Z. *J.Am.Chem.Soc.* **2003,** *125,* 9914-9915.

(76) Rocha-Mendoza, I., Yankelevich, D. R., Wang, M., Reiser, K. M., Frank, C. W., Knoesen, A. *Biophys.J.* **2007,** *93,* 4433-4444.

(77) Mermut, O., Phillips, D. C., York, R. L., McCrea, K. R., Ward, R. S., Somorjia, G. A. *J.Am.Chem.Soc.* **2006,** *128,* 3598-3607.

(78) Kim, J., Somorjai, G. A. *J. Am. Chem. Soc.* **2003,** *125,* 3150.

(79) Knoesen, A., Pakalnis, S., Wang, M., Wise, W. D., Lee, N., Frank, C. W. *IEEE J.Sel.Top.Quantum Electron.* **2004,** *10,* 1154-1163.

(80) Kim, J., Cremer, P. S. *Chem.Phys.Chem.* **2001,** *2,* 543-546.

(81) Nguyen, K., Le Clair, S., Ye, S., Chen, Z. *J. Phys. Chem. B* **2009,** *113,* 12358-12363.

(82) Wang, J., Paszti, Z., Even, M. A., Chen, Z. *J. Phys. Chem. B* **2004,** *108,* 3625-3632.

(83) Liu, J., Conboy, J. C. *J.Am.Chem.Soc.* **2004,** *126,* 8376-8377.

(84) Liu, J., Conboy, J. C. *J.Am.Chem.Soc.* **2004,** *126,* 8894-8895.

(85) Kim, G., Gurau, M. C., Lim, S. M., Cremer, P. S. *J. Phys. Chem. B* **2003,** *107,* 1403-1409.

(86) Wang, J., Paszti, Z., Clarke, M.L., Chen, X., Chen, Z. *J. Phys. Chem. B* **2007,** *111,* 6088-6095.

(87) Krzysztof Murzyn, M.P. *J. Mol. Model* **2003,** *9,* 217-224.

(88) Hore, D.K., Beaman, D. K., Park, D. H., Richmond, G. L. *J.Phys.Chem B* **2005,** *109,* 16846-16851.

(89) Lee, S.-H.,Krimm, S. *Biopolymers* **1998,** *46,* 283-317.

(90) Choi, J.-H., Hahn, S., Cho, M. *Biopolymers* **2006,** *83,* 519-536.

CHAPTER 2

ORIENTATION DETERMINATION OF PROTEIN HELICAL SECONDARY STRUCTURE USING LINEAR AND NONLINEAR VIBRATIONAL SPECTROSCOPY

2.1 Introduction

Proteins and peptides play a crucial role in many biological functions in living organisms, from enzymatic reactions to ion transportation. Proteins are also widely used in many applications such as biosensing, food production, anti-biofouling, and therapeutic agents for various diseases. Because of the importance and prevalence of proteins, their structures have been a subject of study in both science and engineering fields. The α-helix and β-sheet structures are the two most common protein secondary structures, which were proposed by Pauling based on the structural characteristics of amino acids and small peptides in 1951.[1] In this chapter, we will focus on the study of helical secondary structures.

Helices especially α-helices are important structures in membrane associated peptides and membrane proteins. Membrane peptides with α-helical structures play important roles in numerous biological processes. For instance, various natural and synthetic peptides, many of which adopt α-helical structures in cell membranes, have been proposed and tested as antibiotics to prevent bacteria drug resistance.[2-6] The

examination of the structural and orientation information of such helical peptides in cell membranes will aid in the rational design of antimicrobial peptides with improved activities. Membrane proteins with α-helical domains (e.g., potassium ion channels and G proteins) are crucial in cell biological functions such as ion transport and signal transduction, and elucidating relevant orientation information of these helices will lead to a more detailed understanding of function.[7-10]

Pauling's idea of a non-integral α-helical structure was remarkably innovative. He came up with a model of such accuracy that it could not be surpassed for over 40 years. Surprisingly, Pauling came up with the model using a sheet of paper and in a couple of hours, while he was visiting Oxford sick with a cold.[11] Three years after his visit to Oxford, Pauling published the two helical models that he called the α-helix (3.7–residue helix) and gamma-helix (5.1-residue helix).[1,12] Even though the gamma-helical structure has never been discovered in any protein structures, the α-helical one was found to occur most frequently in nature and Pauling's theoretical model was proved to match closely with the x-ray crystallography data of the actual structure. Even back in the days before the x-ray structure was elucidated, Bragg's colleague, organic chemist Todd, personally admitted to Bragg that he preferred Pauling's model over Bragg's which was published a year earlier. Bragg's model was simply proposed through the enumerated possible helical structures with integral numbers of amino acid residues per turn.[13] Perutz also confirmed the α-helix model proposed by Pauling almost immediately after he came across Pauling's paper on the model.[11]

Vibrational spectroscopic techniques have been widely used in the studies of proteins, including the orientation determination of helical structures. Widely used

vibrational spectroscopic techniques include polarized Attenuated Total Reflectance-Fourier Transform Infrared Spectroscopy (ATR-FTIR),[14-28] polarized Raman spectroscopy,[19,20,29-38] and recently Sum Frequency Generation (SFG) vibrational spectroscopy.[39-55] The orientation analyses of helical structures using these techniques require knowledge of the detailed structure of the helices at the atomic level. For example, for polarized ATR-FTIR studies, in order to measure the order parameter, S, of the amide I vibrational mode of a helix, which is necessary to determine its overall orientation, it is essential to know the detailed structure of the helix, as well as the relative angular position between the transition dipole moment and the helical axis.[15,21,23,28] For Raman studies, atomic structural details of helices are also required to correlate the polarized Raman results to the orientation of the helix by projecting the Raman tensor onto the molecular frame of the helix. For SFG, which can be regarded as a combination of infrared (IR) absorption and Raman scattering, to determine the orientation of a helix using polarized SFG spectra, it inevitably requires knowledge of the detailed structure of the helix. Due to the accuracy of Pauling's proposed α-helical structure, it has been used extensively in the orientation determination of α-helices using vibrational spectroscopic techniques.

ATR-FTIR and polarized Raman have been applied to investigate orientation of protein and peptide structures including helical structures.[14,15,23,28,31,33,38] More details about such research will be discussed later in sections 2.3 and 2.6. SFG has several advantages over ATR-FTIR and polarized Raman to study orientation of proteins and peptides at interfaces and in cell membrane environments. Details regarding such advantages have been discussed in a recent review paper[56] and will not be repeated here. The combination

of different vibrational spectroscopic techniques in the study provides more measured parameters for orientation determination of peptides and proteins, aiding in the deduction of more complicated orientation distributions, which will also be discussed in detail later in section 2.6.

SFG Amide I signal of an interfacial α-helical structure was successfully observed in 2003,[57] and subsequently, SFG methodologies were developed to determine the orientation of α-helical structures. First, group theory and the projection operator method were applied to calculate qualitatively the SFG hyperpolarizability tensor and its relation to SFG measured susceptibility tensor.[58] The orientation of fibrinogen at a polymer/protein solution interface (based on its α-helical coiled coils),[59] α-helical melittin in a lipid bilayer,[60] and Gβγ associated with a lipid bilayer (based on its α-helical domains), were then experimentally measured.[61] We found that fibrinogen molecules adopt a broad orientation distribution on the polymer surface; melittin molecules exhibit two well-defined orientations: one parallel to the bilayer surface and another one perpendicular to it; and that the Gβγ orientation is influenced by the lipid composition in the bilayer. In this chapter, we systematically present the detailed methodology to determine the orientation of α-helical structures using SFG. The majority of these details have not been reported previously. We also validate various parameters needed to develop and refine the methodology. This study further extends the method to determine the orientation of 3-10 helices and discusses whether the number of peptide units in a helix would alter the methodology to determine the helix orientation.

2.2 Orientation Determination of an α-Helix

2.2.1 Introduction of Pauling's α-helix

The first and most important assumption that Pauling and his coworkers made in their model of an α-helix was that each peptide bond is planar due to the resonance structure between the carbonyl C=O bond and the amide C-N bond.[1] Based on this assumption, two helical models were constructed and proposed: a gamma-helix and an α-helix, with 5.1 residues per turn and 3.7 residues (later refined to 3.6 residues according to X-ray diffraction results) per turn, respectively.

In a Pauling α-helix, the structure repeats itself every 5.4 Å along the helical axis. Alpha-helices have 3.6 amino acid residues per turn. Each residue is related to the next one by a translation of 1.5 Å along the helical axis and a rotation of 100^{o} (Figure 2.1). One important aspect of this structure is the intra-molecular hydrogen bonding scheme that renders the structure very stable. Every backbone carbonyl C=O and N-H group on a peptide unit is hydrogen-bonded to another N-H and C=O, respectively, on another unit four residues away. Additionally, the backbone C=O groups point in the same direction, while the N-H groups point in the opposite direction.

Extensive research has been done to analyze the three amide I vibrational modes of α- helices[19,33-35,37,62-68]: A, E_1 and E_2. The two modes A and E_1 are IR active, while all three modes are Raman active. Because an SFG active mode needs to be both IR and Raman active, only the A and E_1 modes are SFG active. The A and E_1 modes are parallel and perpendicular to the helical axis, respectively.

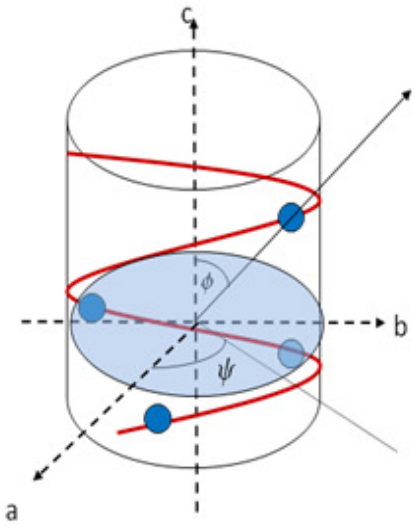

Figure 2.1: Correlation between the direction of the amide I transition dipole moment in one peptide unit and the molecular axis of an α-helix.

The SFG hyperpolarizability tensor can be expressed as a tensor product of the IR transition dipole moment and the Raman polarizability tensor:

$$\beta_{lmn,q} \propto \frac{\partial \alpha_{lm}^{*}}{\partial Q_q}\frac{\partial \mu_n}{\partial Q_q} \qquad \textbf{(2.1)}$$

where (l,m,n) are the molecular coordinate indices, and the superscript "*" denotes the complex conjugate, $\frac{\partial \mu_n}{\partial Q_q}$ and $\frac{\partial \alpha_{lm}}{\partial Q_q}$ are the IR dipole moment and the Raman polarizability derivatives with respect to the normal coordinate of the qth vibrational mode, respectively (in this thesis, we refer to these derivatives as components of IR transition dipole moment and components of Raman polarizability tensor, respectively). As Eq. (2.1) indicates, if both the IR transition dipole moment and Raman polarizability tensor are known, the SFG hyperpolarizability tensor of that vibrational mode can be deduced. In this study, the IR transition dipole moment and Raman polarizability tensor

for a helix are calculated from the IR transition dipole moment and the Raman polarizability tensor of a peptide unit using the bond additivity model according to the α-helix symmetry and structure (Sections 2.2 and 2.3). These calculated quantities are compared to and validated by the experimentally measured quantities acquired by polarized IR and Raman spectroscopic techniques in the literature. The SFG amide I hyperpolarizability tensor for an α-helix is then deduced by incorporating these values into Eq. (2.1).

2.2.2. IR transition dipole moment of an α-helix amide I mode

Higgs successfully applied group theory to characterize and derive the selection rules of the amide I modes of an α-helix in 1953.[19] According to Higgs, the components of the dipole moments (M_+, M_-, M_o) of the nth peptide unit are:

$$M_+(n) = M_+ e^{in\psi} \quad \textbf{(2.2)}$$

$$M_-(n) = M_- e^{-in\psi} \quad \textbf{(2.3)}$$

$$M_o(n) = M_o \quad \textbf{(2.4)}$$

where ψ indicates the angular distance around the helical axis between two adjacent peptide units; $M_+(n)$, $M_-(n)$ and $M_o(n)$ are the dipole moment components of the nth peptide unit that are involved in the absorption of right circularly polarized, left circularly polarized, and linearly parallel polarized IR radiation, respectively; and the terms $e^{in\psi}$ and $e^{-in\psi}$ perform the translations from the first peptide unit to the nth peptide unit. The two types of linearly polarized light, parallel and perpendicular, are referenced to the principal axis of the helix.

The IR absorption intensities of each dipole moment component, for the entire α-helix, can be determined by summing over all the peptide units. For the IR absorption using the right/left circularly polarized or linearly perpendicular polarized light,

$$I^{\perp} = \frac{1}{2}\sum_{i=1}^{n} f_i M_{\pm}^2(i) sin^2\phi_i \qquad \textbf{(2.5)}$$

where ϕ_i is the angle between the transition dipole moment M_i and the helical axis, and f_i is a proportional factor.

For the linearly parallel polarized absorption,

$$I^{//} = \sum_{i=1}^{n} f_i M_o^2 cos^2\phi_i \qquad \textbf{(2.6)}$$

Therefore, the absorption intensity ratio between the perpendicular and the parallel modes is:

$$\frac{I^{\perp}}{I^{\parallel}} = \frac{1}{2}\sum_{i=1}^{18} tan^2\phi_i \frac{M_{\pm}^2(i)}{M_o^2} \qquad \textbf{(2.7)}$$

The angle ϕ_i can be deduced by measuring the dichroic ratio of amide I modes of perfectly aligned α-helical structures. After ϕ_i is deduced, polarized IR measurements can be used to determine the orientation of α-helical structures.

There have been numerous efforts to deduce the angle ϕ_i using IR dichroism from polarized FTIR experiments. In the early 1960's, a series of findings reported ϕ_i values ranging from 30 to 40 degrees. Among these studies, both Miyazawa and Blout (ϕ_i= 29-34°),[24] and Tsuboi (ϕ_i= 39°)[27] reported their measurements on the α-helix of poly-γ-benzyl-L-glutamate. Bradbury *et al.* studied the structure of the ω-form of poly-β-benzyl-L-aspartate (ϕ_i=40°).[17] This type of work has also been done more recently. In 1995, ϕ_i was determined by Axelsen from his studies on peptide L_{24} (ϕ_i<34°),[14] and in 2000 by

Marsh from studies on poly(γ-methyl-L-glutamate)$_x$-co-(γ-*n*-octadecyl-L-glutamate)$_y$ (ϕ_i= 38°).[23] As discussed by Bradbury *et al.*, Miyazawa and Blout assumed the planar orientation in the model instead of uniaxial like others and that caused his result to be slightly different from others. If a uniaxial model had been applied in Miyazawa and Blout's analysis, a range of 33°-37.5° would be deduced from their data, which would be correlated better with other studies.[17]

Since the α-helices used in the research mentioned above may not be ideal and can vary from one sample to another, the amide I signals may not be simple and/or straightforward for analysis. The amide I signal can be affected by the hydrogen bonding scheme and the dipole-dipole coupling among the neighboring groups within a particular α-helical structure. This could explain the discrepancies among the reported ϕ_i values of α-helical structures with a varying number of peptide units, but such discrepancies are not substantial.

Here, a methodology is implemented, similar to that proposed by Suzuki, to calculate the ratio between the dipole moment projections perpendicular and parallel to the principal axis of an α-helix.[26] Wang's corrected ϕ_i angle of 42° is used in these calculations.[59] It is interesting that Marsh also found through transmission FTIR that ϕ_i should be 42°.[23] The results from the calculations are then cross-checked with the calculations from Choi[69] and the experimental data obtained from α-Poly(L-alanine)[37] and PG_{30}[23], which possess well-defined right-handed α-helical structures (see below for more details).

The parallel and perpendicular components (relative to the principal axis) of the amide I IR transition dipole moment of an α-helix are calculated using the bond additivity model. In this model, the dipole moment of each peptide unit in the helix is projected onto the parallel and perpendicular directions in the helix molecular frame. The projections of these dipole moments onto the parallel and perpendicular axes in the molecular frame are then integrated to obtain the perpendicular and parallel dipole moment components of the helix. The calculated IR transition dipole moments for the two IR allowed amide I modes of an α-helix are:

For the A mode (the parallel mode):

$$\left[\frac{\partial \mu}{\partial Q^r}\right](0^o) = \begin{pmatrix} 0 \\ 0 \\ 13.38 \end{pmatrix} \quad \textbf{(2.8)}$$

For the E_1 mode (the perpendicular mode):

$$\left[\frac{\partial \mu}{\partial Q^r}\right](100^o) = \begin{pmatrix} 6.02 \\ 6.02i \\ 0 \end{pmatrix} \quad \textbf{(2.9)}$$

From these results, the ratio of $M_{(y+x)}/M_z$ can be deduced as 0.64. This calculated ratio matches closely with the value of 0.62 obtained from polarized IR measurements using well-aligned α-helical α-Poly(L-alanine) by Lee *et al.*[20] This value also falls within the experimental range of 0.5 to 1.0 determined by polarized IR spectra of α-helical PG30 by Marsh *et al.*[23] Moreover, it is in good agreement with the calculated result from Choi that suggests a $M_{(y+x)}/M_z$ ratio of 0.62.[69] The bond additivity method used to calculate the IR transition dipole moment of an α-helix appears to yield a reasonably accurate $M_{(y+x)}/M_z$ ratio of 0.64.

2.2.3. Raman polarizability tensor of an α-helix amide I mode

The Raman tensors of vibrational modes of various functional groups, such as the ester C=O stretch, the amide I and III modes, and the C-C_{phenyl} stretch, have been successfully described by Tsuboi by investigating Raman spectra of a uniaxial tetragonal aspartame crystal.[30] The Raman tensor for the amide I mode (Figure 2.2) takes the following form:

$$\alpha_{diagonalized} = \begin{pmatrix} 0.05 & 0 & 0 \\ 0 & 0.2 & 0 \\ 0 & 0 & 1.00 \end{pmatrix} \qquad \textbf{(2.10)}$$

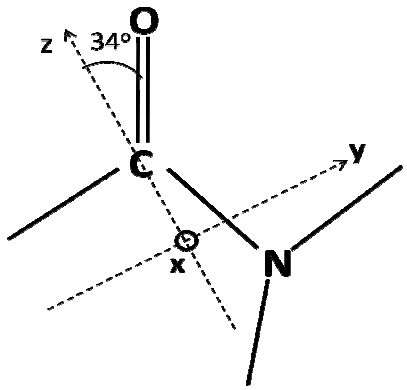

Figure 2.2: Axes for the amide I Raman tensor of a single peptide group.[30]

For a regular helical structure with infinite length, according to its symmetry, the three tensors of the vibrational modes A, E_1 and E_2 can be written as:[34]

$$[\alpha]_A = \frac{1}{2}\begin{pmatrix} \alpha_{11}+\alpha_{22} & \alpha_{12}-\alpha_{21} & 0 \\ \alpha_{21}-\alpha_{12} & \alpha_{11}+\alpha_{22} & 0 \\ 0 & 0 & 2\alpha_{33} \end{pmatrix} \qquad \textbf{(2.11)}$$

$$[\alpha]_{E_1} = \frac{1}{2}\begin{pmatrix} 0 & 0 & \alpha_{13}-i\alpha_{23} \\ 0 & 0 & \alpha_{23}+i\alpha_{13} \\ \alpha_{31}-i\alpha_{32} & \alpha_{32}+i\alpha_{31} & 0 \end{pmatrix} \qquad \textbf{(2.12)}$$

$$[\alpha]_{E_2} = \frac{1}{4}\begin{pmatrix} \alpha_{11} - \alpha_{22} - i(\alpha_{12} + \alpha_{21}) & \alpha_{12} + \alpha_{21} + i(\alpha_{11} - \alpha_{22}) & 0 \\ \alpha_{12} + \alpha_{21} + i(\alpha_{11} - \alpha_{22}) & \alpha_{22} - \alpha_{11} + i(\alpha_{12} + \alpha_{21}) & 0 \\ 0 & 0 & 0 \end{pmatrix} \quad \textbf{(2.13)}$$

Because the E_2 mode is not IR allowed, it is not necessary to consider this mode while calculating the SFG hyperpolarizability, and will thus be ignored in the remainder of this discussion.

In the case of the α-helical structure, the Stokes Raman polarizability tensors of the vibrational modes A and E_1 can be written as the following:

For the A mode:

$$\left[\frac{\partial \alpha}{\partial Q^r}\right](0^o) = \begin{pmatrix} \zeta_r^{aa}(0^o)e^{i\Theta_{\mathrm{Ao}}} & 0 & 0 \\ 0 & \zeta_r^{bb}(0^o)e^{i\Theta_{\mathrm{Ao}}} & 0 \\ 0 & 0 & \zeta_r^{cc}(0^o)e^{i\Theta_{\mathrm{Ao}}} \end{pmatrix} \quad \textbf{(2.14)}$$

where $\zeta_r^{aa}(0^o) = \zeta_r^{bb}(0^o)$.

For the E_1 mode:

$$\left[\frac{\partial \alpha}{\partial Q^r}\right](100^o) = \begin{pmatrix} 0 & 0 & 0\zeta_r^{ca}(0^o)e^{i\Theta_{\mathrm{Eo}}} \\ 0 & 0 & 0\zeta_r^{cb}(0^o)e^{i(\Theta_{\mathrm{Eo}}+\frac{\pi}{2})} \\ \zeta_r^{ac}(100^o)e^{i\Theta_{\mathrm{Eo}}} & \zeta_r^{bc}(0^o)e^{i(\Theta_{\mathrm{Eo}}+\frac{\pi}{2})} & 0 \end{pmatrix} \quad \textbf{(2.15)}$$

$$\left[\frac{\partial \alpha}{\partial Q^r}\right](-100^o) = \begin{pmatrix} 0 & 0 & 0\zeta_r^{ca}(0^o)e^{-i\Theta_{\mathrm{Eo}}} \\ 0 & 0 & 0\zeta_r^{cb}(0^o)e^{-i(\Theta_{\mathrm{Eo}}+\frac{\pi}{2})} \\ \zeta_r^{ac}(100^o)e^{-i\Theta_{\mathrm{Eo}}} & \zeta_r^{bc}(0^o)e^{-i(\Theta_{\mathrm{Eo}}+\frac{\pi}{2})} & 0 \end{pmatrix} \textbf{(2.16)}$$

where $\zeta_r^{ac}(100^o)$=$\zeta_r^{bc}(100^o) = \zeta_r^{ca}(100^o) = \zeta_r^{cb}(100^o)$, Θ_{Eo} and Θ_{Ao} are only generic phase terms. While all amide I groups in different peptide units vibrate in phase in the A mode, there is a phase difference of 100^o in the E_1 mode between two adjacent peptide units.

Based on the symmetry and structure, the Raman polarizability tensors for an α-helix can be obtained, as shown above. The Raman tensor components can now be quantitatively deduced from Tsuboi's Raman tensor of aspartame,[30] which can be used to represent a peptide unit in an α-helix. In order to apply Tsuboi's Raman tensor to the α-helical structure, a transformation needs to be applied to bring Tsuboi's Raman tensor to the first peptide unit of the α-helix in the molecular frame. Pauling proposed an accurate α-helical structure but his model was that of a left-handed helix, while most (if not all) of the α-helical structures in nature are right-handed. The left-handed and the right-handed α-helices are mirror images of each other and therefore the absolute value of the overall calculated Raman tensor is not affected. However, the right-handed version of Pauling's helix will be used in subsequent discussions due to its relevance in nature. The Euler angles transforming Tsuboi's Raman tensor to the first peptide unit in the right-handed version of the Pauling helix are: $\varphi = 0^o$, $\theta = 133.3^o$ and $\psi = 270^o$ using the x-convention rotation. The Euler transformation in the x-convention will yield the following rotation matrix:

$$\xi = \begin{pmatrix} \cos(\psi)\cos(\phi) - \sin(\psi)\cos(\theta)\sin(\phi) & \cos(\psi)\sin(\phi) + \sin(\psi)\cos(\theta)\cos(\phi) & \sin(\psi)\sin(\theta) \\ -\sin(\psi)\cos(\phi) - \cos(\psi)\cos(\theta)\sin(\phi) & -\sin(\psi)\sin(\phi) + \cos(\psi)\cos(\theta)\cos(\phi) & \cos(\psi)\sin(\theta) \\ \sin(\theta)\sin(\phi) & -\sin(\theta)\cos(\phi) & \cos(\theta) \end{pmatrix} \quad \textbf{(2. 17)}$$

With the set of Euler angles listed above, this rotation ξ matrix becomes:

$$\xi_{0^o,133.3^o,270^o} = \begin{pmatrix} 0 & 0.686 & -0.728 \\ 1 & 0 & 0 \\ 0 & -0.728 & -0.686 \end{pmatrix} \quad \textbf{(2.18)}$$

The rotation is applied on the coordinate system (a,b,c) which describes the tensor as:

$$\alpha_{x,y,z} = \xi\ \alpha_{a,b,c}\ \xi^T \qquad \textbf{(2.19)}$$

Therefore,

$$\alpha_1 =$$

$$\begin{pmatrix} 0 & 0.686 & -0.728 \\ 1 & 0 & 0 \\ 0 & -0.728 & -0.686 \end{pmatrix}\begin{pmatrix} 0.05 & 0 & 0 \\ 0 & 0.2 & 0 \\ 0 & 0 & 1.00 \end{pmatrix}\begin{pmatrix} 0 & 0.686 & -0.728 \\ 1 & 0 & 0 \\ 0 & -0.728 & -0.686 \end{pmatrix}^T =$$

$$\begin{pmatrix} 0.624 & 0 & 0.400 \\ 0 & 0.05 & 0 \\ 0.400 & 0 & 0.577 \end{pmatrix} \qquad \textbf{(2.20)}$$

Due to the uniaxial property of the α-helix, all the peptide units are assumed to be approximately identical and can thus be transformed geometrically onto each other. This makes the process of obtaining the helical total Raman tensor much simpler. The Raman polarizability tensor for each peptide unit in the α-helix can be obtained by successively performing 100 degree rotations around the helical axis to move from one peptide unit to the next. The Raman tensor of the entire α-helix can be calculated by multiplying the Raman tensor of each peptide unit with the phase factor in the vibrational mode and then summing over all of them. The A mode vibrations of all the peptide units are all in phase. Therefore, the Raman tensor for the A mode of an ideal α-helix can be calculated as:

$$\alpha_{1-18}$$

$$= \sum_{i=0}^{17} \begin{pmatrix} \cos(100\mathrm{i}) & \sin(100\mathrm{i}) & 0 \\ -\sin(100i) & \cos(100\mathrm{i}) & 0 \\ 0 & 0 & 1 \end{pmatrix}^T \begin{pmatrix} 0.624 & 0 & 0.400 \\ 0 & 0.05 & 0 \\ 0.400 & 0 & 0.577 \end{pmatrix} \begin{pmatrix} \cos(100\mathrm{i}) & \sin(100\mathrm{i}) & 0 \\ -\sin(100i) & \cos(100\mathrm{i}) & 0 \\ 0 & 0 & 1 \end{pmatrix}$$

(2.21)

The Raman polarizability tensors of the E_1 modes can be calculated similarly after incorporating the phase difference between the adjacent peptide units. The deduced Raman polarizability tensors of the A and E_1 modes are:

For the A mode:

$$\left[\frac{\partial \alpha}{\partial Q^r}\right](0^o) = \begin{pmatrix} 6.1 & 0 & 0 \\ 0 & 6.1 & 0 \\ 0 & 0 & 10.4 \end{pmatrix} \quad \textbf{(2.22)}$$

For the E_1 mode:

$$\left[\frac{\partial \alpha}{\partial Q^r}\right](100^o) = \frac{1}{2}\begin{pmatrix} 0 & 0 & 3.6 \\ 0 & 0 & 3.6i \\ 3.6 & 3.6i & 0 \end{pmatrix} \quad \textbf{(2.23)}$$

These results agree very well with experimental results found in the literature. For example, α_{bb}/α_{cc} and α_{cb}/α_{cc} can be calculated to be 0.59 and 0.35, respectively. The calculated α_{bb}/α_{cc} value (0.59) is similar to the widely used value reported by Tsuboi et *al.* of 0.54.[70] In general, the above calculated A and E_1 mode Raman polarizability tensors of an α-helix closely match the experimentally measured values reported in the literatures, which were determined with polarized Raman experiments on well-aligned α-helical samples. For the A mode, an experimental ratio of α_{bb}/α_{cc} within a range of 0.53 to 0.64 was reported, which is in good agreement with our value of 0.59. Many of these values are obtained using the assumption that all the α-helical structures are perfectly aligned along the z-axis (or the fiber axis when fiber samples are used) in the Raman experiments. For example, Wilser *et al.* measured this ratio to be 0.55 according to their polarized Raman studies on the α-helical polypeptide, poly-γ-benzyl-L-glutamate.[29] Using a wool fiber, Rintoul *et al.* measured this value to be 0.62.[71] Ackermann *et al.* obtained a ratio of 0.62 by experiments on α-helices in intact human hair.[72] Overman *et*

al. deduced this value to be 0.58 by performing measurements on α-helical pVIII subunits in the filamentous virus Ff (fd, f1, M13).[31] Tsuboi *et al.* studied the α-helical coat protein in filamentous bacteriophage PH75 and found the value to be 0.64.[38] In the last two experiments the authors did not use the experimentally measured values as α_{bb}/α_{cc}, instead, they used these values and calculated value of 0.54 to determine the orientation of the helices. Perhaps in these samples, the α-helices were actually more or less aligned along the z-axis.

The α_{cb}/α_{cc} value has also been measured experimentally using polarized Raman experiments. Rintoul *et al.* measured this value to be 0.39 by studying a wool fiber. Lee *et al.* investigated well-aligned poly-alanine samples and obtained a value of 0.35.[37] Wilser *et al.* reported this ratio to be between 0.34 and 0.40 in their studies on α-helical poly-γ-benzyl-L-glutamate.[29] These experimental values are all comparable to our calculated value of 0.35. Therefore we believe that this calculated value is also correct. Using these two tensors combined with the transition dipole moment calculated earlier, we can calculate the needed hyperpolarizability components for our later SFG data analysis.

2.2.4. SFG data analysis for α-helices based on the calculated IR transition dipole moment and Raman polarizability

The SFG hyperpolarizability tensor is a third-rank tensor with 27 elements. It is a tensor product of the Raman polarizability tensor and the IR transition dipole moment (Eq. (2.1)). The theoretical background of SFG has been discussed in great details in many publications[39-61,73-76] and will not be repeated here. The discussion will now be

steered toward the application of SFG in the orientation analysis of α-helical structures. The α-helical peptide's orientation can be measured by analyzing SFG amide I spectra collected under polarization combinations of ssp (s-polarized SFG signal beam, s-polarized visible input beam, and p-polarized IR input beam) and ppp. The SFG susceptibility tensor element χ_{ijk} (i, j, k=x,y,z) is related to the SFG molecular hyperpolarizability tensor element β_{lmn} (*l*, *m*, *n* = *a*, *b*, *c*) by a Euler angle projection:[59,75,77,78]

$$\chi_{ijk,q} = N_s \sum_{l,m,n} \langle (\hat{i} \cdot \hat{l})(\hat{j} \cdot \hat{m})(\hat{k} \cdot \hat{n}) \rangle \beta_{lmn,q} \quad \textbf{(2.24)}$$

where N_s is the surface density of α-helical repeating units, the notation "< >" indicates the average value.

For vibrational modes of different symmetries, these relations can be quite different, which were discussed in detail in the literature.[75,78] According to the symmetry of the α-helix, the following relationships can be expressed:[58-60]

For the A mode:

$$\chi_{A,xxz} = \chi_{A,,yyz} = \frac{1}{2} N_s [(1+r) < \cos\theta > -(1-r) < \cos^3\theta >] \beta_{ccc} \quad \textbf{(2.25)}$$

$$\chi_{A,xzx} = \chi_{A,yzy} = \chi_{A,zxx} = \chi_{A,zyy} = \frac{1}{2} N_s [(1-r)(< \cos\theta > - < \cos^3\theta >)] \beta_{ccc} \quad \textbf{(2.26)}$$

$$\chi_{A,zzz} = N_s [r < \cos\theta > + (1-r) < \cos^3\theta >] \beta_{ccc} \quad \textbf{(2.27)}$$

where $r = \beta_{aac} / \beta_{ccc}$

For the E_1 mode:

$$\chi_{E,xxz} = \chi_{E,yyz} = -N_s(<\cos\theta> - <\cos^3\theta>)\beta_{aca} \quad \textbf{(2.28)}$$

$$\chi_{E,xzx} = \chi_{E,yzy} = \chi_{E,zxx} = \chi_{E,zyy} = N_s <\cos^3\theta> \beta_{aca} \quad \textbf{(2.29)}$$

$$\chi_{E,zzz} = 2N_s(<\cos\theta> - <\cos^3\theta>)\beta_{aca} \quad \textbf{(2.30)}$$

where the notation "< >" indicates the average value. θ is the angle between the principal helical axis and the surface normal. When assuming that θ has a delta-distribution, <cosθ>= cosθ. The orientation distribution can be more complicated than a delta-distribution, which will be discussed in more detail later.

Experimentally, the SFG signals from the A and E_1 modes cannot be resolved due to the resolution of our SFG system. The amide I signal can therefore be considered as arising from a contribution of both modes:

$$\chi_{zzz} = \chi_{E,zzz} + \chi_{A,zzz} \quad \textbf{(2.31)}$$

$$\chi_{yyz} = \chi_{xxz} = \chi_{E,yyz} + \chi_{A,yyz} \quad \textbf{(2.32)}$$

$$\chi_{yzy} = \chi_{xzx} = \chi_{zxx} = \chi_{zyy} = \chi_{E,yzy} + \chi_{A,yzy} \quad \textbf{(2.33)}$$

From the above expressions, if β_{aac}/β_{ccc} and β_{aca}/β_{ccc} are known and the combined χ_{zzz}/χ_{yyz} or χ_{zzz}/χ_{yzy} are measured, the orientation angle θ should be able to be deduced. Since the SFG hyperpolarizability is a product of the Raman polarizability and IR transition dipole moment, equations (2.1), (2.8), (2.9) and (2.18) can be combined to give:

$$\frac{\beta_{aac}}{\beta_{ccc}} = \left(\frac{\alpha_{aa}}{\alpha_{cc}}\right)^* \frac{\mu_c}{\mu_c} = \left(\frac{\alpha_{aa}}{\alpha_{cc}}\right)^* = \frac{6.1}{10.4} = 0.59 \quad \textbf{(2.34)}$$

$$\frac{\beta_{aca}}{\beta_{ccc}} = 2 * \left(\frac{\alpha_{ac}}{\alpha_{cc}}\right)^{*} \frac{\mu_a}{\mu_c} = 2 * \frac{3.6}{10.4}\frac{6.02}{13.38} = 0.31 \qquad \textbf{(2.35)}$$

Here, the complex conjugate of the Raman polarizability tensor is used since the Raman process involved in SFG is an anti-Stokes Raman process.

Assuming the orientation angle θ to be a delta-distribution, meaning that all the α-helices adopt an identical orientation, the relationships between each of the ratios χ_{zzz}/χ_{yyz} and χ_{zzz}/χ_{yzy} and θ can be described by the curves shown in Figures 2.3a and 2.3b. However, it can be the case that not all the helices adopt the exact same orientation, and that instead a distribution of orientations is present. In this scenario, the orientation can be assumed as a Gaussian (normal) distribution with a standard deviation σ:

$$p(\theta) = \frac{e^{-\frac{(\theta-\mu)^2}{2\sigma^2}}}{\sqrt{2\pi}*\sigma} \qquad \textbf{(2.36)}$$

$$\langle \cos(\theta) \rangle = N_s \int_0^{\pi} \frac{e^{-\frac{(\theta-\mu)^2}{2\sigma^2}}}{\sqrt{2\pi}*\sigma} \cos(\theta)\sin(\theta)d\theta \qquad \textbf{(2.37)}$$

$$\langle \cos^3(\theta) \rangle = N_s \int_0^{\pi} \frac{e^{-\frac{(\theta-\mu)^2}{2\sigma^2}}}{\sqrt{2\pi}*\sigma} \cos^3(\theta)\sin(\theta)d\theta \qquad \textbf{(2.38)}$$

The above mean values $\langle \cos(\theta) \rangle$ and $\langle \cos^3(\theta) \rangle$ can now be used in the equations (2.25) to (2.30) to describe the relationship between θ and the SFG susceptibility component χ_{ijk}. The variation of the relationship between the ratios χ_{zzz}/χ_{yyz} and χ_{zzz}/χ_{yzy} and θ in terms of different Gaussian distribution width σ is displayed in Figures 2.3a and 2.3b.

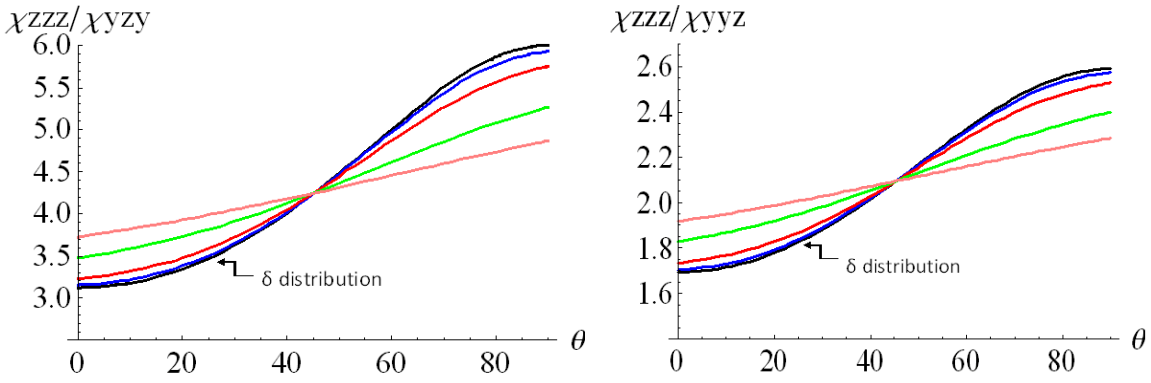

Figure 2.3: Relationships between (a) χ_{zzz}/χ_{yyz} or (b) χ_{zzz}/χ_{yzy} ratio and θ for α-helix in terms of different Gaussian distribution width σ. Black: σ = 0, blue: σ = 5°, red: σ = 10°, green: σ = 20°, pink: σ = 30°. When σ is zero, the distribution is a delta distribution.

2.2.5. The effect of varying the number of peptide units in an α-helical structure on SFG data analysis

The theoretical framework discussed so far has been for ideal α-helical structures, either a unit cell with eighteen peptide units (for five turns) or an infinitely long α-helix. One may pose the question of whether the above SFG data analysis method is still valid if the α-helical species under study does not possess a perfect α-helical structure that has a multiple of repeated helical units, e.g., 18, 36, or 54 amino acids. In nature, many α-helical structures do not have a multiple of repeated helical units; this concern will be addressed in this section.

If we assume that each peptide unit in an ideal α-helical unit (defined as 18 residues) is a "normal" peptide unit, while any peptide units beyond a multiple number of repeated helical units are "extra" units, when the α-helix is very long, the number of

"extra" units is much less than that of "normal" units. In that case, it seems that these "extra" units would not make the SFG data analysis deviate too much from that for an ideal α-helix. If every 3.6 units (one turn) is considered as a repeating unit for an α-helix, then for any α-helix longer than 18 peptide units, the "extra" units are much less than the regular units. For example, for an α-helix with 23 peptide units, 21.6 are regular units, and only 1.4 are extra units. In this case, the deviation from the α-helical symmetry should be minimal, and the SFG data analysis for a perfect α-helix can be approximately applied. If the method discussed above to calculate the hyperpolarizability component ratios α_{bb}/α_{cc} and α_{cb}/α_{cc} was used for α-helices longer than 18 peptide units, their values should be reasonably similar. Hence, the SFG measured susceptibility and orientation angle relation should be also similar.

The above reasoning may not apply, however, for relatively short α-helical structures (e.g., <10 residues). In this case, data analysis for any α-helical peptides that have their number of peptide units not close to 3.6 or 7.2 (e.g., containing 2, 5, or 6 peptide units) may be influenced from the symmetry breaking. However, the occurrence of these short α-helical structures in nature is rare and does not necessitate a discussion here. The focus, instead, will be placed on α-helical structures that have more than ten but less than eighteen peptide units. For these α-helices, the magnitude of the effect of breaking the symmetry of a perfect α-helix on the hyperpolarizability ratios will be discussed. The hyperpolarizability ratios β_{aac}/β_{ccc} and β_{aca}/β_{ccc} of α-helical structures that have 10, 12, 13, 15, 16 and 17 peptide units are calculated. The dependence of the α-helix orientation curve on the helix length is deduced below in order to understand how

the SFG data analysis method is affected by changing the peptide unit number in an α-helix away from eighteen. For comparison, the calculations were also done for α-helical structures with the number of peptide units ranging from 28 to 35. The comparison between these two sets of orientation curves should provide an idea of how the length of the structures affects the deviation from the symmetry of an α-helix unit. This comparison can be found in Figures 2.4a, 2.4b, 2.5a and 2.5b. It is clear from the two sets of curves in both the χ_{zzz}/χ_{yyz} and χ_{zzz}/χ_{yzy} plots that as the number of amino acid residues of the structure becomes larger, the result is less dependent on the number of amino acid residues, leading to less deviations in the relationship between χ_{zzz}/χ_{yyz} and χ_{zzz}/χ_{yzy} and θ from the ideal case. Our findings show that for shorter α-helices, it is important to calculate the molecular hyperpolarizability ratios β_{aac}/β_{ccc} and β_{aca}/β_{ccc} using the bond additivity model with the number of amino acid residues in the particular α-helix under study. Then the relationship between χ_{zzz}/χ_{yyz} or χ_{zzz}/χ_{yzy} and θ can be deduced for SFG data analysis. By taking into account the effects of the peptide chain lengths to establish a specific orientation curve for each α-helical structure, it should provide a more accurate result than using the curve for an ideal helix. For longer α-helices, it is a valid approximation to use the SFG data analysis method developed for an α-helix unit.

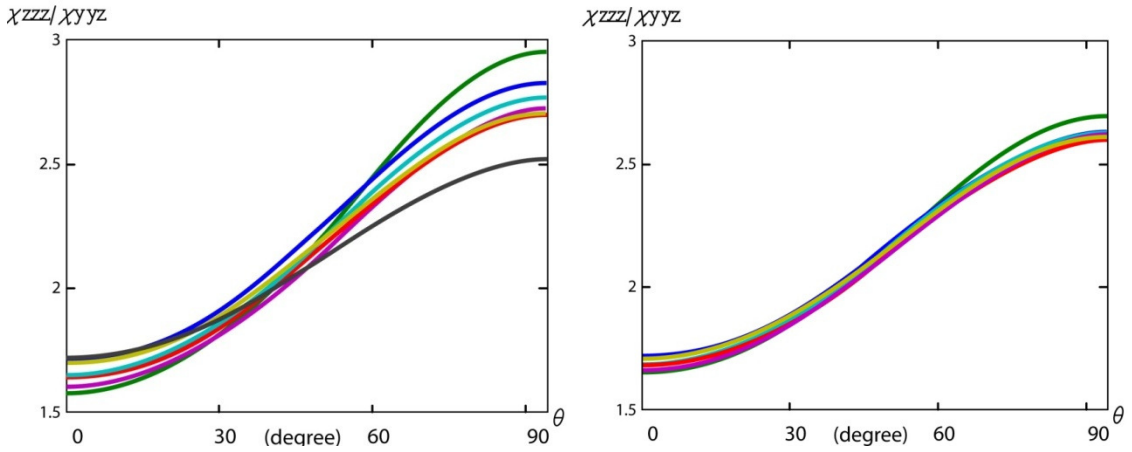

Figure 2.4: Relationship between χ_{zzz}/χ_{yyz} ratio and θ for α-helices with different chain lengths: (a, left) blue: 10, green: 12, red: 13, cyan: 15, purple: 16, yellow: 17, black: 18 residues; (b, right) blue: 28, green: 30, red: 31, cyan: 33, purple: 33, yellow: 35 residues.

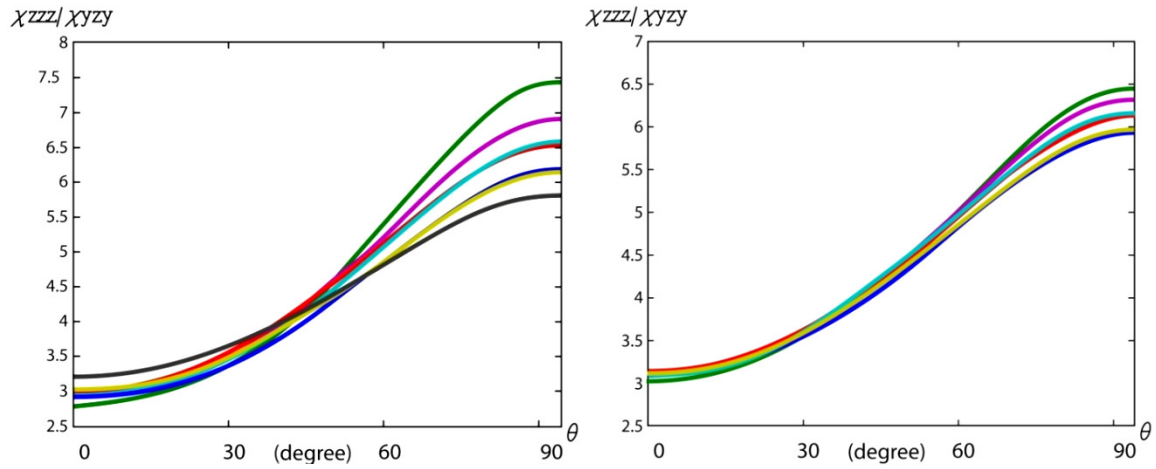

Figure 2.5: Relationship between χ_{zzz}/χ_{yzy} ratio and θ for α-helices with different chain lengths: (a, left) blue: 10, green: 12, red: 13, cyan: 15, purple: 16, yellow: 17, black: 18 residues; (b, right) blue: 28, green: 30, red: 31, cyan: 33, purple: 33, yellow: 35 residues.

2.2.6. Combination of measurements using different vibrational spectroscopic techniques

In section 2.4 the possibility that all α-helices in a sample may not adopt the exact same orientation was discussed, as well as the prospect of using a Gaussian distribution to describe the orientation distribution. To do this, the average orientation and orientation distribution width need to be simultaneously deduced. Also in the same section it was shown that SFG can measure two orientational parameters: $<\cos\theta>$ and $<\cos^3\theta>$. The two macroscopic hyperpolarizability ratios $\chi_{zzz}/\ \chi_{yyz}$ and $\chi_{zzz}/\ \chi_{yzy}$ have been extensively discussed in the orientation analysis above. These two measurements are not independent and thus can only be used to cross-check the accuracy of the data analysis method and the reliability of experimental measurements. To measure $<\cos\theta>$ or $<\cos^3\theta>$ independently, the absolute intensity of SFG signal needs to be obtained, as discussed in detail in our previous publications.[60,79] With two independent measurements, the Gaussian distribution can be deduced. However, the orientation distribution may sometimes be more complicated than a Gaussian distribution.

The same α-helices may adopt two different orientations with separate orientation angles θ_1 and θ_2. If N is the fraction of α-helical molecules tilting at θ_1 to the surface normal, and (1-N) is the fraction of molecules tilting at θ_2 to the surface normal:

$$\langle\cos(\theta)\rangle = N\langle\cos(\theta_1)\rangle + (1-N)\langle\cos(\theta_2)\rangle \qquad \textbf{(2.39)}$$

$$\langle\cos^3(\theta)\rangle = N\langle\cos^3(\theta_1)\rangle + (1-N)\langle\cos^3(\theta_2)\rangle \qquad \textbf{(2.40)}$$

There are now three unknowns: θ_1, θ_2, and N. As discussed previously, SFG can only measure two parameters for the orientation angle (for α-helices). Solely using SFG to deduce all the three unknowns is therefore impossible. As demonstrated in earlier work, it is possible to combine SFG and ATR-FTIR measurements to deduce the three

unknowns.[60] ATR-FTIR has been extensively used in the studies of proteins/peptides at interfaces.[14,15,23,28,33] These studies involve the investigations of the adsorption amount, secondary structures, as well as the orientations of proteins and peptides at interfaces. Excellent reviews on this technique in such studies are available[15,28]; here, a brief review of some of the most relevant aspects of this technique, and its complementarity to SFG in the studies of helical structure orientation at interfaces, will be presented.

In ATR-FTIR studies, the tilt angle of an α-helix can be calculated from the order parameter (S_θ), which is defined as:

$$S_\theta = \frac{3\langle cos^2\theta\rangle - 1}{2} \qquad \textbf{(2.41)}$$

with θ being the tilt angle between the helix's principal axis and the surface normal. The bracket denotes the time and ensemble average. Theoretically, $\langle\cos^2\theta\rangle$ can be determined from the measured intensity ratio in ATR-FTIR using p- and s-polarized IR light.[28] If θ is assumed to have the simplest delta-distribution, the orientation of the helix can be determined from this measured intensity ratio. The advantages and disadvantages of ATR-FTIR have been mentioned in our previous discussions[28,56,74] and will not be reiterated in this chapter. Here, the use of $\langle\cos^2\theta\rangle$ as a third measured parameter obtained by ATR-FTIR, in addition to the two measured SFG parameters, will be shown in solving the two-delta distributions discussed above. For ATR-FTIR:

$$\langle\cos^2(\theta)\rangle = N\langle\cos^2(\theta_1)\rangle + (1-N)\langle\cos^2(\theta_2)\rangle \qquad \textbf{(2.42)}$$

By combining SFG and ATR-FTIR measurements, it is possible to measure θ_1, θ_2, and N simultaneously. The orientation of α-helices may be even more complicated, thus requiring additional measured parameters to deduce these complex orientations. In these

cases, other vibrational spectroscopic techniques, such as Raman and four-wave mixing (FWM), can be utilized.[80] Also, a maximum entropy distribution function can be used as a trial function for orientation distribution.[59,79] Mathematically, this function has the minimum bias with a certain number of measured parameters available. If the orientation distribution is still difficult to deduce after the combined vibrational spectroscopic studies, isotope labeled proteins can be used, similar to those in the NMR studies.

2.2.7 Discussion on the measurement of χ_{zzz} with the near total reflection geometry.

The SFG susceptibility components, χ_{zzz}/χ_{yyz} and χ_{zzz}/χ_{yzy}, can be experimentally probed using SFG spectra collected with different polarization combinations of the input laser beams and output signal beam:

$$I_{ppp} \propto \left| \begin{array}{l} -L_{xx}(\omega)L_{xx}(\omega_1)L_{zz}(\omega_2)\cos\beta\cos\beta_1\sin\beta_2\chi_{xxz} \\ -L_{xx}(\omega)L_{zz}(\omega_1)L_{xx}(\omega_2)\cos\beta\sin\beta_1\cos\beta_2\chi_{xzx} \\ +L_{zz}(\omega)L_{xx}(\omega_1)L_{xx}(\omega_2)\sin\beta\cos\beta_1\cos\beta_2\chi_{zxx} \\ +L_{zz}(\omega)L_{zz}(\omega_1)L_{zz}(\omega_2)\sin\beta\sin\beta_1\sin\beta_2\chi_{zzz} \end{array} \right|^2 \quad \textbf{(2.43)}$$

$$I_{ssp} \propto (-L_{yy}(\omega)L_{yy}(\omega_1)L_{zz}(\omega_2)\sin\beta_2\chi_{yyz})^2 \quad \textbf{(2.44)}$$

$$I_{sps} \propto (-L_{yy}(\omega)L_{zz}(\omega_1)L_{yy}(\omega_2)\sin\beta_1\chi_{yzy})^2 \quad \textbf{(2.45)}$$

where $L_{ii}(\omega)$ is a Fresnel coefficient and local field correction factor and β, β_1 and β_2 are angles of the signal, visible and IR beams with respect to the surface normal, respectively. For an α-helix on an isotropic surface, $\chi_{xzx} = \chi_{zxx}$. Also, in this SFG experimental geometry,

$$L_{xx}(\omega)L_{zz}(\omega_1)L_{xx}(\omega_2)\cos\beta\sin\beta_1\cos\beta_2 \approx L_{zz}(\omega)L_{xx}(\omega_1)L_{xx}(\omega_2)\sin\beta\cos\beta_1\cos\beta_2$$

(2.46)

Thus these two terms cancel each other out in Eq. (2.43), leading to:

$$I_{ppp} \propto \left| \begin{array}{l} -L_{xx}(\omega)L_{xx}(\omega_1)L_{zz}(\omega_2)\cos\beta\cos\beta_1\sin\beta_2\chi_{xxz} \\ +L_{zz}(\omega)L_{zz}(\omega_1)L_{zz}(\omega_2)\sin\beta\sin\beta_1\sin\beta_2\chi_{zzz} \end{array} \right|^2 \qquad \textbf{(2.47)}$$

If the input or output beam angle is close to the critical angle of the total internal reflection, $L_{xx}(\omega)$ is close to zero. Therefore, for the near total reflection geometry,[81]

$$I_{ppp} \propto \left| L_{zz}(\omega)L_{zz}(\omega_1)L_{zz}(\omega_2)\sin\beta\sin\beta_1\sin\beta_2\chi_{zzz} \right|^2 \qquad \textbf{(2.48)}$$

This analysis indicates that ppp signal is the result of destructive interference between the χ_{xxz} and χ_{zzz} components. When a near total reflection geometry is adopted in the SFG experiment, ppp signal probes χ_{zzz}.

2.3. Orientation determination of a 3-10 helix

Although not the most common helical structure in nature, the 3-10 helical structure was proposed almost ten years earlier than the abundant α-helical structure.[82] There have been studies on whether the 3-10 helical structure is actually more common as it may involve as an intermediate step in the protein folding process.[83,84,84-89] A 3-10 helix is characterized by the hydrogen bonds formed between the i^{th} C=O group to the ($i+3)^{th}$ H-N group. The hydrogen bonds in 3-10 helices are stronger than those in α-helices, causing a shorter distance between the oxygen and the hydrogen atoms in the hydrogen bond.[33,90] In this helix, the angular distance between two adjacent amino acid residues is 120^o with an axial translation of 1.95 Å. The pitch is then 5.94 Å, and there are three residues per turn. For 3-10 helices, only A and E_1 modes are both IR and Raman

active, which makes them observable by SFG.[33,90] Below, a similar methodology as that applied for α-helical structures will be applied to the orientation analysis of stable 3-10 helical structures at interfaces. The bond additivity model is applied to calculate the SFG molecular hyperpolarizability ratios β_{aac}/β_{ccc} and β_{aca}/β_{ccc} which will be used to construct the relationship between the macroscopic SFG susceptibility component ratios χ_{zzz}/χ_{yyz} or χ_{zzz}/χ_{yzy} and the tilt angle θ of the helix.

2.3.1 IR transition dipole moment of a 3-10 helix amide I mode

For A mode (the parallel mode):

$$\left[\frac{\partial \mu}{\partial Q^r}\right](0^o) = \begin{pmatrix} 0 \\ 0 \\ 2.121 \end{pmatrix} \quad \textbf{(2.49)}$$

For E_1 mode (the perpendicular mode):

$$\left[\frac{\partial \mu}{\partial Q^r}\right](120^o) = \begin{pmatrix} 1.061 \\ 1.061i \\ 0 \end{pmatrix} \quad \textbf{(2.50)}$$

According to equations (2.49) and (2.50), the ratio $M_{(y+x)}/M_x$ is calculated to be 0.71. In this calculation, the angle between the dipole moment and the helical axis is assumed to be 45°, which was back-calculated from Choi's calculated values of the perpendicular and parallel modes of the transition dipole moment.[69] A value of 45.6° would make our calculation match with Choi's value perfectly. However, upon studies of poly(α-aminoisobutyric acid) using electron diffraction, Malcolm and Walkinshaw approximately set an upper limit of this angle to be about 45°.[90] The value of 45° is therefore believed to be reasonable to use in the calculation.

2.3.2 Raman polarizability tensor of a 3-10 helix amide I mode

To start the process of analyzing the total polarizability of a 3-10 helix, its crystal structure is first required. Malcolm and Walkinshaw have successfully proposed the crystal structure of poly(α-aminoisobutyric acid) using the average values from the crystal structure determinations of 17 independent residues.[91] The coordinates of this crystal structure are shown in Table 2.1.

	x (Å)	y (Å)	z (Å)
C'	1.12	0.54	1.189
O	1.64	0.51	2.304
N	-0.07	1.12	0.957
H	-0.45	1.21	0.018

Table 2.1: Cartesian coordinates of the first peptide link in a 3-10 helix

According to this crystal structure, the peptide unit is approximately planar with the C=O bond almost parallel to the y-axis. The Euler angles that transform Tsuboi's Raman tensor to the first link of the 3-10 helix were calculated to be φ=0°, θ=301.7° and ψ= 270° using the x-convention rotation. The rotation matrix takes the following form:

$$\xi_{0^o,301.7^o,270^o} = \begin{pmatrix} 0 & -0.525 & 0.851 \\ 1 & 0 & 0 \\ 0 & 0.851 & 0.525 \end{pmatrix} \quad \textbf{(2.51)}$$

Therefore,

$$\alpha_1 = \begin{pmatrix} 0 & -0.525 & 0.851 \\ 1 & 0 & 0 \\ 0 & 0.851 & 0.525 \end{pmatrix} \begin{pmatrix} 0.05 & 0 & 0 \\ 0 & 0.2 & 0 \\ 0 & 0 & 1.00 \end{pmatrix} \begin{pmatrix} 0 & -0.525 & 0.851 \\ 1 & 0 & 0 \\ 0 & 0.851 & 0.525 \end{pmatrix}^T = \begin{pmatrix} 0.800 & 0 & 0.357 \\ 0 & 0.05 & 0 \\ 0.357 & 0 & 0.420 \end{pmatrix} \quad \textbf{(2.52)}$$

In the case of 3-10 helix, the uniaxial property is not strictly satisfied, different from that in the α-helix case. However, the C=O bonds only orient slightly (a few

degrees) away from the helical axis. Therefore, the uniaxial property can still be considered so that all the peptide units are assumed to be approximately identical and can be transformed geometrically into each other. The Raman tensor of a 3-10 helix can then be calculated by successively performing the rotation of the Raman tensor of the peptide unit around the helical axis 120^o from one unit to the next and summing over them. For an ideal 3-10 helix, the Raman tensor can be calculated as:

$$\alpha_{1-3} = \sum_{i=0}^{2} \begin{pmatrix} \cos(120i) & \sin(120i) & 0 \\ -\sin(120i) & \cos(120i) & 0 \\ 0 & 0 & 1 \end{pmatrix}^{T} \begin{pmatrix} 0.800 & 0 & 0.357 \\ 0 & 0.05 & 0 \\ 0.357 & 0 & 0.420 \end{pmatrix} \begin{pmatrix} \cos(120i) & \sin(120i) & 0 \\ -\sin(120i) & \cos(120i) & 0 \\ 0 & 0 & 1 \end{pmatrix} \quad \textbf{(2.53)}$$

The calculated polarizability of the A and E1 amide I modes are:

For the A mode:

$$\left[\frac{\partial \alpha}{\partial Q^r}\right](0^o) = \begin{pmatrix} 1.24 & 0 & 0 \\ 0 & 1.24 & 0 \\ 0 & 0 & 1.28 \end{pmatrix} \quad \textbf{(2.54)}$$

For the E_1 mode:

$$\left[\frac{\partial \alpha}{\partial Q^r}\right](120^o) = \frac{1}{2}\begin{pmatrix} 0.55 & -0.55i & 0.55 \\ -0.55i & -0.55 & 0.55i \\ 0.55 & 0.55i & 0 \end{pmatrix} \quad \textbf{(2.55)}$$

2.3.3 SFG data analysis for 3-10 helices based on the calculated IR transition dipole moment and Raman polarizability

The molecular hyperpolarizability ratios β_{aac}/β_{ccc} and β_{aca}/β_{ccc} for an ideal 3-10 helix are:

$$\frac{\beta_{aac}}{\beta_{ccc}} = 2*(\frac{\alpha_{aa}}{\alpha_{cc}})^* \frac{\mu_c}{\mu_c} = (\frac{\alpha_{aa}}{\alpha_{cc}})^* = \frac{1.24}{1.28} = 0.97 \quad \textbf{(2.56)}$$

$$\frac{\beta_{aca}}{\beta_{ccc}} = 2*(\frac{\alpha_{ac}}{\alpha_{cc}})^* \frac{\mu_a}{\mu_c} = 2*\frac{0.55}{1.28}\frac{1.061}{2.121} = 0.43 \quad \textbf{(2.57)}$$

The relationship between each of the ratios χ_{zzz}/χ_{yyz} or χ_{zzz}/χ_{yzy} and the orientation angle θ for 3-10 helices can be deduced using the same methodology as what was adopted to treat the α- helical structures discussed in the previous sections. These relationships are plotted in Figures 2.6a and 2.6b. Figure 2.6b indicates that it is difficult to experimentally determine the orientation angle θ using the relationship between χ_{zzz}/χ_{yzy} and θ because very weak sps signal is expected.

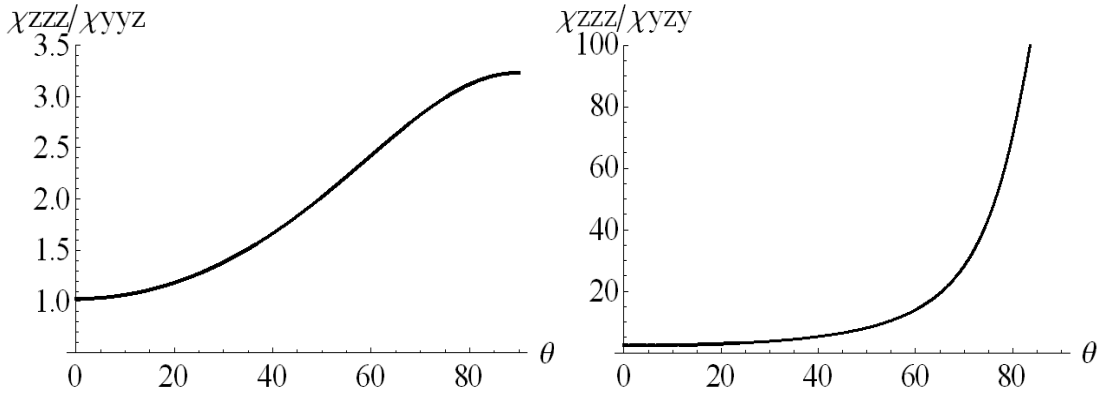

Figure 2.6: Relationship between (a, left) χ_{zzz}/χ_{yyz} or (b, right) χ_{zzz}/χ_{yzy} ratio and θ for a 3-10 helix with a delta-distribution

Similar to α-helices, for 3-10 helices, the above relationships between the SFG susceptibility component ratio and helix orientation angle can also be determined when the orientation distribution is assumed to be a Gaussian distribution instead of a delta-distribution. Also, the dependency of the relationship between χ_{zzz}/χ_{yyz} and θ on the

number of peptide units in the 3-10 helical structure can be investigated, as was done on α-helices above. This dependency (illustrated in Figures 2.7) suggests that the relationship between χ_{zzz}/χ_{yyz} and θ is varied when θ is larger than sixty degrees (meaning that the helix orients nearly parallel the surface). When θ is not large, such a variation is not substantial.

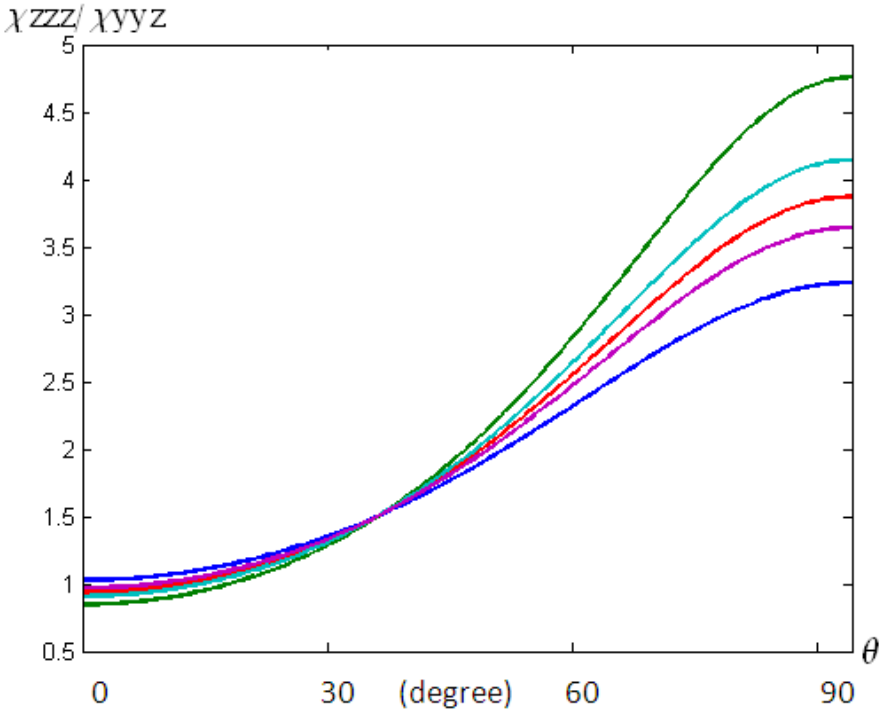

Figure 2.7: Relationship between χ_{zzz}/χ_{yyz} ratio and θ for 3-10 helices with different chain lengths: blue: 3, green: 4, red: 5, cyan: 7, purple: 8 residues

2.4. Conclusion

In this chapter, a methodology to measure the orientation of helical structures, including α-helices and 3-10 helices using polarized SFG measurements, was systematically presented. By adopting the bond additivity model, certain SFG hyperpolarizability component ratios of a helix were computed by calculating the IR

transition dipole moment and Raman polarizability tensor of the helix. The calculated values matched experimental IR and Raman measurements reported in the literature quite well. How the number of peptide units in a helix influences the SFG orientation determination was examined, and a methodology to determine the orientation of any helix that not ideal or perfect regarding the number of peptide units was developed. This method has been recently applied to determine membrane orientations of a variety of α-helical peptides such as magainin 2, MSI-78 and pardaxin, the orientation of α-helical cecropin chemically immobilized on polymer surfaces, and the membrane orientation of the 3-10 helical alamethicin. These studies further validate the method presented in this chapter. This method is likely general and can probably be applied to investigate all other helical structures (e.g., π helices and DNA helical structures) in the future.

2.5 References

(1) Pauling, L., Corey, R. B., Brandon, H. R. *Proc Natl Acad Sci U S A.* **1951,** *37,* 205-211.

(2) Matsuzaki, K. *Biochim. Biophys. Acta* **1999,** *1462,* 1-10.

(3) Sitaram, N., Nagaraj, R. *Biochim. Biophys. Acta,* **1999,** *1462,* 29-54.

(4) Brogden, K. A. *Nat. Rev. Microbiol.* **2005,** *3,* 238-250.

(5) Epand, R. M., Vogel, H.J.; *Biochim. Biophys. Acta,* **1999,** *1462,* 11-28.

(6) Hancock, R. E., Diamond, G. *Trends Microbiol.* **2000,** *8,* 402-410.

(7) Hamasaki, K. M., Eds. *Membrane Proteins: Structure, Function, and Expression Control: International Symposium*, Kyushu University Press, Japan: **1997**

(8) Rydström, J., Ed. *Membrane Proteins: Structure, Function, Assembly*, Cambridge University Press, Cambridge: **1987**

(9) Azzi, A., Masotti, L., Vecli, A., Eds. *Membrane Proteins: Isolation and Characterization*, Springer-Verlag, New York: **1986**

(10) Capaldi, R. A., Ed. *Membrane Proteins and Their Interactions with Lipids*, Marcel Dekker, New York: **1977**

(11) Eisenberg, D. *Proc. Natl. Acad. Sci.* **2003,** *100,* 11207-11210.

(12) Pauling, L., Corey, R. *Proc. Natl. Acad. Sci.* **1951,** *37,* 3235-3240.

(13) Todd, L.A. *The Legacy of Sir Lawrence Bragg,* Science Reviews Limited, Northwood:
1990.

(14) Axelsen, P. H, Kaufman, B. K., McElhaney, R. N., Lewis, R. N. *Biophys. J.* **1995,** *69,* 2770-2781.

(15) Axelsen, P. H., Citra M. J. *Prog. Biophys. molec. Biol.* **1996,** *66,* 227-253.

(16) Bechinger, B., Ruysschaert, J. -M., Goormaghtigh E. *Biophys. J.* **1999,** *76,* 552-563.

(17) Bradbury, E. M., Brown, L., Downie, A. R., Elliot, A., Fraser, R. D. B., Hanby, W. E. *J. Mol. Biol.* **1962,** *5,* 230-247.

(18) Fraser, R. D. B. *J. Chem. Phys.* **1953,** *21,* 1511-1515.

(19) Higgs, P. W. *Proc. R. Soc. Lond. A* **1953,** *220,* 472-485.

(20) Lee, S. -H., Krimm, S. *Biopolymers* **1998,** *46,* 283-317.

(21) Marsh, D. *Methods Enzymol.* **1999,** *294,* 59-92.

(22) Marsh, D. *Biophys. J.* **1998,** *75,* 354-358.

(23) Marsh, D., Müller, M., Schmitt, F. -J. *Biophys J.* **2000,** *78,* 2499-2510.

(24) Miyazawa, T., Blout, E. R. *J. Am. Chem. Soc.* **1961,** *83,* 712-719.

(25) Reisdorf, W. Jr, Krimm, S. *Biophys. J.* **1995,** *69,* 271-273.

(26) Suzuki, E. *Spectrochim. Acta. A.* **1967,** *23,* 2303-2308.

(27) Tsuboi, M. *J. Polymer Sci.* **1962,** *59,* 139-153.

(28) Tamm, L. K., Tatulian, S. A. *Q. ReV. Biophys.* **1997,** *30,* 365-429.

(29) Wilser, W. T., Fitchen, D. B. *J. Chem. Phys.* **1975,** *62,* 720-724.

(30) Tsuboi, M., Ikeda, T., Ueda, T. *J. Raman Spectrosc.* **1991,** *22,* 619-626.

(31) Overman, A. S., Tsuboi, M., Thomas G. J. Jr *J. Mol. Biol.* **1996,** *259,* 331-336.

(32) Chen, L. X., Strauss, H. L., Snyder, R. G. *Biophys. J.* **1993,** *64,* 1533-1541.

(33) Dwivedi, A. M., Krimm, S., Malcolm, B. R. *Biopolymers* **1984,** *23,* 2025-2065.

(34) Fanconi, B., Tomlinson, B., Nafie, L. A., Small, W., Peticolas, W. L. *J. Chem. Phys.* **1969,** *51,* 3993-4005.

(35) Fanconi, B. *Biopolymers* **1973,** *12,* 2759-2776.

(36) Koenig J. L., Sutton, P.L. *Biopolymers* **1970,** *9,* 1229-1237.

(37) Lee, S.-H., Krimm, S. *J. Raman Spectrosc.* **1998,** *29,* 73-80.

(38) Tsuboi, M., Benevides, J. M., Bondre, P., Thomas, G. J., Jr. *Biochemistry* **2005,** *44,* 3091-3100.

(39) Ma, G., Allen, H. C. *Langmuir* **2006,** *22,* 5341-5349.

(40) Moore, F. G., Richmond, G. L. *Acc. Chem. Res.* **2008,** *41,* 739-748.

(41) Opdahl, A., Koffas, T. S., Amitay-Sadovsky, E., Kim, J., Somorjai, G. A. *J. Phys.: Condens. Matter* **2004,** *16,* 659-677.

(42) Richmond, G.L. *Chem. Rev.* **2002,** *102,* 2693-2724.

(43) Rupprechter, G., Weilach, C. *J. Phys.: Condens. Matter* **2008,** *20,* 184019-184036.

(44) Shen, Y.R., Ostroverkhov, V. *Chem. Rev.* **2006,** *106,* 1140-1154.

(45) Shultz, M. J., Baldelli, S., Schnitzer, C., Simonelli, D. *J. Phys. Chem. B* **2002,** *106,* 5313-5324.

(46) Stiopkin, I. V., Jayathilake, H. D., Bordenyuk, A. N., Benderskii, A. V. *J. Am. Chem. Soc.* **2008,** *130,* 2271-2275.

(47) Voges, A. B., Stokes, G. Y., Gibbs-Davis, J. M., Lettan, R. B., Bertin, P. A., Pike, R. C., Nguyen, S. T., Scheidt, K. A., Geiger, F. M. *J. Phys. Chem. C* **2007,** *11,* 1567-1578.

(48) Baldelli, S. *Acc. Chem. Res* **2008,** *41,* 421-431.

(49) Santos, C., Baldelli, S. *J. Phys. Chem. C* **2008,** *112,* 11459-11467.

(50) Anglin, T. C., Conboy, J. C. *Biophys. J.* **2008,** *95,* 186-193.

(51) Dreesen, L., Sartenaer, Y., Humbert, C., Mani, A. A., Methivier, C., Pradier, C. M., Thiry, P. A., Peremans, A. *Chem. Phys. Chem.* **2004,** *5,* 1719-1725.

(52) Gautam, K. S., Dhinojwala, A. *Phys. Rev. Lett.* **2002,** *88,* 145501.1-145501.4.

(53) Gracias, D. H., Chen, Z., Shen, Y. R., Somorjai, G. A. *Acc. Chem. Res.* **1999,** *32,* 930-940.

(54) Holman, J., Ye, S., Neivandt, D. J., Davies, P. B. *J. Am. Chem. Soc.* **2004,** *126,* 14322-14323.

(55) Iwahashi, T., Miyamae, T., Kanai, K., Seki, K., Kim, D., Ouchi, Y. *J. Phys. Chem. B* **2008,** *112,* 11936-11941.

(56) Ye, S., Nguyen, K. T., Le Clair, S.V., Chen, Z. *J. Struct. Biol.* **2009,** in press.

(57) Chen, X., Wang, J., Sniadecki, J. J., Even, M. A., Chen, Z.; *Langmuir* **2005,** *21,* 2262-2264.

(58) Lee, S. -H., Wang, J., Krimm, S., Chen, Z. *J. Phys. Chem. A* **2006,** *110,* 7035-7044.

(59) Wang, J., Lee, S. -H., Chen, Z. *J. Phys. Chem. B* **2008,** *112,* 2281-2290.

(60) Chen, X., Wang, J., Boughton, A. P., Kristalyn, C. B., Chen, Z. *J. Am. Chem. Soc.* **2007,** *129,* 1420.

(61) Chen, X., Boughton, A. P., Tesmer, J. J. G., Chen, Z. *J. Am. Chem. Soc.* **2007,** *129,* 12658-12659.

(62) Elliott, A. *Proc. R. Soc.* **1954,** *226,* 408-409.

(63) Rabolt, J. F., Mo, W. H., Krimm, S. *Macromolecules* **1977,** *10,* 1065-1074.

(64) Itoh, K., Nakahara, T., Shimanouchi, T., Oya, M., Uno, K., Iwakura, Y. *Biopolymers* **1968,** *6,* 1759.

(65) Itoh, K., Shimanouchi,T., Oya, M. *Biopolymers* **1969,** *7,* 649-658.

(66) Masuda, Y., Fukushima, K., Fujii, T., Miyazawa, T. *Biopolymers* **1969,** *8,* 91-99.

(67) Itoh, K., Shimanouchi, T. *Biopolymers* **1970,** *9,* 383-399.

(68) Koenig, J. L., Sutton, P. L. *Biopolymers* **1969,** *8,* 167-171.

(69) Choi, J. -H., Hahn, S., Cho, M. *Biopolymers* **2006,** *83,* 519-536.

(70) Yokote, Y., Kubo, Y., Takahashi, R., Ikeda, T., Akahane, K., Tsuboi, M. *Bull. Chem. Soc. Jpn.* **2007,** *80,* 1148-1156.

(71) Rintoul, L., Carter, E. A., Stewart, S. D., Fredericks, P. M. *Biopolymers* **2000,** *57,* 19-28.

(72) Ackermann, K. R., Koster, J., Schlucker, S. *J. Biophotonics* **2008,** *1,* 419-424.

(73) Lambert, A. G., Davies, P. B., Neivandt, D. J. *App. Spec. Rev.* **2005,** *40,*

(74) Chen, X., Clarke, M. L., Wang, J., Chen, Z. *Intern. J. Mod. Phys. B* **2005,** *19,* 691-713.

(75) Moad, J. A., Simpson, G. *J. Phys. Chem. B* **2004,** *108,* 3548-3562.

(76) Li, Q., Hua, R., Cheah, I. J., Chou, K. C. *J. Phys. Chem. B* **2008,** *112,* 694-697.

(77) Simpson, G., Perry J.M., Ashmore-Good, C.L. *Phys. Rev. B* **2002,** *66,* 165437.

(78) Hirose, C., Akamatsu, N., Domen, K. *J. Chem. Phys.* **1992,** *96,* 997-1004.

(79) Wang, J., Paszti, Z., Even, M.A., Chen, Z. *J. Am. Chem. Soc.* **2002,** *124,* 13302-13305.

(80) Wang, J., Paszti, Z., Clarke, M. L., Chen, X., Chen, Z. *J. Phys. Chem. B* **2007,** *111,* 6088-6095.

(81) Wang, J., Even, M. A., Chen, X., Schmaier, A. H., Waite, J. H., Chen, Z. *J. Am. Chem. Soc.* **2003,** *125,* 9914-9915.

(82) Huggins, M. *Chem. Rev.* **1943,** *32,* 195-218.

(83) Millhauser, G. L. *Acc. Chem. Res.* **1999,** *32,* 1027-1033.

(84) Tirado-Rives, J., Jorgensen, W. L. *Biochemistry* **1991,** *30,* 3864-3871.

(85) Tobias, D. J., Brooks, C. L. *Biochemistry* **1991,** *30,* 6059-6070.

(86) Tobias, D. J., Mertz, J. E., Brooks, C. L. *Biochemistry* **1991,** *30,* 6054-6058.

(87) Brooks, C.L. *J. Phys. Chem.* **1996,** *100,* 2546-2549.

(88) Sheinerman, F. B., Brooks, C. L. *J. Am. Chem. Soc.* **1995,** *117,* 10098-10103.

(89) Brooks, C. L. I., Case, D. A. *Chem. Rev.* **1993,** *93,* 2487-2502.

(90) Malcolm, B. R., Walkinshaw, M. D *Biopolymers* **1986,** *25,* 607-625.

(91) Paterson, Y., Rumsey, S. M., Benedetti, E., Nemethy, G., Sheraga, H. A. *J. Am. Chem. Soc.* **1981,** 2947-2955.

CHAPTER 3

MOLECULAR INTERACTION BETWEEN MAGAININ 2 AND MODEL MEMBRANES *IN SITU*

3.1. Introduction

Isolated from the African clawed frog *Xenopus laevis*, Magainins have been shown to have antimicrobial activity.[1-3] At low concentrations, magainin peptides are able to disrupt the bacterial cell membrane, leading to cell death. At these concentrations, however, magainin peptides have been shown to be harmless to mammalian cells.[2] The Magainin family is considered to be the most well-studied group of peptides among all antimicrobial peptides. Magainins have been shown to have antimicrobial activity against a large number of bacterial strains, and it is believed that they have a great therapeutic potential in the treatment of bacterial, fungal, and protozoan infections in humans.[2] Among its family, Magainin 2 possesses a broad antimicrobial spectrum with high potency. Experimental tests have shown that Magainin 2 is about 5 to 10 times more potent than Magainin 1.[2] Extensive studies have been carried out to understand the antimicrobial activity of Magainin 2 using different techniques ranging from experimental methods such as External Reflection-Fourier Transform Infrared spectroscopy (ER-FTIR), neutron reflectivity,[4] oriented circular dichroism,[5,6] X-ray diffraction,[7] confocal laser scanning microscopy,[8] differential scanning calorimetry,

solid-state NMR,[9] atomic force microscopy[10] and fluorescence spectroscopy[11-13] to molecular dynamics simulations.[14,15]

Many of the above efforts were trying to unveil the differences in the interaction schemes of Magainin 2 with bacterial cells as opposed to mammalian cells. Even though a consensus has not been reached, it is generally believed that Magainin 2 disrupts bacterial cells by forming toroidal pores (wormholes) in the membrane; whereas it binds horizontally to the mammalian cell membranes and hence exhibits no disruptive activity.[16-18]

The lipid compositions of cell membranes play a significant role in the ability of many antimicrobial peptides to distinguish between bacterial cell membranes and mammalian cell membranes. Bacterial cell membranes consist of a substantial amount of lipids with negatively charged head groups (e.g., phosphatidylglycerol – PG) in addition to neutral lipids (e.g., phosphatidylethanolamine – PE). Mammalian cell membranes, on the other hand, mainly have zwitterionic lipids (e.g., phosphatidylcholine – PC) and other components (e.g., cholesterol). Most antimicrobial peptides contain amino acids that are positively charged, and this electrostatic attraction between the negatively charged lipids and the positive charges on the antimicrobial peptides is believed to be the driving force for their binding to bacterial cell membranes, but not mammalian ones.

Sum Frequency Generation (SFG) vibrational spectroscopy is a non-linear optical spectroscopic technique that is becoming more prevalent in the studies of a variety of interfaces due to its intrinsic surface/interface sensitivity. The advantages and strengths of using SFG in interfacial studies have been previously discussed extensively,[19-27] which

will not be repeated in detail here. In this chapter, we will report the results obtained from SFG studies on Magainin 2 in mammalian and bacterial model membranes. Attenuated Total Reflectance – Fourier Transform Infrared spectroscopy (ATR-FTIR) was also used in this study as a supplemental technique to SFG. The combination of SFG and ATR-FTIR in the study of peptide-membrane interactions was shown to be valuable in our previous publication on the interactions between melittin and lipid bilayers.[28] In this chapter, SFG and ATR-FTIR data indicated similar Magainin 2 orientations in the respective lipid bilayers. This is the first report on the quantitatively measured average orientation angles of Magainin 2 molecules in a model bacterial cell membrane (a single POPG/POPG bilayer) *in situ* using SFG. The modes of action of Magainin 2 on both mammalian and bacterial cell membranes can be proposed through Magainin 2 orientations and SFG observations of lipid bilayers.

3.2. Materials and methods

Magainin 2 (GIGKWLHSAKKFGKAFVGEIMNS) was purchased from Bachem (Torrance, CA). Hydrogenated 1-Palmitoyl-2-Oleoyl-*sn*-Glycero-3-[Phospho-*rac*-(1-glycerol)] (POPG) and 1-Palmitoyl-2-Oleoyl-*sn*-Glycero-3-Phosphocholine (POPC) were ordered from Avanti Polar Lipids (Alabaster, AL).

For SFG experiments, right-angle CaF_2 prisms purchased from Altos (Trabuco Canyon, CA) were soaked in toluene overnight and then sonicated in Contrex AP solution from Decon Labs (King of Prussia, PA) before the first use. Before each lipid deposition, the CaF_2 prisms were stored in Contrex AP solution overnight and then rinsed with water before immersing in methanol for an hour. The prisms were rinsed thoroughly

with a large amount of deionized water and then cleaned in a glow discharge plasma chamber for 4 minutes immediately before the bilayer preparation. Substrates were tested by collecting SFG signals from their surfaces, and no contamination was detected.

We used the Langmuir-Blodgett and Langmuir-Schaefer (LB/LS) method to deposit the proximal and the distal leaflets, respectively.[29, 30] A KSV2000 LB system and ultrapure water from a Millipore system (Millipore, Bedford, MA) were used throughout the experiments during the bilayer preparation, which is briefly described below. A prism was attached to a sample holder via one right-angle face. The other right-angle face was perpendicularly immersed in the water inside the Langmuir trough. An appropriate amount of lipid chloroform solution was then gently spread onto the water surface, and the chloroform was allowed to evaporate. The lipid monolayer area was compressed by two barriers at a rate of 5 mm/min until a surface pressure of 34 mN/m was reached. The prism was lifted out of the subphase at a rate of 1 mm/min. A monolayer of lipid on the prism was thus prepared. A 2 mL reservoir was placed in a large trough slightly deeper than it so that water could cover it. The right-angle surface of the prism with the monolayer was horizontally lowered to contact the monolayer deposited on the water surface (with a surface pressure of 34 mN/m) of the trough to form a lipid bilayer. After the formation of the bilayer, the extra lipids at the air-water interface were removed using a micropipette. Water in the large trough was drained while keeping the bilayer immersed in water inside the small reservoir so that a much smaller amount of peptide/protein would be sufficient for the experiment. The bilayer was immersed in water throughout the entire experiment, and a small amount of water was added to the reservoir, when needed, to compensate for water evaporation during lengthy experiments.

For the Magainin 2-bilayer interaction experiments, a specific volume of the Magainin 2 aqueous stock solution was injected into the small reservoir of 2 mL to achieve the desired concentration. A magnetic microstirrer was used to ensure a homogeneous concentration distribution of peptide molecules in the subphase below the bilayer. All experiments were carried out at room temperature (~24^{o}C), at which both POPG and POPC bilayers are in the fluid phase.

Details of the SFG setup in our laboratory have been described in previous publications and will not be repeated here.[31, 32] Input laser beams were incident onto the prism through one of the right-angle faces and then reflected by the other right-angle face coated with the bilayer (Figure 3.1). The prism was arranged such that total reflection of the 532-nm green beam was achieved. Under these conditions, the infrared (IR) beam was not totally reflected. For orientation analysis, SFG spectra were collected using ssp (s-polarized output SFG signal, s-polarized input visible beam and p-polarized input IR beam) and ppp polarization combinations. Details about the analysis of SFG spectra will be presented later in section 3.3.

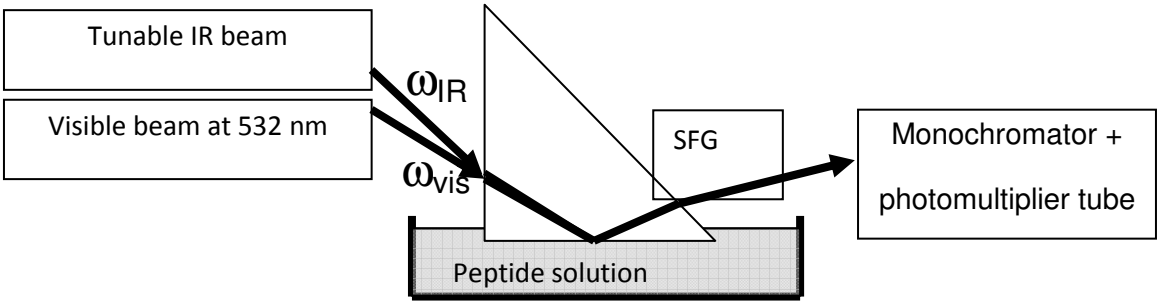

Figure 3.1: Schematic of the near total reflection experimental geometry in SFG

ATR-FTIR experiments were carried out with a Nicolet Magna 550 FTIR spectrometer using a detachable ZnSe total internal reflection crystal (Specac Ltd. RI, United Kingdom). The LB/LS method was used to deposit the lipid bilayers onto the ZnSe crystal surface that had been pre-cleaned with methanol, Contrex AP solution, deionized water and eventually treated in a glow discharge plasma chamber for 2 minutes immediately before the bilayer preparation. After the lipid bilayer was deposited onto the crystal, the water that kept the bilayer hydrated was flushed multiple times with D_2O to avoid signal confusion between the O-H bending mode and the peptide amide I mode, and to ensure a better S/N ratio in the peptide amide I band region. Next, 3.2 μL of a 400 μM Magainin 2 stock solution was injected into the subphase of 1.6 mL to achieve the desired concentration. S and P polarized ATR-FTIR spectra of Magainin 2 in the lipid bilayer were taken for orientation analysis after the system reached equilibrium (about one hour).

3.3. SFG Data analysis

Magainin 2 is known to possess no well-defined secondary structure in aqueous solutions.[33-36] However, CD, FTIR and solid-state NMR studies suggest that it folds into an α-helical structure in the presence of phospholipid bilayers.[33-39] It is believed that magainin 2 forms dimer or trimers when the peptide-to-lipid ratio is above 0.02,[12] which is much higher than the ratio we deal with in our SFG experiments. Therefore, we can assume that the peptide orientation we determine here is the average tilt angle of single magainin molecules. The average orientation of Magainin 2 molecules was calculated

based on the orientation of the amide C=O bonds, which are held up in the direction of the helical axis by the hydrogen bonds within the peptide molecules. This average orientation was deduced by analyzing the polarized SFG amide I signal (between 1600 to 1700 cm^{-1}). SFG amide I spectra are deconvoluted such that the alpha-helical spectral component (centered at ~1655 cm^{-1}) can be extracted from the band. In addition, SFG spectra collected from the lipid bilayer in the C-H stretching frequency regime (2800 cm^{-1} to 3000 cm^{-1}) (with or without the peptides) were investigated according to the thin film model as discussed in one of our previous publications.[40]

The peptide's orientation information can be obtained by SFG using polarization combinations of ssp and ppp collected in the amide I regime. The SFG susceptibility tensor element χ_{ijk} (i, j, k = x, y, z) is related to the SFG molecular hyperpolarizability tensor element β_{lmn} (*l*, *m*, *n* = *a*, *b*, *c*) by Euler angle projections.[41] The relationship between the SFG susceptibility tensor elements for α-helices, the orientation angle (θ) and the hyperpolarizability components can be expressed as:

For the A mode:

$$\chi_{A,xxz} = \chi_{A,,yyz} = \frac{1}{2} N_s[(1+r) < \cos\theta > -(1-r) < \cos^3\theta >]\beta_{ccc}$$
$$\chi_{A,xzx} = \chi_{A,yzy} = \chi_{A,zxx} = \chi_{A,zyy} = \frac{1}{2} N_s[(1-r)(< \cos\theta > - < \cos^3\theta >)]\beta_{ccc} \quad \textbf{(3.1)}$$
$$\chi_{A,zzz} = N_s[r < \cos\theta > +(1-r) < \cos^3\theta >]\beta_{ccc}$$

Where $r = \beta_{aac}/\beta_{ccc}$

For the E_1 mode:

$$\chi_{E,xxz} = \chi_{E,yyz} = -N_s(< \cos\theta > - < \cos^3\theta >)\beta_{aca}$$

$$\chi_{E,xzx} = \chi_{E,yzy} = \chi_{E,zxx} = \chi_{E,zyy} = N_s(<\cos^3\theta>\beta_{aca} \quad \textbf{(3.2)}$$

$$\chi_{E,zzz} = 2N_s(<\cos\theta> - <\cos^3\theta>)\beta_{aca}$$

where N_s is the surface density of the α-helical repeat units. The SFG hyperpolarizability tensor elements can be deduced from Raman and IR properties of the α-helical molecules, which makes it possible to deduce the relations among these elements, as we showed in the previous chapter. From these deductions, we obtained r= 0.61 and β_{aca}= $0.33\beta_{ccc}$ with the adoption of the bond additivity model on an α-helical symmetry that consists of 23 amino acid residues.[42]

We have developed a methodology to determine the orientation of α-helical structures using SFG amide I spectra collected with different polarization combinations.[28,41,42] This method is based on the SFG data analysis for an α-helix with one unit length (eighteen amino acids) or infinitely long. We also complete the methodology by considering α-helices with number of amino acid residues different than multiples of one unit (i.e., with the number of amino acids not being a multiple of 18). We presented a systematic discussion on the determination of α-helix (as well as 3-10 helix) orientation using SFG in the previous chapter. The current SFG study on magainin orientation can be considered as a successful application of the method.

3.4. Results and Discussions

3.4.1 SFG and ATR-FTIR Amide I Spectra.

3.4.1.1 Magainin 2 in a POPG/POPG lipid bilayer.

It has been shown that the minimum inhibitory concentration (MIC) of Magainin 2 against *E. coli* is around 20 μM.[43] The positively charged Magainin 2 molecules tend to target anionic lipids in the cell membrane via electrostatic attraction. *E. coli* cell membranes only contain about 32% anionic lipids,[44] thus a purely negatively charged lipid bilayer should require a lower peptide concentration for disruption than MIC. In this set of experiments, we employed anionic POPG lipids to represent the bacterial cell membrane, and therefore a lower concentration of 800 nM of Magainin 2 was believed to be sufficient to ensure effective interactions between Magainin 2 and the POPG bilayer. Even at this 25-fold lower concentration than the MIC against *E. coli*, Magainin 2 exhibited excellent SFG signal strength (Figure 3.2), enabling for a reliable orientation analysis of Magainin 2 molecules in the bilayer using SFG.

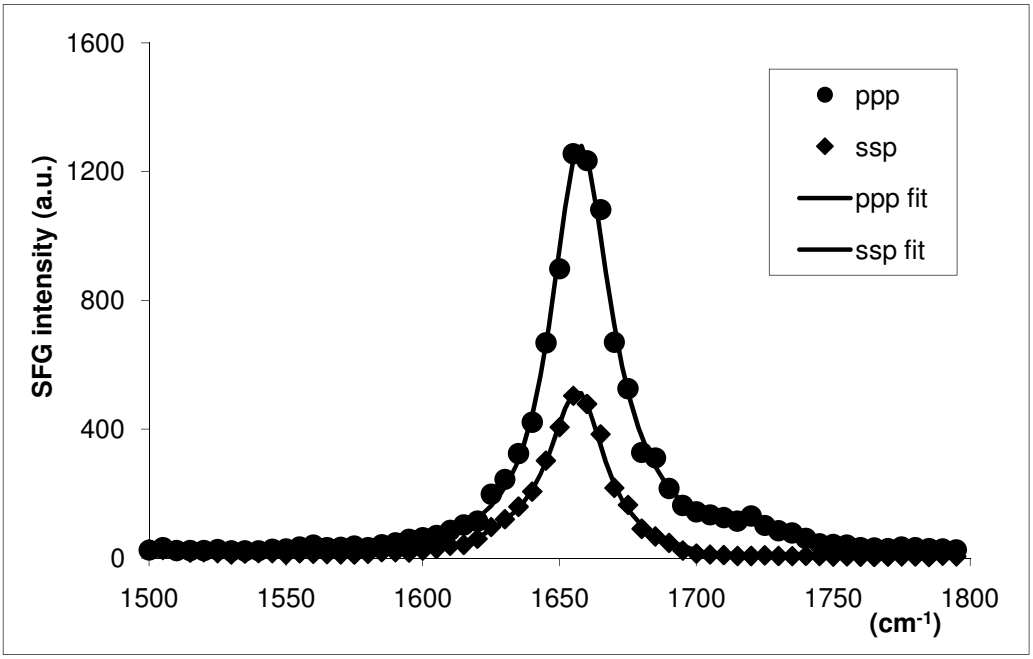

Figure 3.2: SFG ppp and ssp spectra collected from a POPG bilayer in contact with a 800 nM Magainin 2 solution in the C=O stretching frequency region

1657 cm-1	Amplitude	Damping coefficient	Xppp/Xssp
ppp	480	13.5	1.55
ssp	287	12.5	

Table 3.1: Fitting parameters of the SFG amide I signal collected from a POPG bilayer in contact with a 800 nM Magainin 2 solution

Before we discuss the interactions between the POPG bilayer with magainin 2 of a peptide solution of 800 nM, we first present the results on a lower magainin 2 concentration of 200 nM. The CaF_2 supported POPG/POPG bilayer was in contact with 2 mL deionized water, then 1 μL of the peptide stock solution was introduced. No discernable SFG signal in the amide I region could be detected after 1 hour (data not shown), but some changes in the lipid signal were observed (see later discussions for more details). This can be explained by the fact that the α-helical Magainin 2 peptides could be lying down on the bilayer surface, generating a much weaker SFG amide I signal than that generated from vertically oriented peptides in the bilayers, but still causing changes in the bilayer organization (see Section 3.4.2). Magainin 2 has an amphiphilic α-helical structure, which allows the peptide molecules to lie on the membrane surface at low peptide concentration.[45,11]

A higher peptide concentration experiment was then carried out in which 4 μL Magainin 2 stock solution was added to the water subphase to reach a concentration of 800 nM. Magainin 2 was allowed to interact with the POPG/POPG bilayer and SFG spectra were collected. Figure 3.2 displays SFG spectra in the amide I range of Magainin

2 in the POPG bilayer after the signal had stabilized (one hour). Both ssp and ppp spectra exhibit a dominant peak centered at 1657 cm^{-1}. According to the previous vibrational spectroscopic studies on protein/peptide amide I signals and our previous research on melittin, the amide I mode (dominated by the C=O stretching mode) of the α-helical peptide units is centered at around 1655 cm^{-1}.[28,29,46-48] The amide I peak center affirms that Magainin 2 adopted a well-defined α-helical structure in the POPG bilayer. The correlation between the ratio χ_{ppp}/χ_{ssp} and the peptide orientation angle θ for Magainin 2 is plotted in Figure 3.3. According to the measured SFG signal, the χ_{ppp}/χ_{ssp} ratio for Magainin 2 in the POPG/POPG bilayer is about 1.55. It can be deduced from Figure 3.3 that Magainin 2 adopts a transmembrane orientation in POPG bilayers (Table 3.1). Quantitatively, the tilt angle (θ) between the helical principal axis of the Magainin 2 molecule and the POPG bilayer surface normal was found to be around 22 degrees if a δ orientation distribution is assumed.

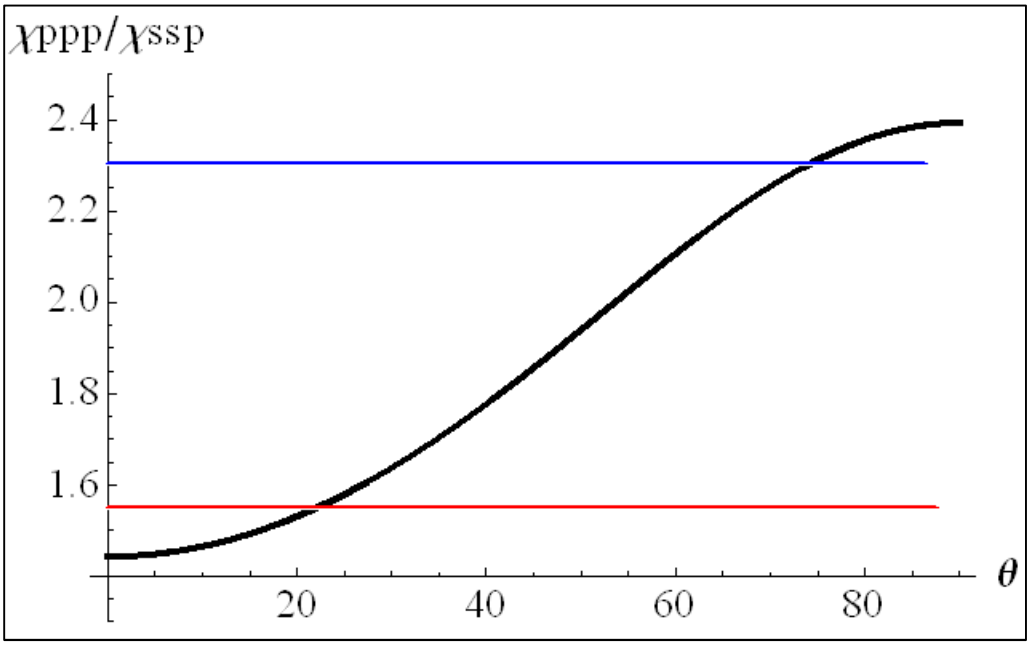

Figure 3.3: Relationship between the χ_{ppp}/χ_{ssp} ratio and the helix orientation angle of Magainin 2

ATR-FTIR was used as a supplemental technique to our SFG measurements. As mentioned above, the amide I signal of an α-helical peptide is centered at about 1655 cm^{-1}. Due to the strong H_2O bending mode in this frequency range, which may complicate our amide I ATR-FTIR signal analysis, we used a Magainin 2 D_2O solution in the ATR-FTIR study. The amide I signal undergoes a slight red-shift for α-helical peptides when D_2O is used to make the solution. In our ATR-FTIR experiment with Magainin 2 and a POPG lipid bilayer in a D_2O solution, we observed a peak maximum at 1652 cm^{-1}, indicating a Magainin 2 α-helical conformation in the POPG bilayer (Figure 3.4).[46] The peak center position is in good agreement with a recent study of Magainin 2 interacting with DPPG monolayers using ER-FTIR.[4]

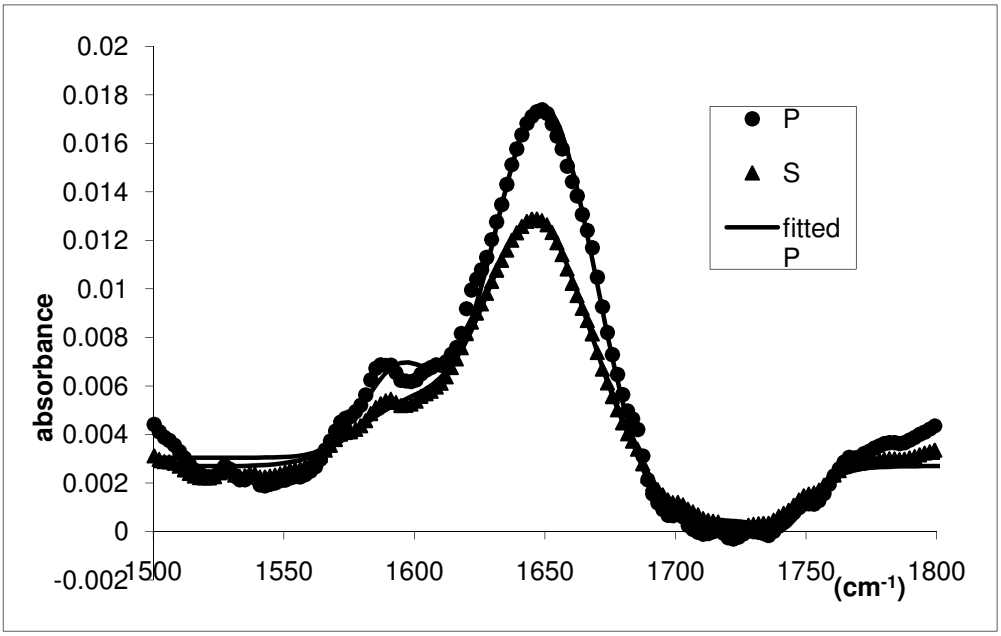

Figure 3.4: p and s polarized ATR-FTIR spectra collected from a POPG bilayer in contact with a 800 nM Magainin 2 solution in the C=O stretching frequency region

While fitting the ATR-FTIR amide I signal of Magainin 2, we also included a minor peak at around 1644 cm^{-1} to account for the C=O bonds that adopted a random coil structure for the "in-solvent" Magainin 2 molecules that did not fold into helical structures.

Using the polarized ATR-FTIR measurement, the dichroic ratio of the 1652 cm^{-1} peak of Magainin 2 (800 nM) in a POPG lipid bilayer was determined to be 2.79, which gives the order parameter S_θ a value of 0.662. The average angle θ between the helical axis of the Magainin 2 molecule and the bilayer surface normal was calculated to be approximately 20 degrees if a delta orientation distribution is assumed. This is in excellent agreement with the SFG data. As we discussed in our previous publications and in chapter 2, SFG measures $\langle\cos\theta\rangle$ and $\langle\cos^3\theta\rangle$, while ATR-FTIR measures $\langle\cos^2\theta\rangle$.[28] Since SFG and ATR-FTIR measure different orientation parameters, the excellent agreement between the two methods indicates that Magainin 2 adopts a well-defined orientation (δ-distribution or an orientation distribution with a narrow width) in the POPG bilayer. If the orientation distribution is not narrow, the results should be substantially different when deduced from different measured parameters, like $\langle\cos\theta\rangle$, $\langle\cos^2\theta\rangle$, and $\langle\cos^3\theta\rangle$. Here both SFG and ATR-FTIR studies show that magainin 2 adopts transmembrane orientation when its concentration is 800 nM, different from what was observed when the concentration is 200 nM.

Our spectroscopic measurements match the published results from Molecular Dynamics simulations performed on a constructed Magainin 2 toroidal-pore model.[14] In this simulation, a Magainin pore that consisted of five Magainin 2 molecules, 138 1-

palmitoyl-2-oleoylphosphatidylethanolamine POPE and 46 POPG molecules was left equilibrating for 250 ps. During this period of time the reorientation of Magainin 2 molecules was observed. Magainin 2 molecules lining the pores were found to tilt at about 21 degrees from the membrane normal.

3.4.1.2 Magainin 2 in a POPC/POPC lipid bilayer

A POPC bilayer was used as a representation of the mammalian cell membrane. Different from POPG, POPC is a zwitterionic lipid. For this set of experiments, a higher Magainin 2 concentration of 2.0 μM was used. At this peptide concentration, discernable SFG amide I signal was detected, allowing for a reliable analysis of the peptide orientation (Figure 3.5). A supplemental ATR-FTIR experiment at the same concentration of Magainin 2 (2.0 μM) was also carried out, but no amide I signal was detected (data not shown). This is due to the fact that the Magainin 2 coverage on the POPC/POPC bilayer was not high enough to produce detectable ATR-FTIR signal.

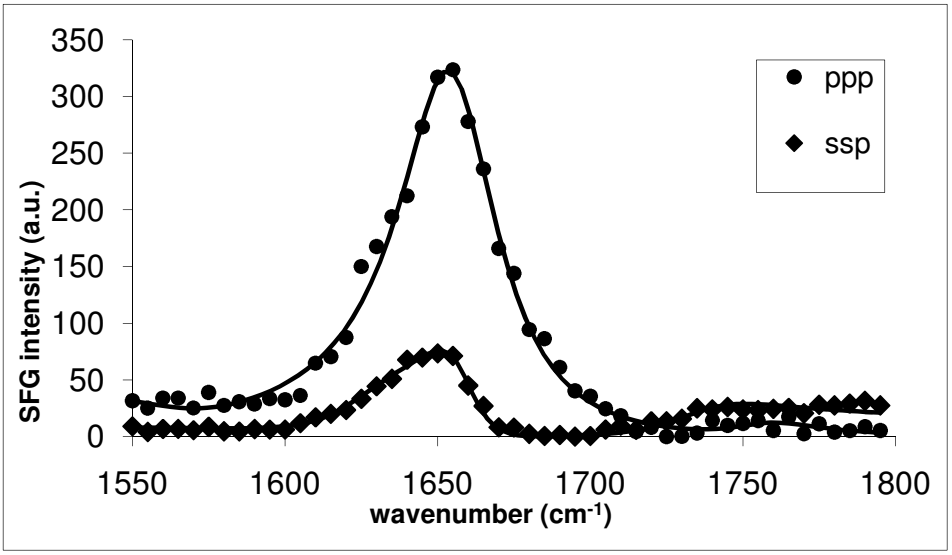

Figure 3.5: SFG ppp and ssp spectra collected from a POPC bilayer in contact with a 2.0 μM Magainin 2 solution in the C=O stretching frequency region.

1657 cm^{-1}	Amplitude	Damping coefficient	χ_{ppp}/χ_{ssp}
ppp	350	20	2.3
ssp	152.5	20	

Table 3.2: Fitting parameters of the SFG amide I signal collected from a POPC bilayer in contact with a 2.0 μM Magainin 2 solution

From the SFG ssp and ppp polarized spectra (Figure 3.5), the average tilt angle (θ) of Magainin 2 in the POPC/POPC bilayer was determined to be ~75 degrees if a delta orientation distribution is assumed (Table 3.2), which is very different from that in the POPG/POPG bilayer. This result strongly agrees with previous findings in the literature stating that Magainin 2 lies down on the surface of l-Palmitoyl-2-stearoyl-(n-doxyl)-α-phosphatidylcholine [n-doxyl-PCs (n = 5, 10, and 12)] lipid vesicles at an angle of approximately 79 degrees ± 5 degrees relative to the surface normal.[33, 37, 49]

3.4.2 SFG spectra of POPG and POPC lipid bilayers.

The behavior of the lipids was monitored in our SFG experiments by the observation of SFG spectra in the C-H stretching frequency regime (2800 – 3000 cm^{-1}). Magainin 2 should not contribute substantial SFG signal in the C-H stretching spectral region.[4] As displayed in Figures 3.6, SFG spectral features in the C-H stretching region are significantly different between POPG/POPG and POPC/POPC lipid bilayers before the Magainin 2 interaction. The weaker SFG signal of the neutral POPC/POPC bilayer shown in Figure 3.6 (spectrum a) compared to that of the charged POPG/POPG bilayer

(spectrum b) indicates that lipid bilayers with zwitterionic headgroups are more ordered and therefore more symmetrical. The better order of the POPC bilayer compared to POPG bilayer in water might be due to the different interactions between the water molecules and the headgroups of lipid molecules. For lipids that are in fluid phase at room temperature, it is difficult to quantitatively investigate the average orientation of the lipid chain due to the rapid flip-flop and lateral displacement of the lipid molecules. Therefore the discussion below is qualitative.

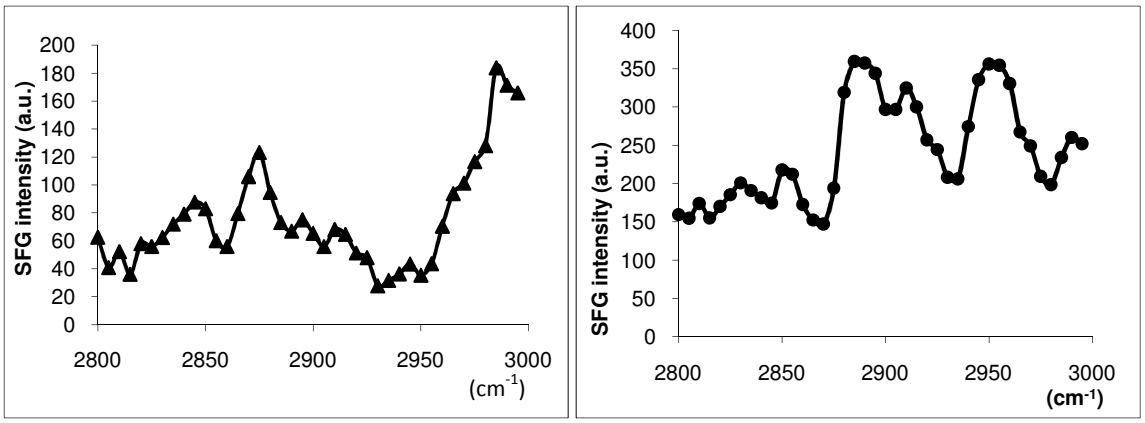

Figure 3.6: SFG spectra collected from a. POPC/POPC bilayer (left) and b. POPG/POPG bilayer (right) before in contact with magainine 2 in the C-H stretching frequency region.

Similar spectral features can be seen in Figure 3.7 for both the POPG/POPG bilayer (with 200 nM Maiganin 2, spectrum 7b) and the POPC/POPC bilayer (with 2.0 μM Magainin 2, spectrum 7a). This striking similarity might indicate that similar interactions are taking place in both cases. In Section 4.1.2, we indicated that magainin 2 molecules orient relatively parallel to the POPC bilayer surface. It is therefore likely that magainin 2 molecules adopt a similar orientation on the POPG bilayer at low concentrations. This interpretation agrees with what was discussed regarding the amide I

band analysis (i.e. low signal would indicate a parallel orientation). Because there is a change in the lipid C-H stretching signal, magainin 2 molecules must adsorb to the bilayer, but only with a low surface coverage.

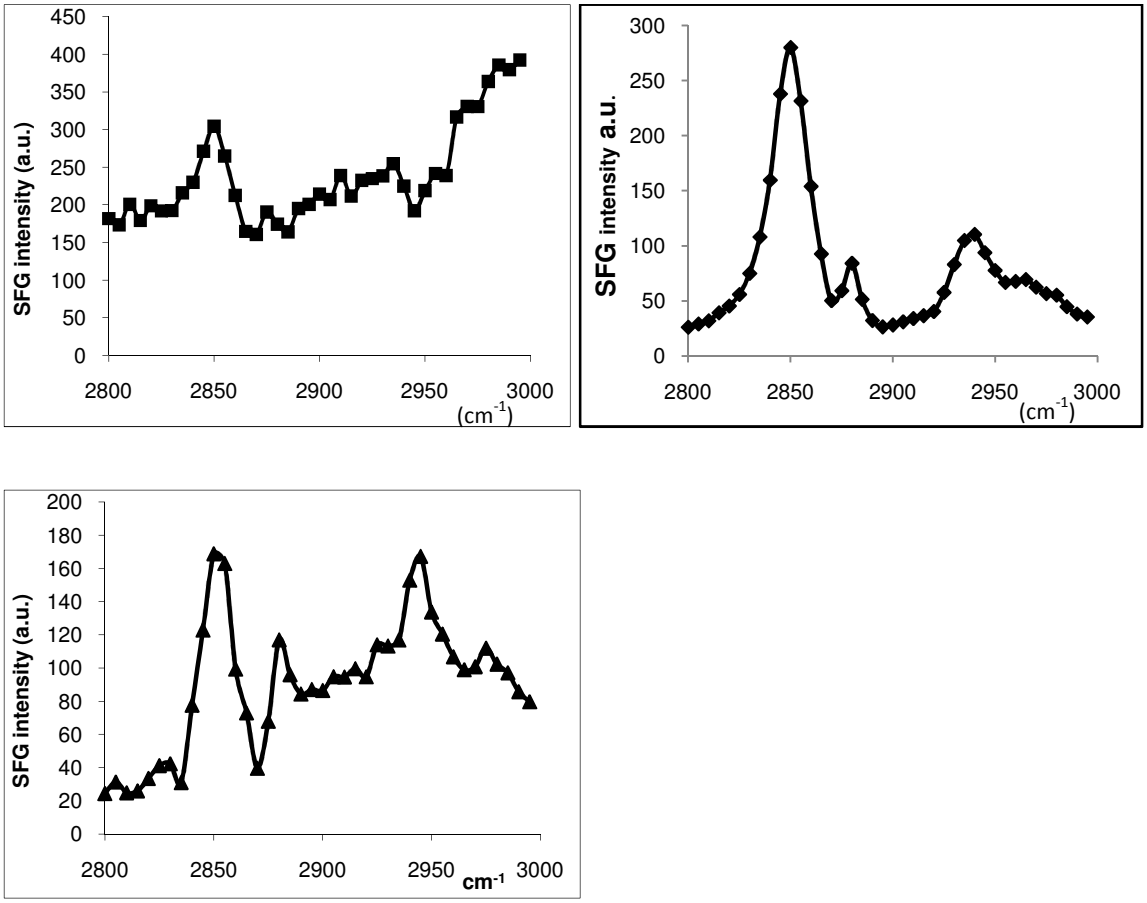

Figure 3.7: SFG spectra collected from a. POPC/POPC bilayer in contact with 2.0 uM magainin 2 solution (top left); b. POPG/POPG bilayer in contact with 200 nM magainin 2 solution (top right); c. POPG/POPG bilayer in contact with 800 nM magainin 2 solution in the C-H stretching frequency region (bottom).

In Figure 3.7, when comparing the two spectra of POPG/POPG with 800 nM Magainin 2 (spectrum c) and POPC/POPC with 2.0 μM Magainin 2 (spectrum a), it can be seen that they have similar spectral features as well, except for the peak at 2880 cm^{-1} representing the symmetric stretch of the methyl group. In the POPG/POPG bilayer, a

dramatic drop in the overall spectral intensity was observed after the addition of peptide (compare spectrum 7c to 6b). A possible interpretation for this would be the formation of a toroidal pore, which would cause the lipid side chains to tilt and form a connection between the two leaflets. Because of the rapid flip-flop that would be induced from this process, this pore lining phenomenon would significantly enhance the symmetry of the bilayer and reduce overall POPG/POPG bilayer SFG signal. In addition to this, the CH_2 symmetric stretch peak at 2850 cm^{-1} could arise from the lipid side chains that are tilted along the pores.

3.5. Conclusion

We have successfully applied SFG and ATR-FTIR to measure the average tilt angle of Magainin 2 molecules in negatively charged (POPG) and zwitterionic (POPC) lipid bilayers in the fluid phase. It was found that SFG has a much better detection limit, which can be used to study interfacial molecules when the surface coverage is much lower. SFG orientation analysis on α-helical structures is based on a methodology developed in our lab, which was summarized in detail in chapter 2.[42] For the cases where both SFG and ATR-FTIR signals can be detected, SFG and ATR-FTIR can measure different orientation parameters. Our SFG results can be well correlated to ATR-FTIR conclusion, demonstrating the reliability of the measurements. This also further validates our SFG orientation analysis methodology presented in chapter 2. All the experiments were performed *in situ* under biologically relevant conditions. The modes of action of Magainin 2 on these two different model membranes for bacterial cells and mammalian cells were discussed according to the deduced average orientation of the peptide

molecules and the investigation of the lipid bilayer SFG signals. The transmembrane orientation of Magainin 2 molecules and the possible rapid flip-flop induced led us to believe that the peptide forms toroidal pores in POPG/POPG lipid bilayers at a peptide concentration of 800 nM. On the other hand, the "more tilt or lie down" orientation of the peptide's molecules and the disturbance of lipid chains are evident for the carpet-like mechanism when Magainin 2 interacts with POPC/POPC bilayer. This research, along with our previous SFG studies on lipid bilayers,[28,50-54] demonstrates that SFG is a powerful technique to elucidate molecular interactions between various molecules and model cell membranes in situ.

3.6 References

(1) Maloy, W. L., Kari, U. P. *Biopolymers* **1995**, *37*, 105-122.

(2) Zasloff, M., Martin, B., Chen, H. C. *Proc. Natl. Acad. Sci. USA* **1988,** *85*, 910-913.

(3) Berkowitz, B. A, Bevins, C. L., Zasloff, M. A. *Biochem. Pharmacol*. **1990**, *39*, 625-629.

(4) Lad, M. D., Birembaut, F., Clifton, L. A., Frazier, R. A., Webster, J. R. P., Green, R. J. *Biophys. J.* **2007,** *92*, 3575-3586.

(5) Ludtke, S., He, K., Heller, W., Harroun, T., Yang, L., Huang, H. *Biochemistry* **1996,** *35*, 13723-13728.

(6) Chen, F. Y., Lee, M. T., Huang, H. W. *Biophys. J.* **2003,** *84*, 3751-3758.

(7) Ludtke, S., He, K., Huang, H. *Biochemistry* **1995,** *35*, 16764-16769.

(8) Imura, Y., Choda, N., Matsuzaki K. *Biophys. J.* **2008,** *95*, 5757-5765.

(9) Hallock, J. K., Lee, D. K., Ramamoorthy, A. *Biophys. J.* **2003,** *84*, 3052-3060.

(10) Mecke, A., Lee, D. K., Ramamoorthy, A., Orr, B. G., Banaszak Holl, M. M. *Biophys. J.* **2005,** *89*, 4043-4050.

(11) Gregory, S. M., Pokorny, A., Almeida, P. F. F. *Biophys. J.* **2009,** *96*, 116-131.

(12) Matsuzaki, K., Murase, O., Tokuda, H., Funakoshi, S., Fujii, N., Miyajima, K. *Biochemistry*. **1994,** *33*, 3342-3349.

(13) Matsuzaki, K., Murase, O., Fujii, N., Miyajima, K. *Biochemistry* **1996,** *35*, 11361-11368.

(14) Murzyn, K., Pasenkiewicz-Gierula, M. *J. Mol. Model.* **2003,** *9*, 217-224.

(15) Illya, G., Deserno, M. *Biophys. J.* **2008,** *95*, 4163-4173.

(16) Matsuzaki, K. *Biochim. Biophys. Acta* **1998,** *1376*, 391-400.

(17) Wieprecht, T., Beyermann, M., Seelig, J. *Biochemistry* **1999,** *38*, 10377-10387.

(18) Matsuzaki, K., Murase, O., Tokuda, H., Funakoshi, S., Fujii, N., Miyajima, K. *Biochemistry* **1994,** *33*, 3342-3349.

(19) Miranda, P. B., Shen, Y. R. *J. Phys. Chem. B* **1999,** *103*, 3292-3307.

(20) Kim, J., Somorjai, G. A. *J. Am. Chem. Soc.* **2003,** *125*, 3150-3158

(21) Kim, J., Cremer, P. S. *Chem. Phys. Chem.* **2001,** *2*, 543-546.

(22) Baldelli, S. *Acc. Chem. Res* **2008,** *41,* 421-431.

(23) Voges, A. B., Al-Abadleh, H. A., Musorrariti, M. J., Bertin, P. A., Nguyen, S. T., Geiger, F. M. *J. Phys. Chem. B* **2004,** *108*, 18675-18682.

(24) Li, Q. F., Hua, R., Chea, I. J., Chou, K. C. *J. Phys. Chem. B* **2008,** *112*, 694-697.

(25) Ye, H. K., Gu,Z. Y., Gracias, D. H. *Langmuir* **2006,** *22*, 1863-1868.

(26) Yatawara, A. K., Tiruchinapally, G., Bordenyuk, A. N., Andreana, P. R., Benderskii, A. V. *Langmuir* **2009,** *25*, 1901-1904.

(27) Perry, A., Ahlborn, H., Space, B., Moore, P. B. *J. Chem. Phys.* **2003,** *118*, 8411-8419.

(28) Chen, X., Wang, J., Boughton, A. P., Kristalyn, C. B., Chen, Z. *J. Am. Chem. Soc.* **2007,** *129*, 1420-1427.

(29) Tamm, L. K., Mcconnell, H. M. *Biophys. J.* **1985,** *47*, 105-113.

(30) Thompson, N. L., Palmer, A. G. *Comm. Mol. Cell. Biophys.* **1988,** *5*, 39-56.

(31) Wang, J., C. Y. Chen, S. M. Buck, Z. Chen. *J. Phys. Chem. B.* **2001,** *105*, 12118-12125.

(32) Wang, J., Z. Paszti, M. A. Even, Z. Chen *J. Am. Chem. Soc.* **2002,** *124*, 7016-7023.

(33) Matsuzaki, K., Harada, M., Handa, T., Funakoshi, S., Fujii, N., Yajima, H., Miyajima, K. *Biochim. Biophys. Acta* **1989,** *981*, 130-134.

(34) Jackson, M., Mantsch, H. H., Spencer, J. *Biochemistry* **1992,** *31*, 7289-7293.

(35) Wieprecht, T., Dathe, M., Schumann, M., Krause, E., Beyermann, M., Bienert, M. *Biochemistry* **1996,** *35*, 10844-10853.

(36) Williams, R. W., Starman, R., Taylor, K. M. P., Gable, K., Beeler, T., Zasloff, M. *Biochemistry* **1990,** *29***,** 4490-4496.

(37) Matsuzaki, K., Harada, M., Funakoshi, S., Fujii, N., Miyajima, K. *Biochim. Biophys. Acta* **1991,** *1063*, 162-170.

(38) B. Bechinger, M. Zasloff, Opella, S. J. *Prot. Sci.* **1993,** *2*, 2077-2084.

(39) Hirsh, D. J., Hammer, J., Maloy, W. L., Blazyk, J., Schaefer, J. *Biochemistry* **1996,** *35*, 12733-12741.

(40) Wang, J., Paszti, Z., Even, M. A., Chen, Z. *J. Phys. Chem. B.* **2004,** *108*, 3625-3632.

(41) Wang, J., Lee, S. H., Chen, Z. *J. Phys. Chem. B* **2008,** *112*, 2218-2290.

(42) Nguyen, K., Le Clair, S. V., Ye, S., Chen, Z. *J. Phys. Chem. B* **submitted,**

(43) Imura, Y., Nishida, M., Matsuzaki, K. *Biochim. Biophys. Acta* **2007,** *1768*, 2578-2585.

(44) Anisimova, E. V., Badyakina, A. O., Vasil'eva, N. V., Nesmeyanova, M. A. *Microbiology* **2005,** *74*, 147-152.

(45) Brasseur, R. *J. Biol. Chem.* **1991,** *266,* 16120-16127.

(46) Tamm, L. K., Tatulian, S. A. *Q. ReV. Biophys.* **1997,** *30*, 365-429.

(47) Axelsen, P. H., Kaufman, B. K., McElhaney, R. N., Lewis, R. N. A. H. *Biophys. J.* **1995,** *69*, 2770-2781.

(48) Axelsen, P. H., Citra, M. J. *Prog. Biophys. Molec. Biol.* **1996,** *66*, 227-253.

(49) Bechinger, B., Kim, Y., Chirlian, L. E., Gesell, J., Neumann, J. M., Montal, M., Tomich, J., Zasloff, M., Opella, S. J. *J. Biomol. NMR* **1991,** *1*, 167-173.

(50) Ye, S., Nguyen, K., Le Clair, S. V., Chen, Z. *J. Struct. Biol.*, **2009**, *in press*

(51) Chen, X., Boughton, A. P., Tesmer, J. J. G., Chen, Z. *J. Am. Chem. Soc.*, **2007**, *129*, 12658-12659.

(52) Chen, X., Wang, J., Kristalyn, C. B., Chen, Z. *Biophys. J.*, **2007**, *93*, 866-875.

(53) Chen, X., Chen, Z. *Biochim. Biophys. Acta*, **2006**, *1758*, 1257-1273 .

(54) Chen, X., Tang, H., Even, M. A., Wang, J., Tew, G. N., Chen, Z. *J. Am. Chem. Soc.*, **2006**, *128*, 2711-2714.

CHAPTER 4

SFG STUDY ON A MEMBRANE ANCHORED PROTEIN: *CYTOCHROME b5*

4.1 Introduction

Membrane proteins constitute approximately one third of all the proteins in nature and are involved in a variety of essential biological processes, ranging from cellular communications to the metabolism of exogenous and endogenous compounds. Due to the hydrophobicity of most integral membrane proteins, a complex network of proteins that assist the folding/unfolding (chaperones) is required to carefully refold and shuttle these proteins to their proper locations in the cell membrane after translation.[1-6] For most membrane proteins residing in the endoplasmic reticulum (ER), their insertion into the ER membrane typically begins with the association of signal recognition particle (SRP) to the hydrophobic sequence of the nascent polypeptide chain.[7] Afterward, the ribosome-nascent-chain-SRP complex binds with the SRP receptor on the ER membrane and is subsequently delivered to the Sec61 protein-conducting channel. However, not all the proteins need the convenience of this co-translational pathway for ER membrane insertion, particularly for those belong to the class of membrane anchored proteins. There are indeed two distinct pathways which deliver the membrane anchored proteins to the ER. Even though the mechanisms of the two pathways are distinctive, these pathways themselves do not need to be mutually exclusive: certain membrane anchored proteins

can follow both mechanisms to ultimately find their ways to the ER.[8] The membrane anchoring tail of membrane anchored proteins mostly lies in the C-terminal and remains inaccessible to SRP or to the ER membrane until the complete polypeptide chain is released from the ribosome. Thus, these proteins must rely on other post-translational mechanism for ER membrane insertion. While some membrane anchored proteins require the assistance of other cytoplasmic proteins for bilayer insertion, others are known to be readily to associate and insert into the plasma membrane.[9-12]

The spontaneous insertion of certain membrane anchored proteins into lipid bilayers is of particular interest in both structural biology and membrane biophysics. In order for membrane anchored proteins to insert into the bilayer, an enormous energy barrier must be overcome such that these proteins must have evolved a particular structural feature that is capable of such an endeavor. While many structural features of membrane anchored proteins are well characterized and studied, their interactions with cell membranes and the mechanisms with which they insert into the membranes continue to remain as an enigma.[11] In this chapter, we examine the interaction and topology of membrane anchored proteins in model membranes (lipid bilayers) using SFG vibrational spectroscopy. The membrane anchored protein used in this study is cytochrome b_5 (*Cyt* b_5). *Cyt* b_5 belongs to a family of heme proteins whose intimate interactions with P450 catalyze a variety of oxidation reactions. *Cyt* b_5 inserts spontaneously into the ER membrane *in vivo* and shown to be inactive when its α-helical anchoring tail is removed. Interestingly, the membrane integration of *Cyt* b_5 is believed to be able to take place with pure phospholipids without the presence of any other protein. The binding of this protein

is shown to be correctly localized at the ER when expressed in cell, which is a strong evidence for an existing protein-free machinery that governs the targeting of *Cyt* b_5.[13-16]

Cyt b_5 is a heme protein which widely presents in animals, plants, fungi and bacteria. *Cyt* b_5 exists in both soluble and membrane bound forms.[17] One of the most important functions of *Cyt* b_5 is to interact with Cytochrome P450, catalyzing a variety of oxidation reactions. There has been extensive research studying the interactions between these two cytochrome proteins. In this dissertation research, we only focus on the binding behavior of *Cyt* b_5 to lipid bilayers. *Cyt* b_5 contains two distinct domains separated by a trypsin-sensitive region.[18] The larger, and catalytic domain that holds the heme group, is comprised of approximately 90 amino acid residues. This domain is usually called the water-soluble domain, whose function is to transfer electron to a variety of donors and acceptors within the ER. The three-dimensional crystal structure of this heme binding domain has been characterized by X-ray crystallographic and NMR studies.[19, 20] The other domain (the so called "membrane anchoring domain" or "tail") of *Cyt* b_5 is a smaller hydrophobic domain of around 40 residues that anchors the globular domain to the ER membrane. This domain contains an α-helical membrane anchoring tail[21] and a linker connecting this part and the water soluble domain. The linker region is a 15 residues long region whose specific sequence was found to be unimportant for its functions. However, this linker has to be of a sufficient length (7-8 residues) to guarantee the effective interaction between the protein and the Cytochrome P450.[22] In the following discussions, we will also call the α-helical membrane insertion part as "membrane anchoring tail" as well. It has been found that the post-translational membrane association of *Cyt* b_5 is ATP independent because no ATP was required for this particular

process. This ATP independent membrane association of *Cyt* b_5 suggests that either the membrane insertion of *Cyt* b_5 does not need to be assisted by cytosolic factors or that its insertion mechanism is different from those that are synaptobrevin-mediated.[23, 24]

The interaction of *Cyt* b_5 with lipid membranes has been an area of constant debate over the years. From fluorescence quenching experiments and trypsin digestion assays, it was proposed that the membrane anchoring tail could adopt two different conformations: a hairpin helix that only spans half of the bilayer[25, 26] or a single α-helix that spans the whole bilayer.[26-28] The hairpin helix conformation is believed to be loosely associated with the bilayer and was observed to undergo exchange between liposomes in solution. Interestingly, when *Cyt* b_5 is reconstituted in lipid vesicles through detergent dialysis, no exchange of *Cyt* b_5 between liposomes was observed, which indicates the helix may have spanned the whole bilayer and the protein is tightly anchored to the membrane. This brings into focus the importance of the membrane anchor conformation when it interacts with the bilayer and its role in facilitating membrane insertion. Importantly, the hairpin helix conformation seems energetically unfavorable; however, this conformation can be a transient or intermediate state that when sufficient energy is provided, it is able to convert into its membrane spanning form.[29-31] In order to better understand this phenomenon, the *in vitro* binding of *Cyt* b_5 to lipid bilayers will be rigorously investigated by SFG.

As already shown in the previous chapters, SFG is an extremely sensitive optical technique and is capable of providing detailed information on the interactions at the membrane interface. More importantly, unlike other bulk solution techniques, SFG only detects signals from molecules that bind to the membrane surface, allowing for the

monitoring of both structural and chemical changes that occur during the course of binding in real time. Thus, with SFG, it is possible to probe, in real time, the interactions between *Cyt b_5* and lipid bilayers with unprecedented sensitivity and time resolution.

4.2 Materials and experimental procedures

^{15}N labeled full length and mutant versions rabbit *Cyt b5* used in this study was expressed in *E.coli* C41 cells using the pLW01 plasmid[32] with the purity of >90%.[33] Deuterated dimyristoylphosphatidylcholine (dDMPC), dilauroylphosphatidylcholine (DLPC) and dipalmitoylphosphatidylcholine *(*DPPC*)* were purchased from Avanti Polar Lipids (Alabaster, AL) and used without any further purification. HEPES buffer (10 mM, pH= 7.3) was used in making the protein solutions and stabilizing the pH of the reaction media. The CaF_2 prisms (purchased from Altos, Trabuco Canyon, CA) were cleaned in toluene, soap, methanol and then rinsed thoroughly with DI water before being treated in a glow discharge plasma chamber for 4 minutes immediately before the deposition of lipid monolayers. We used the Langmuir-Blodgett and Langmuir-Schaefer (LB/LS) method to deposit the proximal and the distal leaflets onto the prisms, respectively.[34, 35] The lipid bilayer deposition process is the same as that used in chapter 3, which has been described in many of our earlier publications and will not be reiterated here.[36-38]

The details of our SFG experiments are the same as those in chapter 3 and will not be repeated here. An experimental geometry similar to the total reflection geometry used in ref. 39 was used but with different input and output beam angles. The angles of the visible and signal inside the substrate (68°) were close to the critical angle (69°) for total internal reflection at the interface of CaF_2 (with a layer of lipid bilayer) and water (or

dilute protein/peptide solution), which allowed for the collection of SFG vibrational spectra by the near total reflection geometry.

The temperature controlled experiment was done using a hot plate and a thermal couple sensing the temperature of the reaction medium. A micro stir bar was used to gently stir the solution at 60 rpm to regulate the heat within the medium.

4.3 Orientation of full length *Cyt b_5* in a dDMPC/dDMPC lipid bilayer

As mentioned above, a full length *Cyt b_5* molecule consists of a membrane anchoring tail, a soluble domain hosting the heme group,[40] and a linker which links the above two domains. The linker is unstructured, hence is able to provide a significant amount of rotational freedom as well as random movement to the soluble domain. The membrane anchoring tail is simply a 20-22 residue α- helix, whose membrane orientation can be determined using SFG.[37, 41, 42] However, in the case of *Cyt b_5*, there are also other helical structures reside in the protein's water soluble domain that might contribute observable SFG signal. Fortunately, by using symmetry arguments, we showed that no substantial SFG signal is generated from the α-helical structures in the soluble domain due to the SFG signal cancellation arisen from the symmetric arrangement of these helical structures (the four major helices holding the heme group are positioned in opposite directions). This was verified by using NLOPredict, a visualization program that was developed by a collaboration between the laboratory of Garth Simpson Group at Purdue University and the Scientific Data Analysis Lab, a Pervasive Technology Lab of Indiana University, to assist the interpretation of second order nonlinear optical processes.[43, 44] The symmetric vibrational mode of the α-helix, the most effective vibrational mode that shows the symmetry property of an α-helical containing structure,

was calculated for both the water soluble and membrane anchoring tail of *Cyt* b_5 using NLOPredict. The deduced SFG susceptibility of the water soluble domain (when positioned in highly probable manners) is at least one order of magnitude smaller compared to the smallest SFG susceptibility of the membrane anchor tail (Figures 4.1 and 4.2). Therefore, we believe that when determining the orientation of the membrane anchor α-helix of *Cyt* b_5 using SFG, the neglect of the SFG signal contribution from the α-helical structures in the soluble domain will only lead to, at most, several degrees (should be less than five degrees) of error in the membrane anchoring tail's tilt angle. It is this property (the cancellation of the α-helical structures' SFG susceptibilities in the soluble domain) of this particular protein that makes the "direct" SFG orientation analysis of the α-helical anchor group feasibly reliable.

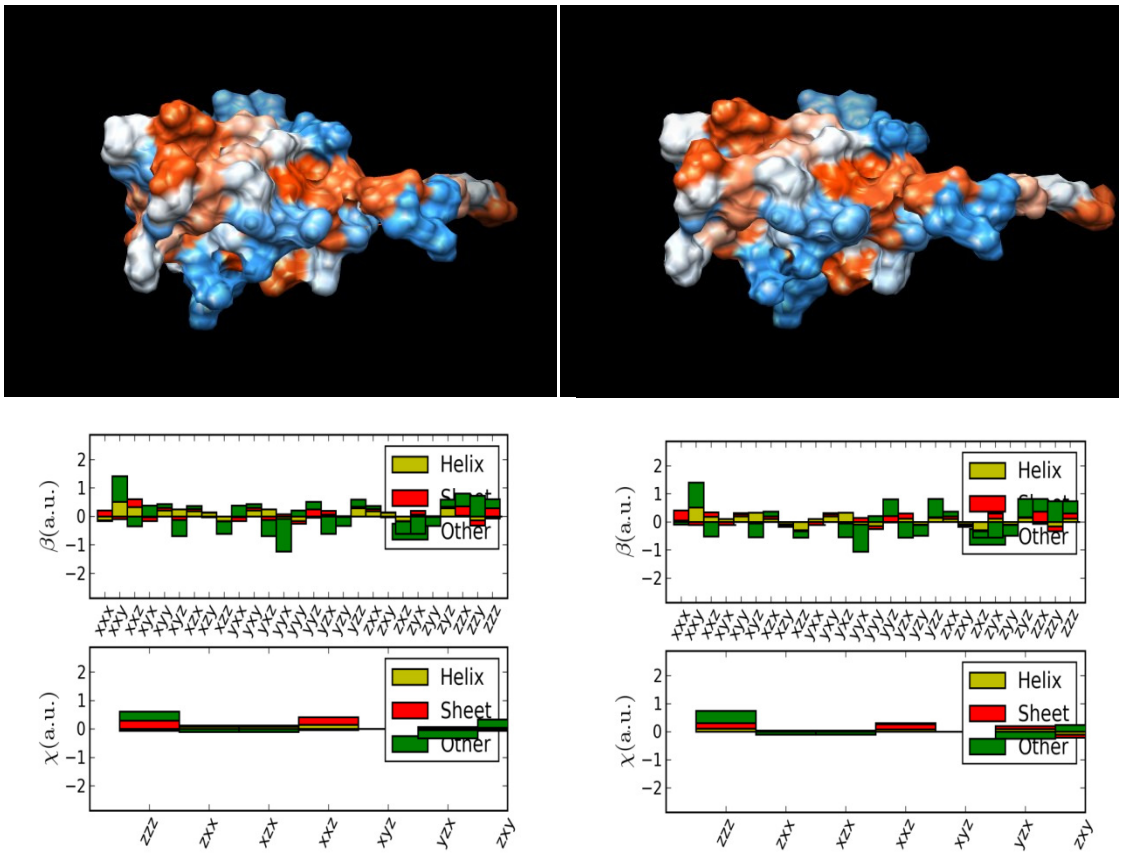

Figure 4.1: Macroscopic $\chi^{(2)}$ quantities of *Cyt b5* water soluble domain calculated by NLOpredict.
Left: when the anchoring tail is likely to adopt the transmembrane orientation in the lipid bilayer.
Right: when the anchoring tail is likely to adopt the horizontal orientation on top of the lipid bilayer.

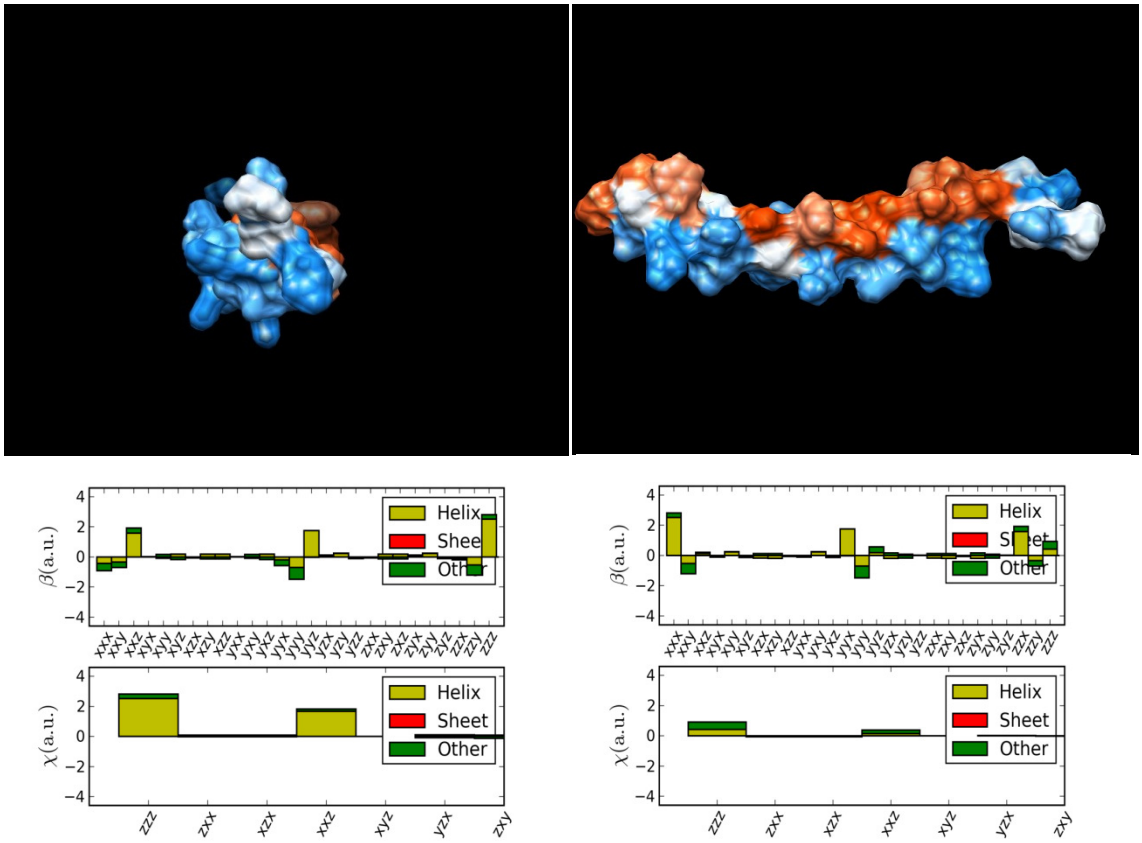

Figure 4.2: Macroscopic $\chi^{(2)}$ quantities of the magainin 2, which has the similar length as the *Cyt b5*'s anchoring tail. Calculated by NLOpredict.
Left: when the anchoring tail adopts the transmembrane orientation in the lipid bilayer.
Right: when the anchoring tail adopts the horizontal orientation on top of the lipid bilayer.

Since the *Cyt* b_5 soluble domain does not contribute substantially to the observable SFG amide I signal from α-helical structures, the orientation analysis of the anchoring tail can be performed using the orientation analysis on a single α-helix in the

lipid bilayer. The methodology to determine a single α-helical structure orientation using the SFG amide I signals with different polarization combinations has been described in great detail in chapter 2 and will be used in this study.

SFG spectra were collected from full length *Cyt b_5* in a dDMPC/dDMPC bilayer using ssp and ppp polarizations of the input and output laser beams (Figure 4.3). The SFG spectra were dominated by a peak centered at approximately 1655 cm^{-1}, contributed by the α-helical anchoring tail. The orientation of the α-helical anchoring tail can be calculated using the fitted ppp and ssp signal strength ratio of the 1655 cm^{-1} peak and the relationship between this ratio and the orientation of a 22 amino acid long α-helix (Figure 4.4). It was found by SFG experiments that the membrane anchoring tail of the full length *Cyt b_5* inserted into the dDMPC/dDMPC bilayer at a tilt angle of 14 degrees in relative to the bilayer surface normal. This tilt angle agrees excellently well with the NMR results ($15^o \pm 3^o$) obtained by Dürr and colleagues using solid state NMR.[45]

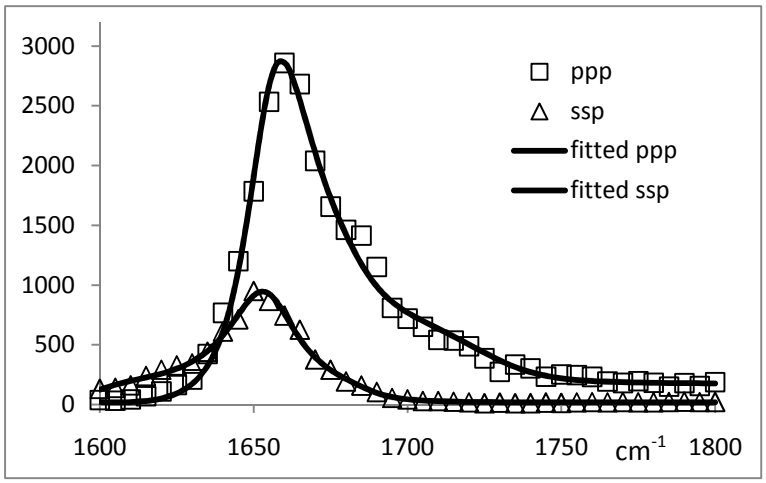

Figure 4.3: ssp and ppp polarized SFG amide I band of *Cyt b5* in dDMPC/dDMPC lipid bilayer.

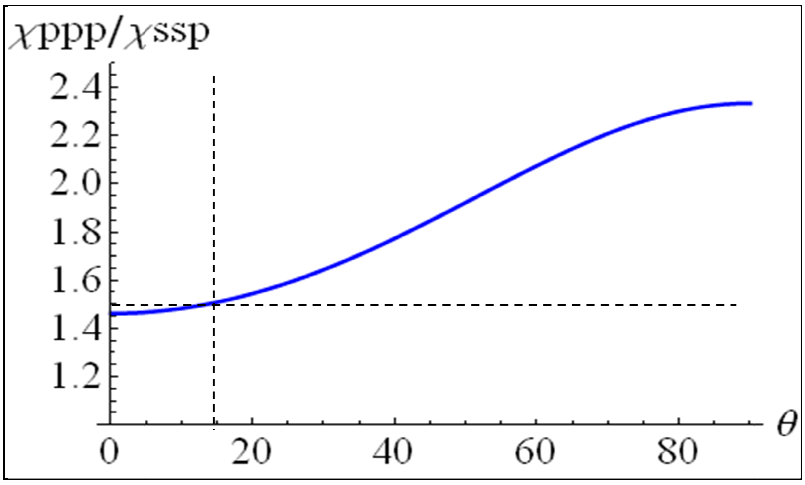

Figure 4.4: The relationship between χ_{ppp}/χ_{ssp} ratio of the α-helix and the helical tilt angle.

4.4 Orientation of Mutant-*Cyt b_5* (*Mcyt b_5*) in the dDMPC/dDMPC lipid bilayer

In addition to the full length *Cyt b_5* studied above, we also investigated a mutant *Cyt b_5* (*MCyt b_5*) in which the linker connecting the water soluble domain and the membrane anchoring tail was deleted. This study investigates the exact influences of the linker region to how *Cyt b5* interacts with the cell membrane. Experiments were carried out to collect SFG spectra from the *MCyt b_5* protein in a dDMPC/dDMPC bilayer. Surprisingly, the SFG amide I signal from the *MCyt b_5* while interacting with a dDMPC/dDMPC bilayer was much weaker than that we obtained from the full length *MCyt b_5* presented above (Figures 4.3 and 4.6).

The lower SFG amide I signal of *MCyt b_5* suggests an overall more horizontal orientation of the *MCyt b_5*'s membrane anchoring tail at the interface in comparison to the full length *Cyt b_5* because when an α-helical structure aligns more towards the surface normal, we expect stronger SFG signal generated (Figure 4.5). We performed a quick

orientation analysis from the difference in SFG amide I intensities (in ppp polarization combination) at 1655 cm^{-1} collected from the full length *Cyt* b_5 and the *MCyt* b_5. This quick analysis does not use the SFG ssp polarized signal; therefore, it is independent to the approach that uses both ppp and ssp signals. Because the experimental conditions were identical in the full length *Cyt b5* and *Mcyt b5* experiments, the intensity difference observed must have caused by the difference in orientation of the two protein molecules at the membranes, not by the difference in the protein coverage.

The SFG signal collected with the ppp polarization combinations from the full length *Cyt* b_5 was about 4 times higher than the ppp signal detected from the *MCyt* b_5 (Figures 4.3 and 4.6). The fitting results indicate that the SFG susceptibility component χ_{zzz} generated by the full length *Cyt* b_5 associated with a dDMPC/dDMPC bilayer is 2.24 times higher than that of the dDMPC/dDMPC bound *MCyt* b_5. Assuming the protein coverage in both experiments on *Cyt* b_5 and *MCyt* b_5 to be similar (which is reasonable due to the absence of the electrostatic driving force), with the previously determined tilt angle of the full length *Cyt* b_5*'* anchoring-tail in the dDMPC/dDMPC lipid bilayer, we are able to deduce the tilt angle of the *MCyt* b_5*'* anchoring-tail in the bilayer (Figure 4.5). This method results in a tilt angle of about 70 degrees of the *MCyt* b_5's anchoring-tail versus the surface normal in the dDMPC/dDMPC bilayer.

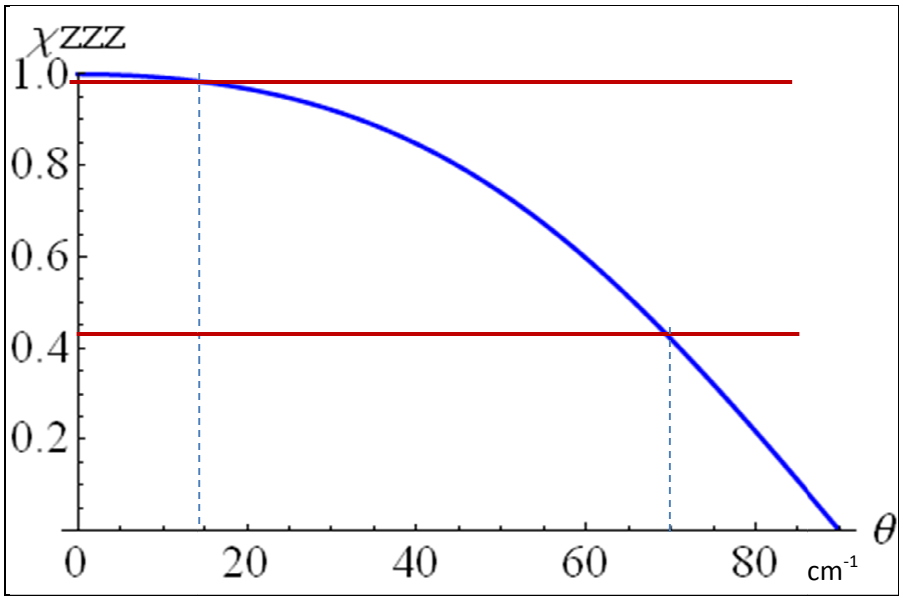

Figure 4.5: The relationship between χ_{zzz} of the α-helix and the helical tilt angle.

To further confirm the orientation of the α-helical membrane anchoring tail of the *MCyt b_5'* anchoring-tail in the dDMPC/dDMPC lipid bilayer, a more vigorous approach as presented in chapter 2 was employed, which uses the SFG amide I ppp and ssp signal ratio (this is also the same method to deduce the full length *Cyt b_5* orientation above). Using this approach, it was found that *MCyt b_5* tilts with an angle of 73 degrees, which correlates well to the 70 degrees deduced above using an independent approach based on the absolute intensity. The good agreement in the two independent approaches confirms the negligibility of the SFG amide I signal contribution from the α-helical structures reside in water soluble domain.

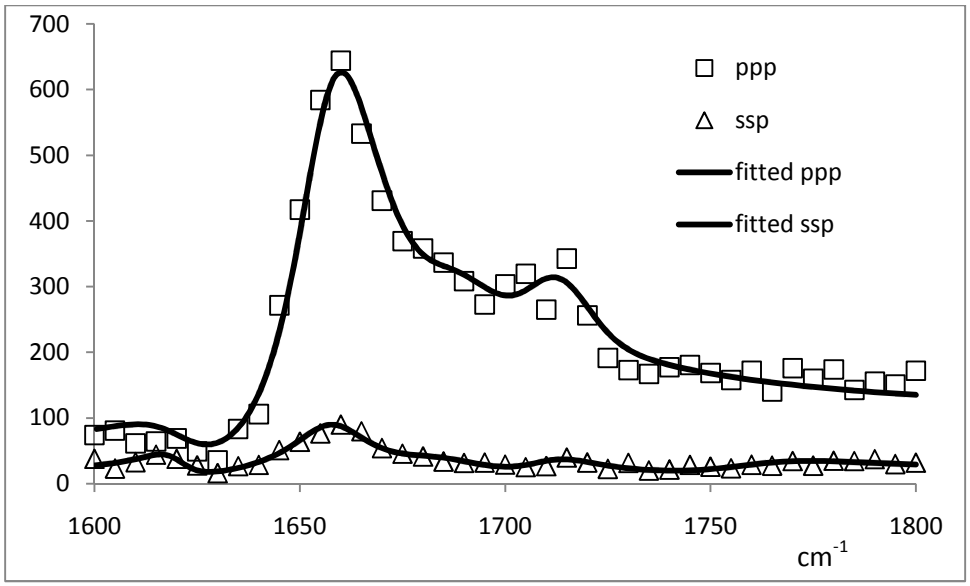

Figure 4.6: ssp and ppp polarized SFG amide I band of Mcyt b5 in dDMPC/dDMPC lipid bilayer.

4.5 Time dependent studies on the interactions of the full length *Cyt b_5* and the *MCyt b_5* with the dDMPC/dDMPC lipid bilayer

Time dependent studies on the interactions of the full length *Cyt b_5* and the *MCyt b_5* with the dDMPC/dDMPC bilayer also exhibit distinct differences. Although the kinetics of the protein adsorption or binding is difficult to interpret accurately by SFG signal intensity alone due to the dependency of the SFG signal on both the protein coverage and orientation, we can still observe a more dynamic behavior of the full length *Cyt b_5* while interacting with lipid bilayers. For the *MCyt b_5* adsorption onto the dDMPC/dDMPC lipid bilayer, the SFG signal reached a plateau within one hour, indicating that it took about one hour for *MCyt b_5* to reach an equilibrium state while interacting with the bilayer. In the case of the full length *Cyt b_5*, it took the protein about 1 hour and 30 minutes to fully interact with the dDMPC/dDMPC lipid bilayer (both

experiments were carried out with the same protein concentration) (Figure 4.7). This suggests that the full length *Cyt* b_5 undergoes either a more complex interaction mechanism or one that just takes a longer time than that of the *Mcyt b5*.

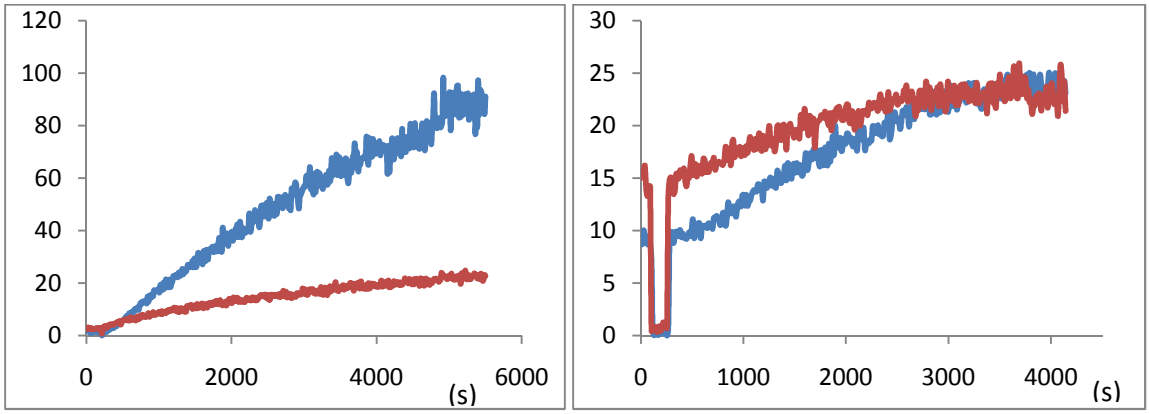

Figure 4.7: ppp polarized time dependent plots of the peak at 1655 cm^{-1} (α-helical peak center, blue) and 1725 cm^{-1} (carbonyl C=O stretch of the lipids, red) of *Cyt b5* (left) and *MCyt b5* (right) in dDMPC/dDMPC lipid bilayers.

4.6 Observing the dDMPC/dDMPC lipid bilayer signal changes caused by the full length *Cyt* b_5 and the *MCyt* b_5

We studied the behavior of the dDMPC/dDMPC lipid bilayer after its interaction with *Cyt* b_5 by observing the SFG signal in the C-D stretch frequency regime (2000 cm^{-1} to 2300 cm^{-1}). The lipid terminal CD_3 group has a symmetric stretching vibrational mode at around 2070 cm^{-1}, a Fermi resonance peak at around 2145 cm^{-1}, and an asymmetric stretching peak at around 2160 cm^{-1}.[46] According to the C_{3v} point group, a relationship of the SFG susceptibility ratio of the asymmetric/symmetric mode and the interfacial tilt angle of the CD_3 group was then established (Figure 4.8). From this figure, one can see that the observed asymmetric peak grows as the tilt angle (versus the surface normal) of

the CD_3 group increases. When the CD_3 terminal group aligns with the surface normal, the asymmetric peak should be relatively small in the ssp SFG spectrum. SFG spectra in ssp polarization combination were collected from the dDMPC/dDMPC lipid bilayer in the C-D stretching frequency region after the bilayer interact with the full length *Cyt* b_5 and *MCyt* b_5 (Figure 4.9). This figure indicates that the SFG spectra from the dDMPC/dDMPC bilayer after interacting with *Cyt* b_5 and *MCyt* b_5 are substantially different, showing different interaction mechanisms must have happened in the two cases.

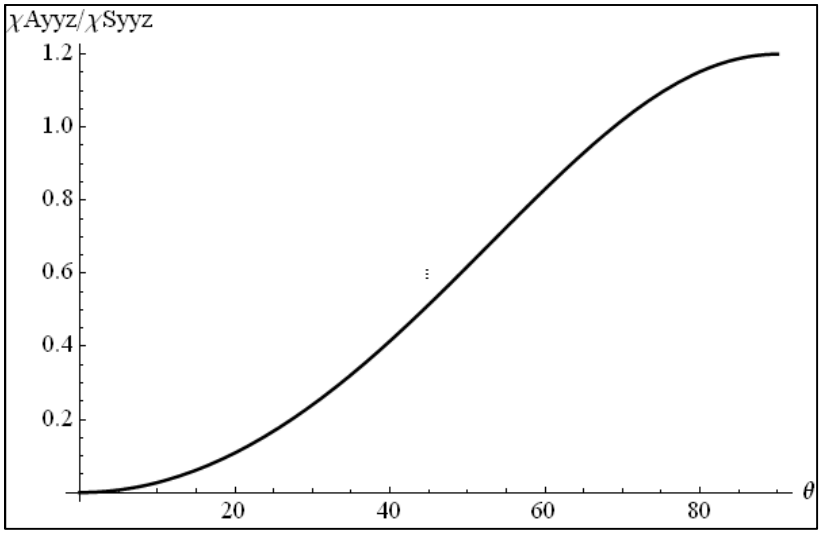

Figure 4.8: the relationship between χ_{Ayyz}/χ_{Syyz} of CD_3 group.

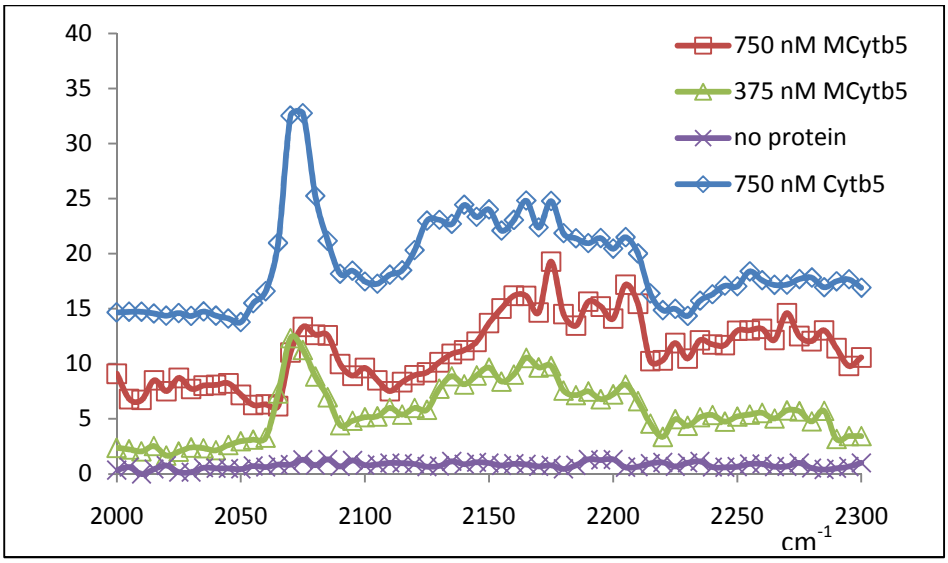

Figure 4.9: ssp SFG spectra of the dDMPC/dDMPC lipid bilayers (in CD regime) upon their interaction with *Cyt b5* (375 nM) and *MCyt b5* (375 and 750 nM).

By comparing the intensity ratio between the asymmetric C-D stretching peak at 2160 cm^{-1} and the symmetric C-D stretching signal at 2070 cm^{-1} of the CD_3 groups, we observed that the CD_3 terminal groups of the dDMPC/dDMPC bilayer after interacting with the full length *Cyt* b_5 have an average smaller tilt angle than after interacting with *MCyt* b_5 (Figure 4.9). This must be due to the fact that *MCyt* b_5*'* anchoring tails tilt more towards the bilayer surface when interacting with the bilayer, causing the membrane thinning effect, thus change the lipid chain orientation significantly. In the case of the full length *Cyt* b_5, the protein's anchoring tails adopt a trans-membrane orientation, causing less change of the lipid chain orientation. Besides, the Cyt b5 anchoring tail's transmembrane orientation allows the *Cyt b5*'s water soluble domain to keep a crucial distance of 15 to 20 Å from the membrane interfacial region for the *Cyt b5-Cyt P450* complex formation.[47] Being detached from the lipid bilayer interface, the full length *Cyt b5*'s water soluble domain would have minimal lipid thinning effect on the bilayer, which

was observed in our experiments. We believe that the results obtained from the SFG studies on the lipid bilayer in the C-D stretching frequency region support our SFG orientation analysis of the protein presented above based on the SFG spectra collected in the amide I frequency region.

4.7 Effects of the linker length on the *MCyt b_5* – lipid bilayer interactions

Our above research demonstrated the crucial role which the linker plays in the interaction between *Cyt b_5* and the lipid bilayer. It was found that for the interaction between *Cyt b_5* and Cyt P450 to occur, the *Cyt b_5* linker length needs to be at least 7-8 amino acid residues long. It was also observed that a longer linker would not substantially affect the interaction between the two cytochomes.[48] Therefore, we chose to study *Cyt b5* with linker of eight amino acids or shorter. In this chapter, we define the full length *Cyt b5* to be the protein with an eight residues long linker. We believe that the linker facilitates the insertion of the *Cyt b_5*'s anchor tail into the lipid bilayer. With the help of a flexible linker, *Cyt b_5* can be inserted into the dDMPC/dDMPC bilayer effectively. When the linker was deleted from the protein, the membrane anchoring tail of *MCyt b_5* more or less laid down on the lipid bilayer surface, undergoing no insertion into the bilayer. In order to systematically quantify the linker's effect, we studied different versions of mutant *Cyt b_5* with various linker lengths by deleting different numbers of amino acid residues in the linker. In addition to the full length *Cyt b_5* and *MCyt b_5* studied above which have 8 and 0 amino acid residues in the linker, mutant *Cyt b_5* molecules with linkers of 2 and 6 residues long were also studied. Identical SFG experiments were performed to determine the orientations of these two mutant *Cyt b_5*'s membrane anchoring tails in the dDMPC/dDMPC bilayer. The orientations of *Cyt b_5*'s membrane

anchoring tails with different linker lengths in the dDMPC/dDMPC bilayer are summarized in Table 4.1. It was shown clearly in this table that the linker length affects the orientation of the *Cyt* b_5's membrane anchoring tails in the bilayers and thus the orientation of *Cyt* b_5 molecules. When the linker is short, e.g., with 0 or 2 residues, mutant *Cyt* b_5's anchoring tails more or less lie down on the bilayer surface (with tilt angle to be around 70 degrees versus the bilayer normal). When the linker's length reaches 6 residues, the mutant *Cyt* b_5's membrane anchoring tail tilts in the bilayer at an angle of 50 degrees. For the full length *Cyt* b_5 with 8 amino acids, *Cyt* b_5 more or less spans the entire lipid bilayer, with a tilt angle of about 14 degrees.

linker's length	ppp/ssp ratio	tilt angle
0	2.24	73^o
2	2.21	70^o
6	1.92	50^o
8	1.50	14^o

Table 4.1: The helical tilt angles of the anchoring tails corresponding to their linker lengths.

This study demonstrates that it is not only the presence of the linker is important for the membrane insertion of the anchoring tail of *Cyt* b_5 molecules, but also its length plays decisive role in the membrane anchoring. Previous studies in the literature on the interactions between *Cyt* b_5 and Cyt P450 suggested that the *Cyt* b_5 linker length needs to be at least 7-8 amino acid residues long for the protein to function.[48] We observed this same critical linker length for the interaction of *Cyt* b_5 and lipid bilayers "directly" using SFG.

4.8 Temperature dependent study on the insertion of *MCyt b_5's* anchoring tail into the dDMPC/dDMPC lipid bilayer

Our study presented above demonstrated the difference in the bilayer binding of the full length *Cyt b_5* and the *MCyt b_5*: The full length *Cyt b_5*'s membrane anchoring tail inserts readily into a dDMPC/dDMPC lipid bilayer at room temperature; whilst the *MCyt b_5*'s anchoring tail lies more or less horizontally on the lipid bilayer surface. An experiment that is aimed for *MCyt b_5* to overcome the energy barrier of the insertion of the membrane anchoring tail into the hydrophobic region of the lipid bilayer was, therefore, designed and carried out. In this experiment, the temperature of the reaction medium (or the subphase in contact with the bilayer) was increased in a step-wise manner while the orientation of the membrane anchoring tail of *MCyt b_5* in the lipid bilayer was monitored at different temperatures using SFG. We believe that the thermal energy provided in the experiment would increase the fluidity of the lipid bilayer as well as the mobility of the *MCyt b_5* molecules; hence, *MCyt b_5* molecules are able to overcome the energy barrier of the membrane insertion.

While elevating the temperature from 25 ^{o}C to 40 ^{o}C, we observed a dramatic increase of the SFG amide I signal collected in the ppp polarization combination (Figure 4.10). This observed SFG signal intensity increase was not caused by more proteins adsorbed onto the bilayer at a higher temperature, because the *MCyt b_5* solution in contact with the bilayer was replaced by HEPES (pH=7.3) at room temperature after the interaction initially reached equilibrium. Therefore, the protein coverage at higher temperatures could not be larger than that at room temperature. From the orientation analysis of the helical structure using SFG amide I band, the SFG signal intensity

increases when the tilt angle θ decreases (Figure 4.5). In other words, when the α-helical membrane anchoring tail inserts into the lipid bilayer (changes from a more horizontal orientation to a more vertical orientation), we should expect stronger SFG signal generated from this α- helical structure. We believe this to be strong evidence that the adsorbed *MCyt* b_5 molecules went through a reorientation process in the bilayer at higher temperatures.

When the temperature is even higher, besides the protein's reorientation process, an induced change in the membrane protein coverage may have also occurred. This can explain the SFG signal intensity drop when the temperature is changed from 40 ^{o}C to 45 ^{o}C. As mentioned above, the proteins in the subphase were removed. When the temperature is high enough (e.g., >40 ^{o}C), membrane anchored *MCyt* b_5 molecules might become more mobile and thus may be able to leave the more fluidic lipid bilayer to the subphase. This would lead to a loss in SFG signal intensity (Figure 4.10).

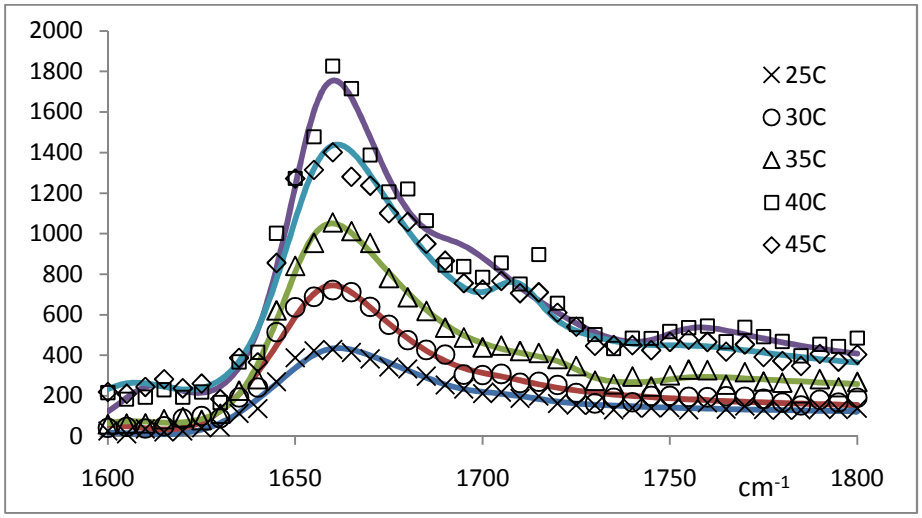

Figure 4.10: SFG amide I band in ppp polarization combination of Mcyt b5 in dDMPC/dDMPC lipid bilayer at different temperatures.

To quantify the orientation of the α-helical membrane anchoring tail of *MCyt b_5* in the lipid bilayer at different temperatures, SFG spectra were collected from *MCyt b_5* in the amide I frequency region using both ssp and ppp polarization combinations. Using the signal strength ratio of the ppp and ssp spectra, as discussed in detail in chapter 2, the tilt angle θ of the membrane anchoring tail was determined at five different temperatures: 25 ^{o}C, 30 ^{o}C, 35 ^{o}C, 40 ^{o}C and 45 ^{o}C, as shown in Figure 4.11 and Table 4.2. It was found that the membrane anchoring tail of *MCyt b_5* indeed can insert into the hydrophobic region of the lipid bilayer when the temperature is higher than 30 ^{o}C, even though at the room temperature it more or less lies down on the bilayer surface (Figure 4.11).

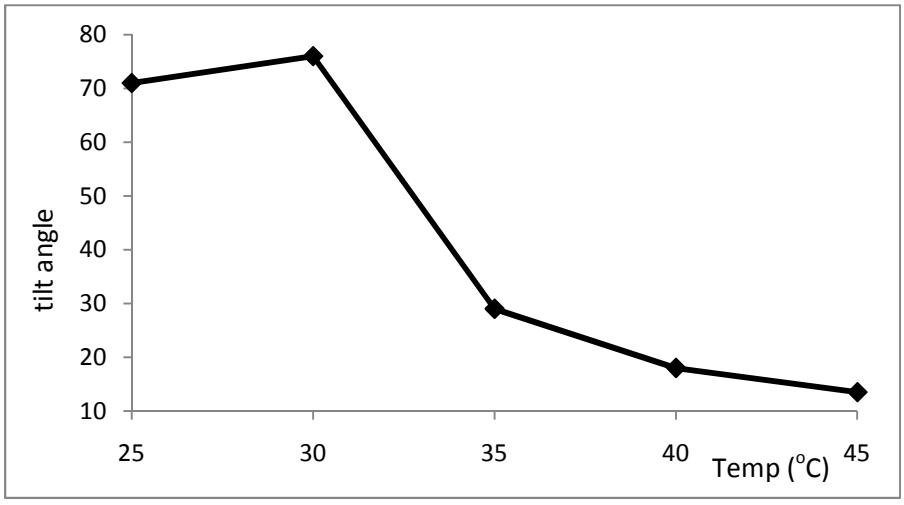

Figure 4.11: The helical tilt angle of the anchoring tail at each temperature.

	cytb5			Mctyb5	
	ppp/ssp ratio	tilt angle		ppp/ssp ratio	tilt angle
dDMPC/dDMPC 25C	1.50	14		2.24	73
dDMPC/dDMPC 30C	N/A	N/A		2.27	76
dDMPC/dDMPC 35C	N/A	N/A		1.63	29

dDMPC/dDMPC 40C	N/A	N/A		1.53	18
dDMPC/dDMPC 45C	N/A	N/A		1.50	14
DLPC/DLPC 30C	1.60	26		2.26	75
DLPC/DLPC 45C	N/A	N/A		1.60	26
DPPC/DPPC 30C	N/A	N/A		N/A	N/A
DPPC/DPPC 45C	1.48	10		N/A	N/A

Table 4.2: Temperature controlled SFG studies on the interaction of *Cyt b5* and *Mcyt b5* with lipid bilayers.

4.9 Studies on the interactions between *Cyt b_5*/*MCyt b_5* and lipid bilayers composed of different lipids of various chain lengths.

The results presented in the previous section showed that raising the temperature facilitates the insertion of *MCyt b_5* into the lipid bilayer. As we discussed, one of the possible reasons responsible for this observation is that the lipids are more fluidic at a higher temperature. To investigate the effect of the lipid fluidity on the interactions between the lipid bilayer and *Cyt b_5* or *MCyt b_5*, in addition to the dDMPC bilayer, we included lipids with different lengths in the study, including dilauroylphosphatidylcholine (DLPC) and dipalmitoylphosphatidylcholine *(*DPPC*)* lipid bilayers. DLPC, DMPC and DPPC have different acyl chain lengths of 12, 14 and 16 carbons. Their fluid to gel phase transition temperatures are 5^{o}C, 23^{o}C and 41^{o}C, respectively. Since these three types of lipid bilayers have different thicknesses, this study should also shed light on the effect of

lipid bilayer thicknesses (or hydrophobic thicknesses) on the orientation of *Cyt b_5*/*MCyt b_5*'s membrane anchoring tails.

The orientation of *MCyt b_5* in the DLPC/DLPC lipid bilayer was investigated by collecting SFG spectra with ppp and ssp polarization combinations. It was found that at 30°C, *MCyt b_5's* anchoring tails orient similarly in both DLPC/DLPC and DMPC/DMPC lipid bilayer. The tilt angle was determined to be around 75 degrees relative to the lipid bilayer normal. When the temperature of the interaction medium was raised to 45°C, we observed the insertion of the *MCyt b_5* membrane anchoring tail into the hydrophobic region of the lipid bilayer with a tilt angle of around 25 degrees. The interaction between *MCyt b_5* and the DLPC/DLPC lipid bilayer is similar to that between *MCyt b_5* and the DMPC/DMPC lipid bilayer, except that the tilt angles of the *MCyt b_5* anchor in the two bilayers at 45°C are slightly different, which will be discussed further below.

Full length *Cyt b_5* interacts with DLPC/DLPC and DMPC/DMPC lipid bilayers in the similar manner. The *Cyt b_5* α-helical membrane anchoring tail can readily insert into the hydrophobic region of the DLPC/DLPC lipid bilayer at room temperature, as observed when *Cyt b_5* interacts with the dDMPC/dDMPC lipid bilayer discussed above. The tilt angle of the *Cyt b_5* membrane anchor was deduced to be around 25 degrees versus the bilayer normal using the ppp and ssp SFG signal strength ratio.

SFG spectra were also collected from *Cyt b_5* and *MCyt b_5* in the DPPC/DPPC bilayer using different polarization combinations. When the DPPC/DPPC bilayer is used, only very weak amide I SFG signal can be obtained from both *Cyt b_5* and *MCyt b_5* upon their interactions with the lipid bilayer. For *MCyt b_5*, almost no discernible SFG amide I signal was observed in the DPPC/DPPC bilayer regardless of the temperature (between

room temperature and 45°C). This is either because the *MCyt b_5* membrane anchoring tail lies more or less flat on the surface due the stiffness of DPPC/DPPC bilayer which prohibits the insertion of the membrane anchoring tail, or because the *MCyt b_5* coverage on the lipid bilayer is just too low.

Our research above indicates that it is easier for the full length *Cyt b_5* to insert into a lipid bilayer compared to *MCyt b_5*. Even so, the full length *Cyt b_5* could not interact strongly with the DPPC/DPPC lipid bilayer, yielding an extremely weak SFG signal at most temperatures. At 45°C (right above the transition temperature of DPPC), however, relatively stronger SFG signal was collected from the *Cyt b_5* in the DPPC/DPPC bilayer. However, the intensity was still not comparable to what we obtained from the experiments on *Cyt b_5* in the dDMPC/dDMPC and DLPC/DLPC lipid bilayers. At this temperature, it was deduced that the anchoring tail of *Cyt b_5* can insert into the hydrophobic region of the DPPC/DPPC lipid bilayer with a tilt angle of around 10 degrees, which is similar to the tilt angle of this helical structure in a dDMPC/dDMPC lipid bilayer at room temperature (Table 4.2). Since the orientations of the *Cyt b_5*'s anchoring tails are similar, the lower SFG signal obtained here must be due to the lower protein membrane coverage.

Different tilt angles of the membrane anchoring tails of *Cyt b_5*5 or *MCyt b_5* were experimentally observed in different bilayers of lipids with varying lengths. It was found that the anchoring tail spans the entire hydrophobic region of the ER,[30] therefore this hydrophobic thickness of the ER bilayer can have an effect on the tilt angle of this transmembrane helical anchoring tail. When the lipids have different lengths, the hydrophobic thicknesses of the lipid bilayers should vary. The experiments on different

lipid bilayers should reveal the correlation between the membrane anchoring tail tilt angle and the hydrophobic thicknesses of the lipid bilayers. The hydrophobic thickness is directly proportional to the low dielectric region, which accommodates the protein's membrane anchoring tail. For the three lipid bilayers studied here, the low dielectric region of the DLPC/DLPC lipid bilayer is the thinnest, and that of the DPPC/DPPC lipid bilayer is the thickest.

The length of the α-helical *Cyt* b_5 membrane anchoring tail can be calculated using the structural properties of an α-helix. The α-helical anchor is composed of 22 peptide units. According to the α-helical structure, each of the peptide unit is 1.5 Å long along the principal axis of the α-helix, yielding the total length of the anchor tail to be about 33 Å. Assuming that the membrane anchoring tail inserts completely into the DLPC/DLPC lipid bilayer with a low dielectric region of 30 Å,[49, 50] by a simple geometry calculation, the tilt angle of the membrane anchoring tail is deduced to be between 25 and 30 degrees, depending on whether we take into account the last amino acid residue that does not belong to the helix. This straight forward calculation surprisingly produces a result that matches the tilt angle solved by SFG. When *Cyt* b_5 and *MCyt* b_5 insert into the DLPC/DLPC bilayer at 30 ^{o}C and 45 ^{o}C respectively, the orientations in both cases were determined to be 26 degrees.

According to the orientation of *Cyt* b_5 and *MCyt* b_5 inserted into the DMPC/DMPC bilayer, given the membrane anchoring tail's tilt angle, this simple calculation can be used to deduce the thickness of the low dielectric region of the DMPC/DMPC bilayer. It was calculated to be between 32 and 33.5 Å, in excellent agreement with the simulated result obtained by Gambu and coworkers.[51] However, the

calculation breaks down when applied to the DPPC/DPPC lipid bilayer because the thickness of the low dielectric region of the dDMPC/dDMPC lipid bilayer already approaches the length of the *Cyt* b_5's helical membrane anchoring tail. Without any constrains arisen from the thickness of the membrane, the helical anchor structure now can insert into the DPPC/DPPC lipid bilayer with a more or less vertical orientation, as observed when *Cyt* b_5 inserted into the DPPC/DPPC bilayer at 45°C.

4.10 Conclusion

SFG has been successfully applied to study the interactions between the α-helical membrane anchoring tail of *Cyt* b_5 and various lipid bilayers. The orientations of the anchoring tails of full length *Cyt* b_5 and various versions of mutant *Cyt* b_5 interacting with lipid bilayers were quantitatively determined. It was found that the linker connecting the soluble domain and the membrane anchoring tail in *Cyt* b_5 plays an important role in the insertion of the *Cyt* b_5 membrane anchoring tail into the lipid bilayer. The full length *Cyt* b_5 was found to be able to anchor to the DLPC/DLPC and DMPC/DMPC bilayers. Without the linker, the membrane anchoring tail of *MCyt* b_5 is unable to insert into the lipid bilayer hydrophobic region. Even with the presence of a shorter linker, the protein's anchoring tail cannot adopt a transmembrane orientation while associating with the lipid bilayers. The SFG results also indicated that thermal energy assists the insertion of the protein's anchoring tail into the lipid bilayers. We believe that this SFG study on interactions between *Cyt* b_5 and lipid bilayers is important not only in understanding the binding mechanism of *Cyt* b_5 to cell membranes, but also in understanding the pathway that membrane anchored proteins follow in finding their ways to the ER. This study

opens up a possibility of applying SFG to a more thorough investigation of the mechanisms which tail anchored proteins may adopt at work.

4.11 References

(1) Richardson, R.T., Alekseev, O. M., Grossman, G., Widgren, E. E., Thresher, R.;Wagner, E. J., Sullivan, K. D., Marzluff, W. F., O'Rand, M. G. *J. Biol. Chem.* **2006,** *281,* 21526-21534.

(2) Alekseev, O.M., Richardson, R. T., Alekseev, O., O'Rand, M. G. *Reprod. Biol. Endocrinol.* **2009,** *7,* 45-45.

(3) Ellis, R.J. *Trends. Biochem. Sci.* **2006,** *31,* 395-401.

(4) Ruoppolo, M., Orrù, S., Talamo, F., Ljung, J., Pirneskoski, A., Kivirikko, K. I., Marino, G., Koivunen, P. *Protein Sci.* **2003,** *12,* 939-952.

(5) Frickel, E.M., Riek, R., Jelesarov, I., Helenius, A., Wuthrich, K., Ellgaard, L. *Proc. Natl. Acad. Sci. U.S.A.* **2002,** *99,* 1954-1959.

(6) Fenton, W.A., Horwich, A. L. *Q. Rev. Biophys.* **2003,** *36,* 229-256.

(7) Leslie, M. *J. Cell Biol.* **2005,** *171,* 13-14.

(8) High, S., Abell, B. M. *Biochem. Soc. Trans.* **2004,** *32,* 659-662.

(9) Kutay, U., Hartmann, E., Rapoport, T. A. *Trends Cell Biol.* **1993,** *3,* 72-75.

(10) Lecomte, F.J., Ismail, N., High, S. *Biochem. Soc. Trans.* **2003,** *31,* 1248-1252.

(11) Borgese, N., Colombo, S., Pedrazzini, E. *J. Cell Biol.* **2003,** *161,* 1013-1019.

(12) Borgese, N., Brambillasca, S., Colombo, S. *Curr. Opin. Cell Biol.* **2007,** *19,* 368-375.

(13) Mitoma, J., Ito, A. *EMBO J.* **1992,** *11,* 4197-4203.

(14) Kutay, U., Ahnert-Hilger, G., Hartmann, E., Wiedenmann, B., Rapoport, T. A. *EMBO J.* **1995,** *14,* 217-223.

(15) Linstedt, A.D., Foguet, M., Renz, M., Seelig, H. P., Glick, B. S., Hauri, H. P. *Proc. Natl. Acad. Sci. U.S.A.* **1995,** *92,* 5102-5105.

(16) Pedrazzini, E., Villa, A., Borgese, N. *Proc. Natl. Acad. Sci. U.S.A.* **1996,** *93,* 4207-4212.

(17) Douglas, R.H., Hultquist, D. E. *Proc. Natl. Acad. Sci. U. S. A.* **1978,** *75,* 3118-3122.

(18) Spatz, L. and Strittmatter, P. *Proc. Natl. Acad. Sci. U.S.A.* **1971,** *68,* 1042-1046.

(19) Durley, R., Mathews, F. S. *Acta. Crystallogr.* **1996,** *D52,* 65-76.

(20) Muskett, F.W., Kelly, G. P., Whitford, D. *J. Mol. Biol.* **1996,** *258,* 172-189.

(21) Hanlon, M.R., Begum, R. R., Newbold, R. J., Whitford, D., Wallace, B. A. *Biochem. J.* **2000,** *352,* 117-124.

(22) Clarke, T.A., Im, S. C., Bidwai, A., Waskell, L. *J. Biol. Chem.* **2004,** *279,* 36809-36818.

(23) Kim, P.K., Janiak-Spens, F., Trimble, W. S., Leber, B., Andrews, D. W. *Biochemistry* **1997,** *36,* 8873-8882.

(24) Schmidt-Mende, J., Bieck, E., Hugle, T., Penin, F., Rice, C. M., Blum, H.E., Moradpour, D. *J. Biol. Chem.* **2001,** *276,* 44052-44063.

(25) Visser, L., Robinson, N. C., Tanford, C. *Biochemistry* **1975,** *14,* 1194-1199.

(26) Ladokhin, A.S., Wang, L., Steggles, A. W., Malak, H., Holloway, P. W. *Biochemistry* **1993,** *32,* 6951-6956.

(27) Kuroda, K., Kinoshita, J. Y., Honsho, M., Mitoma, J. Y., Ito, A. *J. Biochem. (Tokyo).* **1996,** *120,* 828-833.

(28) Takagaki, Y., Radhakrishnan, R., Wirtz, K. W. A., Khorana, H. G. *J. Biol. Chem.* **1983,** *258,* 9136-9142.

(29) Enoch, H., Fleming, P. J., Strittmatter, P. *J. Biol. Chem.* **1979,** *254,* 6483-6488.

(30) Vergères, G., Ramsden, J., Waskell, L. *J. Biol. Chem.* **1995,** *270,* 3414-3422.

(31) Riley, M.L., Wallace, B. A., Flitsch, S. L., Booth, P. J. *Biochemistry* **1997,** *36,* 192-196.

(32) Bridges, A., Gruenke, L., Chang, Y. T., Vakser, I. A., Loew, G., Waskell, L. *J. Biol. Chem.* **1998,** *273,* 17036-17049.

(33) Mulrooney, S.B., Waskell, L. *Protein Expr. Purif.* **2000,** *19,* 173-178.

(34) Tamm, L.K., Mcconnell, H. M. *Biophys. J.* **1985,** *47,* 105-113.

(35) Thompson, N.L., Palmer, A. G. *Comm. Mol. Cell. Biophys.* **1988,** *5,* 39-56.

(36) Chen, X., Boughton, A.P., Tesmer, J.J.G., Chen, Z. *J. Am. Chem. Soc.* **2007,** *129,* 12658-12659.

(37) Chen, X., Wang, J., Boughton, A. P., Kristalyn, C. B.,Chen, Z. *J.Am.Chem.Soc.* **2007,** *129,* 1420-1427.

(38) Chen, X., Wang, J., Kristalyn, C. B., Chen, Z. *Biophys. J* **2007,** *93,* 866-875.

(39) Wang, J., Even, M. A., Chen, X., Schmaier, A. H., Waite, J. H., Chen, Z. *J. Am. Chem. Soc.* **2003,** *125,* 9914-9915.

(40) Spatz, L., Strittmatter, P. *Proc. Natl. Acad. Sci. U.S.A.* **1971,** *68,* 1042-1046.

(41) Nguyen, T. K., Le Clair, S. V., Ye, S., Chen, Z. *J. Phys. Chem. B* **2009,** *113,* 12169-12180.

(42) Wang, J., Lee, S. H., Chen, Z. *J. Phys. Chem. B* **2008,** *112,* 2281-2290.

(43) Moad, A.J., Moad, C. W., Perry, J. M., Wampler, R. D., Goeken, G. S., Begue, N. J., Shen, T., Heiland, R., Simpson, G. J. *J. Comp. Chem.* **2007,** *28,* 1996-2002.

(44) Wampler, R.D., Moad, A. J., Moad, C. W., Heiland, R., Simpson, G. J. *Acc. Chem. Res.* **2007,** *40,* 953-960.

(45) Dürr, U.H.N., Yamamoto, K., Im, S. C., Waskell, L., Ramamoorthy, A. *J. AM. CHEM. SOC.* **2007,** *129,* 6670-6671.

(46) Liu, J., Conboy, J. C. *Langmuir* **2005,** *21,* 9091-9097.

(47) Dürr, U.H.N., Waskell, L., Ramamoorthy, A. *Biochim. Biophys. Acta* **2007,** *1768,* 3235-3259.

(48) Takematsu, H., Kozutsumi, Y., Suzuki, A., Kawasaki, T. *Biochem. Biophys. Res. Commun.* **1992,** *185,* 845-851.

(49) Sayyed-Ahmad, A., Kaznessis, Y. N. *PLoS ONE 4(3)* **2009,** *4,* e4799.

(50) Damodaran, K.V., Merz Jr., K. M. *Biophys. J.* **1994,** *66,* 1076-1087.

(51) Gambu, I., Roux, B. *J. Phys. Chem. B* **1997,** *101,* 6066-6072.

CHAPER 5

ORIENTATION DETERMINATION OF INTERFACIAL β-SHEET STRUCTURES *IN SITU*

5.1 Introduction

Biological surfaces and interfaces provide unique environments for a wide variety of protein activities. For example, after a biomedical material is implanted, the first body reaction is protein adsorption. The structure and activity of the surface adsorbed proteins determine later body reactions, mediating whether the biomaterial is accepted or rejected by the body. Additionally, surface immobilized proteins serve as sensing units for biosensors; their interfacial structures play crucial roles in biosensing performance. Cell membranes are interfacial environments that host many critical cellular processes such as trans-membrane transport and cellular communication. Membranes can also be susceptible to antimicrobial activity. These processes are governed by membrane-associated proteins and peptides. Given the strong relationship between structure and function found in biologically active molecules, the orientation that a membrane-associated protein or peptide assumes at an interface is naturally important. In order to study the interfacial orientation of complex proteins, it is necessary to examine orientations of common secondary structures that are components of peptides and proteins on surfaces and at interfaces. The most commonly seen secondary structures are

α-helices and β-sheets. We have developed systematic means to determine interfacial orientation of α-helices in the previous chapters.[1-3] In this research, we will investigate orientation of β-sheet structure on surfaces/at interfaces.

The β-sheet structure was first proposed by Astbury in 1931; that model was not accurate until the refinements made by Pauling and Corey in 1951.[4] It is a widely distributed secondary structure found in a diverse range of proteins. Many membrane-associated proteins and peptides have β-sheet or β-barrel components. Porins, for instance, are an extremely important family of membrane spanning β-barrel proteins that facilitate the transport of ions across cell membranes. Determining the orientation of this structure, and more importantly the way the structure adapts to changing environments, is crucial in having a detailed understanding of the protein's functional mechanisms.[5] Transformational changes of protein components to β-sheets have also been observed and are believed to be crucial malfunctions that lead to diseases such as mad cow disease and Creutzfeldt-Jakob disease. The formation of β-sheets producing fibrous structures occurs at interfaces, which can disrupt cellular processes.[6] These amyloid β-peptide (Aβ-) fibrous plaques can accumulate on the brain, leading to Alzheimer's disease. [7] The occurrence of β-sheet structures in membrane-associated proteins as well as in Aβ-plaques raises much interest about β-sheet orientation. Therefore, the ability to determine the structural information of the β-sheets, including orientation of β-sheets at interfaces and on surfaces, could aid in the understanding of protein behaviors.

A wide range of spectroscopic techniques have been applied to the study of interfacial proteins and peptides. For instance, Attenuated Total Reflectance Fourier Transform Infrared spectroscopy (ATR-FTIR) and Raman spectroscopic techniques have

been extensively used to study surface peptides, providing orientation information of peptides while they are adsorbed on surfaces.[8-31] Nuclear Magnetic Resonance (NMR) techniques have also been successfully applied to determine detailed structural information regarding membrane-associated peptides, including interaction mechanisms of adsorbed peptides.[32-40]

As discussed in the previous chapters, SFG has recently been developed into a powerful technique to investigate surfaces and interfaces.[2,41-65] SFG measures the second order nonlinear response of a system, $\chi^{(2)}$, which is intrinsically surface sensitive, allowing peptides and proteins to be selectively studied while they are in interfacial environments such as in lipid bilayers or on polymer surfaces. In addition, SFG has been demonstrated to be an extremely sensitive technique, allowing interfacial proteins and peptides to be studied *in situ* and at biological concentrations.[50, 51, 66-84] Protein (or peptide) - membrane interactions can also be studied in real time, revealing adsorption kinetics as well as orientation and structural changes as the proteins interact with surfaces or cell membranes. Therefore, in comparison with ATR-FTIR, Raman spectroscopy and NMR, SFG has many significant advantages such as superb detection limit, near background free detection and real time *in situ* study capability. SFG has been successfully applied to the orientation determination of interfacial α-helices.[1-3, 85] Here we will focus on the β-sheet, specifically the anti-parallel β-sheet structure.

In this work, we successfully applied the bond additivity model to calculate the IR transition dipole moment, the Raman polarizability and eventually the SFG hyperpolarizability of the anti-parallel β-sheet. The hyperpolarizability tensor components are related to the SFG chiral and achiral signal strength, which allows for the

orientation analysis of this particular structure at interfaces. The orientation of tachyplesin I, an anti-parallel β-sheet structure, was analyzed at both polymer and lipid bilayer interfaces. The possibility of determining the orientation of β-sheet structure is of great importance in the structural analysis of large proteins which consist of both α-helical and β-sheet structures. The orientation information of these proteins now can be investigated by two independent yet complementary SFG approaches (by studies of α-helical and β-sheet components), which will enhance the viability of the technique.

5.2 Experimental

Materials

C-terminal amidated tachyplesin I (**NH_2-K-W-C-F-R-V-C-Y-R-G-I-C-Y-R-R-C-R-$CONH_2$**) was purchased from GenScript USA Inc. (Piscataway, NJ) with >95% purity. Tachyplesin I is an antimicrobial peptide that is extracted from the horseshoe crab hemocytes. Tachyplesin I adopts anti-parallel β-sheet structure, which is stabilized by the two disulfide bonds. It is also because of these two disulfide bonds that the peptide's secondary structure is much more stable than these β-sheet structures that are held up just by hydrogen bonds. Polystyrene (PS) used in this research was PS standard, purchased from Scientific Polymer Products Inc, with a molecular weight of 393,400. The sulfonated PS (s-PS) was prepared from such PS standard. The sulfonation reaction has been described previously.[86] PS and PS with 15% sulfonation were used for the SFG experiments. Both the lipids, hydrogenated and deuterated 1,2-dipalmitoyl (D26)-sn-glycero-3-phosphoglycerol (DPPG and dDPPG), used in this report were purchased from Avanti Polar Lipids Inc (Alabaster, AL).

Lipid bilayer deposition

Single lipid bilayers, which can have two different leaflets, were prepared on CaF_2 right angle prisms (Altos Photonics, Bozeman, MT). Langmuir-Blodgett and Langmuir-Schaefer (LB/LS) methods were used to deposit the proximal and then the distal leaflets, respectively. A KSV2000 LB system and ultrapure water from a Millipore system (Millipore, Bedford, MA) were used throughout the experiments for bilayer preparation. The bilayer was immersed in water inside a 2-mL reservoir during the experiment and a small amount of water could be added to the reservoir to compensate for evaporation when needed for long timescale experiments. For tachyplesin I-bilayer interaction experiments, 10 μL of 0.25 mg/ml tachyplesin I solution was injected into the reservoir. A magnetic micro-stirrer was used at a rate of 100 rpm to ensure a homogeneous concentration distribution of peptide molecules in the subphase below the bilayer.

SFG experiments

The details of our SFG setup and experimental design have been previously thoroughly described.[2, 87, 88] Polymer films were prepared by spin coating 1 wt% polymer solutions onto CaF_2 prisms at a speed of 2400 rpm. Spectra were collected in ssp (s-SFG, s-visible, p-IR), ppp and spp polarizations using our previously reported near total reflection geometry.[81]

ATR-FTIR experiments

The ATR-FTIR spectra were collected on a Nicolet 550 spectrometer (Thermo Fisher Scientific. Inc., MA, USA). A thin polymer film was solution cast onto a germanium substrate from a 0.1 wt % polymer solution. 50 μL of 0.05 mg/ml

tachyplesin I solution in D_2O (Sigma Aldrich, St. Louis, MO) was injected into the ATR trough, and S and P polarized spectra were collected approximately one hour after the injection of peptide. The chamber was purged with nitrogen before and during the data collection, and the spectra were collected using 256 scans/spectrum.

5.3. Orientation determination of β-sheet

The SFG hyperpolarizability tensor, β, can be described as a tensor product of the IR transition dipole moment and the Raman polarizability tensor[3, 89, 90],

$$\beta_{lmn,q} \propto \frac{\partial \alpha^*_{lm}}{\partial Q_q} \frac{\partial \mu_n}{\partial Q_q} \qquad \textbf{(5.1)}$$

where l, m, and n are the molecular coordinates, $\frac{\partial \alpha_{lm}}{\partial Q_q}$ and $\frac{\partial \mu_n}{\partial Q_q}$ are the Raman polarizability and IR dipole moment derivatives with respect to the normal mode coordinate of the q^{th} vibrational mode, respectively. Throughout this chapter these derivatives will be referred to as the components of the Raman polarizability tensor and IR transition dipole moment. As equation (5.1) indicates, if both the IR transition dipole moment and the Raman polarizability tensor are known, the SFG hyperpolarizability tensor for the vibrational mode of interest can be deduced. It is widely accepted that the anti-parallel β-sheet adopts D_2 symmetry.[91-93] Applying this symmetry point group, the Raman polarizability tensor and the IR transition dipole of the four peptide units that comprise the β-sheet repeating unit can be projected onto the molecular coordinate system using the bond additivity model. The calculation of the hyperpolarizability tensor will be presented in detail in sections 5.3.4.

5.3.1 Anti-parallel β-sheet structure and D_2 point group symmetry

For a structure with D_2 point group symmetry, there are three IR active (B_1, B_2 and B_3) and four Raman active amide I vibrational modes (A, B_1, B_2 and B_3). The four modes are: [93-97]

$$\nu(0,0) = \nu_0 + D_{10} + D_{01} + D_{11} = 1668\ cm^{-1}$$
$$\nu(0,\pi) = \nu_0 + D_{10} - D_{01} - D_{11} = 1685\ cm^{-1} \quad \textbf{(5.2)}$$
$$\nu(\pi,0) = \nu_0 - D_{10} + D_{01} - D_{11} = 1636\ cm^{-1}$$
$$\nu(\pi,\pi) = \nu_0 - D_{10} - D_{01} + D_{11} = 1723\ cm^{-1}$$

where ν_0 is the unperturbed peptide unit frequency and D_{10} and D_{01} account for the intrachain and interchain couplings, respectively. The term D_{11} represents the coupling of the transition dipoles between adjacent strands. A graphical illustration of these four vibrational modes is presented in Figure 5.1.

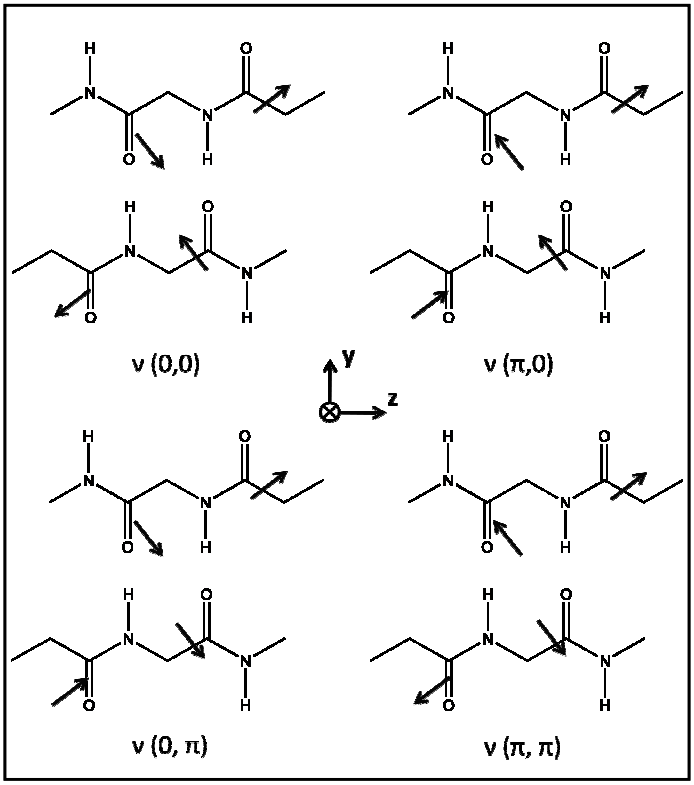

Figure 5.1: Four amide I vibrational modes of a repeating unit of an anti-parallel β-sheet

5.3.2 The Raman polarizability tensor of an anti-parallel β-sheet

The Raman tensor for the amide I mode (Figure 5.2) has been proposed by Tsuboi and colleagues by investigating Raman spectra of a uniaxial tetragonal aspartame.[30] For β-sheet structures, the principle x-axis of Tsuboi's polarizability tensor is found to be significantly more in line with the C=O bond; this tilt angle is only 22 degrees (instead of 34.5 degrees in α-helical structures).[96] This refinement was made by adjusting this tilt angle so that the Raman intensity ratio $\frac{I_{cc}}{I_{bb}}$ matches the experimental observations on *Bombyx mori* silk ($\frac{I_{cc}}{I_{bb}}$ = 0.304), *Nephila edulis* spidroin ($\frac{I_{cc}}{I_{bb}}$ = 0.406), *S. c. ricini* fibroin silk ($\frac{I_{cc}}{I_{bb}}$ = 0.257), and fowl feather barb ($\frac{I_{cc}}{I_{bb}}$ = 0.429).[95, 96, 98] For the β-sheet, the polarizability tensor can be written in the given molecular frame as defined in Figure 5.2.

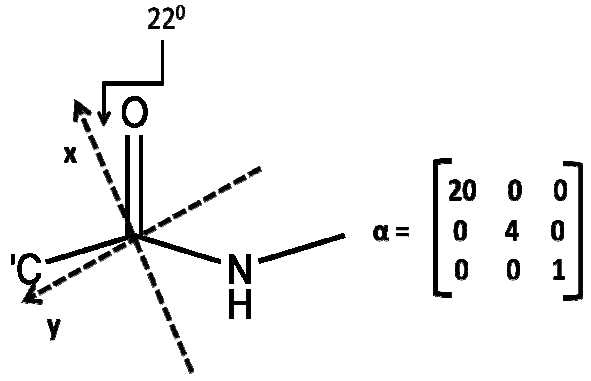

Figure 5.2: A peptide unit and its transition Raman polarizability tensor in the given molecular frame of the β-sheet

Given this polarizability tensor and its corresponding molecular frame, an Euler transformation can be used to impose this tensor in the molecular coordinate system onto the four peptide units of the Pauling-Corey β-sheet. The Euler transformation used here follows the z-y-z convention, which has a matrix in the form of

$$\xi = \begin{pmatrix} -\sin(\psi)\cos(\phi) + \cos(\psi)\cos(\theta)\cos(\phi) & \sin(\psi)\cos(\phi) + \cos(\psi)\cos(\theta)\sin(\phi) & -\cos(\psi)\sin(\theta) \\ -\cos(\psi)\sin(\phi) - \sin(\psi)\cos(\theta)\cos(\phi) & \cos(\psi)\cos(\phi) - \sin(\psi)\cos(\theta)\sin(\phi) & \sin(\psi)\sin(\theta) \\ \sin(\theta)\cos(\phi) & \sin(\theta)\sin(\phi) & \cos(\theta) \end{pmatrix} \quad \textbf{(5.3)}$$

and the rotations are carried out using equation (5.4).

$$\alpha_{xyz} = \xi \alpha_{abc} \xi^T \quad \textbf{(5.4)}$$

We define a positive rotation as a rotation in the counter-clockwise direction. The four Euler angle sets used to rotate the peptide units comprising the β-sheet repeating unit from Tsuboi's frame into Pauling-Corey's frame are: (φ_1=292°, θ_1= 113°, ψ_1= 0°), (φ_2=112°, θ_2= 247°, ψ_2= 0°), (φ_3=112°, θ_3= 67°, ψ_3= 0°) and (φ_4=292°, θ_4= 293°, ψ_4= 0°). The first Raman polarization tensor of the anti-parallel β-sheet structure in the Pauling-Corey coordinate system can be calculated as:

$$\alpha_1 = \begin{pmatrix} -0.15 & 0.36 & -0.92 \\ 0.93 & 0.37 & 0 \\ 0.34 & -0.85 & -0.39 \end{pmatrix} \begin{pmatrix} 20.00 & 0 & 0 \\ 0 & 4.00 & 0 \\ 0 & 0 & 1.00 \end{pmatrix} \begin{pmatrix} -0.15 & 0.36 & -0.92 \\ 0.93 & 0.37 & 0 \\ 0.34 & -0.85 & -0.39 \end{pmatrix}^T =$$

$$\begin{pmatrix} 1.80 & -2.17 & -1.89 \\ -2.17 & 17.75 & 5.12 \\ -1.89 & 5.12 & 5.44 \end{pmatrix} \quad \textbf{(5.5)}$$

The four resulting Raman polarization tensors after the rotation are

$$\alpha_1 = \begin{pmatrix} 1.80 & -2.17 & -1.89 \\ -2.17 & 17.75 & 5.12 \\ -1.89 & 5.12 & 5.44 \end{pmatrix}, \qquad \alpha_2 = \begin{pmatrix} 1.80 & -2.17 & 1.89 \\ -2.17 & 17.75 & -5.12 \\ 1.89 & -5.12 & 5.44 \end{pmatrix},$$

$$\alpha_3 = \begin{pmatrix} 1.80 & 2.17 & 1.89 \\ 2.17 & 17.75 & 5.12 \\ 1.89 & 5.12 & 5.44 \end{pmatrix}, \qquad \alpha_4 = \begin{pmatrix} 1.80 & 2.17 & -1.89 \\ 2.17 & 17.75 & -5.12 \\ -1.89 & -5.12 & 5.44 \end{pmatrix}. \qquad \textbf{(5.6)}$$

The transition Raman polarizability tensor of the A, B_1, B_2 and B_3 modes of the repeating unit of the β-sheet structure can be calculated from these Raman polarizability tensors, with the phase differences of these modes being considered (Figure 5.1).

A mode:

$$\alpha_{\nu(0,0)} = \sum_{i=1}^{4} \alpha_i = \begin{pmatrix} 7.2 & 0 & 0 \\ 0 & 71.00 & 0 \\ 0 & 0 & 21.76 \end{pmatrix} \qquad \textbf{(5.7)}$$

B_1 mode:

$$\alpha_{\nu(0,\pi)} = \cos(\pi)\alpha_1 + \cos(\pi)\alpha_2 + \cos(0)\alpha_3 + \cos(0)\alpha_4 = \begin{pmatrix} 0 & 8.68 & 0 \\ 8.68 & 0 & 0 \\ 0 & 0 & 0 \end{pmatrix} \qquad \textbf{(5.8)}$$

B_2 mode:

$$\alpha_{\nu(\pi,0)} = \cos(0)\alpha_1 + \cos(\pi)\alpha_2 + \cos(\pi)\alpha_3 + \cos(0)\alpha_4 = \begin{pmatrix} 0 & 0 & -7.56 \\ 0 & 0 & 0 \\ -7.56 & 0 & 0 \end{pmatrix} \qquad \textbf{(5.9)}$$

B_3 mode:

$$\alpha_{\nu(\pi,\pi)} = \cos(\pi)\alpha_1 + \cos(0)\alpha_2 + \cos(\pi)\alpha_3 + \cos(0)\alpha_4 = \begin{pmatrix} 0 & 0 & 0 \\ 0 & 0 & -20.48 \\ 0 & -20.48 & 0 \end{pmatrix} \qquad \textbf{(5.10)}$$

As seen from these modes, the A mode dominates the Raman spectra of the anti-parallel β-sheet structures, which was also experimentally observed.[95]

5.3.3 IR transition dipole moment of an anti-parallel β-sheet

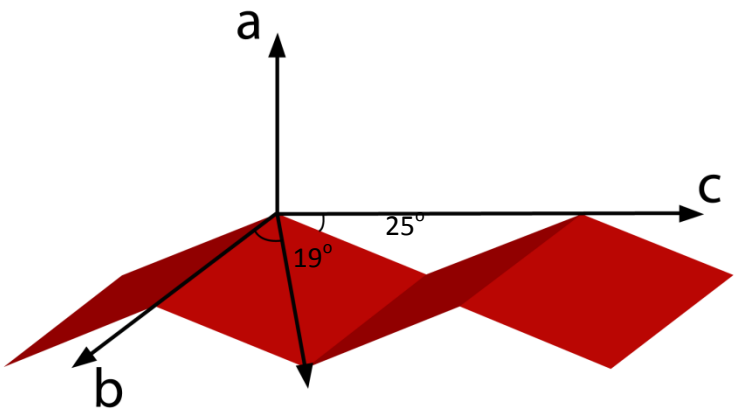

Figure 5.3: Orientation of the IR transition dipole moment of the individual peptide unit comprising the anti-parallel β-sheet structure. The dipole moment lies in the plane that is inclined at an angle of 25° to the strand axis, and makes an angle of 19° to the axis that connects the two successive α-carbons of the two strands.

The calculation of the IR transition dipole moment of the individual peptide unit comprising one repeating unit of the anti-parallel β-sheet structure (shown in Figure 5.3)[99] has been reported by Marsh.[93] We slightly modified Marsh's projection by transforming the dipole moment of the peptide unit into Tsuboi's frame, followed by a transformation into the Pauling-Corey frame using the Euler transformation that was introduced previously in section 5.3.2. We have verified the outcome of this approach (projection followed by rotation) with the results obtained from the conventional projection to ensure that the proper rotational operations were performed. The final calculated dipole moments of the four peptide units are

$$\mu_1 = \begin{pmatrix} -0.13 \\ 0.95 \\ 0.30 \end{pmatrix}, \mu_2 = \begin{pmatrix} 0.13 \\ -0.95 \\ 0.30 \end{pmatrix}, \mu_3 = \begin{pmatrix} -0.13 \\ -0.95 \\ -0.30 \end{pmatrix}, \mu_4 = \begin{pmatrix} 0.13 \\ 0.95 \\ -0.30 \end{pmatrix} \qquad \textbf{(5.11)}$$

From these transition dipole moments of the four individual peptide units in a β-sheet repeating unit (Figure 5.1), one can see that the symmetric A mode is inactive in IR spectroscopy. The overall transition dipole moment of the B_1, B_2 and B_3 vibrational modes can be calculated: [94]

B_1 mode: $$\mu_{\nu(0,\pi)} = \cos(\pi)\mu_1 + \cos(\pi)\mu_2 + \cos(0)\mu_3 + \cos(0)\mu_4 = \begin{pmatrix} 0 \\ 0 \\ -1.2 \end{pmatrix} \quad \textbf{(5.12)}$$

B_2 mode: $$\mu_{\nu(\pi,0)} = \cos(0)\mu_1 + \cos(\pi)\mu_2 + \cos(\pi)\mu_3 + \cos(0)\mu_4 = \begin{pmatrix} 0 \\ 3.80 \\ 0 \end{pmatrix} \quad \textbf{(5.13)}$$

B_3 mode: $$\mu_{\nu(\pi,\pi)} = \cos(\pi)\mu_1 + \cos(0)\mu_2 + \cos(\pi)\mu_3 + \cos(0)\mu_4 = \begin{pmatrix} 0.52 \\ 0 \\ 0 \end{pmatrix} \quad \textbf{(5.14)}$$

The calculated overall dipole moment is indeed supported by the experimental observations with a strong peak at 1635 cm^{-1}. This low frequency mode was assigned to the B_2 representation, while the high frequency absorption peak at 1685 cm^{-1} was assigned to be the B_1 representation (Figure 5.1 and equation 5.2). If we define the molecular (a, b, c) frame to be superimposed with the lab (x, y, z) coordinate system, the B_2 mode of the β-sheet structure is y polarized, and the B_1 mode is z polarized. As one can see from the calculated dipole moments, the strong mode is along the y axis, which belongs to the B_2 representation. Additionally, the calculated intensity ratio between the B_1/B_2 modes agrees fairly well with the value reported by Choi et al. Applying normal mode analysis of the amide I vibrations, Choi reported the B_1/B_2 intensity to be around 0.11 versus our calculated value of 0.10. However, Choi's calculation predicts quite different peak centers for the B_1 and B_2 modes as previously done by the work of Miyazawa, Tsuboi, Krimm and Marsh.[100]

5.3.4 SFG data analysis for anti-parallel β-sheet structures based on the calculated IR transition dipole moment and Raman polarizability tensor.

The SFG hyperpolarizability tensor, β, is a third-rank tensor with 27 elements. It is a tensor product of the Raman polarizability tensor and the IR transition dipole moment. Hence, a vibrational mode is only SFG active when it is both IR and Raman active. Therefore, B_1 (components μ_c and α_{ab}), B_2 (μ_b and α_{ac}) and B_3 (μ_a and α_{bc}) vibrational modes of the anti-parallel β-sheet are SFG active. Conventionally, chiral signal was believed to arise primarily from the double resonance SFG process, in which the Raman tensor is asymmetric.[101, 102] However, Shen and colleagues used perturbation theory of vibrational SFG to predict that the generation of chiral signal is plausible in vibrational SFG without the requirement of an asymmetric Raman tensor.[101, 103] Evidentially, our laboratory has also experimentally observed strong chiral vibrational SFG signal with the anti-parallel β-sheet, which was also predicted by Simpson and coworkers.[81, 104]

In this chapter, we report the SFG achiral signal observed in ssp polarization combination and the SFG chiral signal observed in spp polarization.[81, 105]

$$\chi_{ssp}^{(2)} = L_{yyz}\chi_{yyz}^{(2)} \quad \textbf{(5.15)}$$

$$\chi_{spp}^{(2)} = L_{yxz}\chi_{yxz}^{(2)} + L_{yzx}\chi_{yzx}^{(2)} \quad \textbf{(5.16)}$$

The normalized Fresnel factors L_{yyz}, L_{yzx} and L_{yxz} are calculated to be 11.0, 5.2 and 1.0, respectively for our experimental geometry which has been described in our previous publications.[2, 88] These Fresnel coefficients were normalized relative to L_{yxz} so that the

refractive index of the interfacial medium (PS/peptide solution interface and lipid bilayer with the peptides) does not need to be determined explicitly.

To relate the molecular SFG hyperpolarizability, β_{abc}, to the macroscopic SFG susceptibility, $\chi^{(2)}_{xyz}$, we use a set of three Euler angles φ, θ, and ψ representing the in-plane rotation, the tilt angle and the twist angle, respectively. The transformation matrix therefore can be written as

$$R = (R_3(\psi\psi)R_2(\theta)R_1(\varphi))^T =$$

$$\left[\begin{pmatrix} \cos(\psi\psi) & \sin(\psi\psi) & 0 \\ -\sin(\psi\psi) & \cos(\psi\psi) & 0 \\ 0 & 0 & 1 \end{pmatrix}\begin{pmatrix} \cos(\theta) & 0 & -\sin(\theta) \\ 0 & 1 & 0 \\ \sin(\theta) & 0 & \cos(\theta) \end{pmatrix}\begin{pmatrix} \cos(\varphi) & \sin(\varphi) & 0 \\ -\sin(\varphi) & \cos(\varphi) & 0 \\ 0 & 0 & 1 \end{pmatrix}\right]^T =$$

$$\begin{pmatrix} \cos(\psi)\cos(\theta)\cos(\varphi) - \sin(\psi)\sin(\varphi) & -\sin(\psi)\cos(\theta)\cos(\varphi) - \cos(\psi)\sin(\varphi) & \sin(\theta)\cos(\varphi) \\ \cos(\psi)\cos(\theta)\sin(\varphi) + \sin(\psi)\cos(\varphi) & -\sin(\psi)\cos(\theta)\cos(\varphi) - \cos(\psi)\cos(\varphi) & \sin(\theta)\sin(\varphi) \\ -\cos(\psi)\sin(\theta) & \sin(\psi)\sin(\theta) & \cos(\theta) \end{pmatrix}$$

(5.17)

The macroscopic SFG susceptibility quantity, $\chi^{(2)}_{xyz}$, can be described by the molecular hyperpolarizability tensor components: [90, 106-110]

$$\chi^{(2)}_{IJK} = \sum_{i'j'k'=x'y'z'} N_S\langle R_{Ii'}R_{Jj'}R_{Kk'}\rangle\beta_{i'j'k'} \qquad \textbf{(5.18)}$$

The three vibrational modes of the anti-parallel β-sheet can be observed in the laboratory coordinate system by the following relations:

B_1 mode:

$$\chi^{(2)}_{yyz} = \frac{1}{2}N_s(\cos(\theta)\cos(\psi)\sin(\psi) - \cos^3(\theta)\cos(\psi)\sin(\psi)) * \beta_{abc}$$

$$\chi^{(2)}_{zzz} = N_s(\cos^3(\theta)\cos(\psi)\sin(\psi) - \cos(\theta)\cos(\psi)\sin(\psi)) * \beta_{abc}$$

$$\chi^{(2)}_{yzx} = \tfrac{1}{2}N_s\sin^2(\theta)\cos^2(\psi) * \beta_{abc} \qquad \textbf{(5.19)}$$

$$\chi^{(2)}_{yxz} = -\frac{1}{2}N_s\cos^2(\theta) * \beta_{abc}$$

B_2 mode:

$$\boldsymbol{\chi^{(2)}_{yyz} = \frac{1}{2}N_s(\cos(\theta)\cos(\psi)\sin(\psi) - \cos^3(\theta)\cos(\psi)\sin(\psi)) * \beta_{acb}}$$

$$\chi^{(2)}_{zzz} = N_s(\cos^3(\theta)\cos(\psi)\sin(\psi) - \cos(\theta)\cos(\psi)\sin(\psi)) * \beta_{acb} \quad \textbf{(5.20)}$$

$$\chi^{(2)}_{yzx} = -\frac{1}{2}N_s\cos^2(\theta) * \beta_{acb}$$

$$\chi^{(2)}_{yxz} = \frac{1}{2}N_s\sin^2(\theta)\cos^2(\psi) * \beta_{acb}$$

B_3 mode:

$$\boldsymbol{\chi^{(2)}_{yyz} = \frac{1}{2}N_s(\cos(\theta)\cos(\psi)\sin(\psi) - \cos^3(\theta)\cos(\psi)\sin(\psi)) * \beta_{bca}}$$

$$\chi^{(2)}_{zzz} = N_s(\cos^3(\theta)\cos(\psi)\sin(\psi) - \cos(\theta)\cos(\psi)\sin(\psi)) * \beta_{bca}$$

$$\chi^{(2)}_{yzx} = \tfrac{1}{2}N_s\cos^2(\theta) * \beta_{bca} \quad \textbf{(5.21)}$$

$$\chi^{(2)}_{yxz} = -\frac{1}{2}N_s\sin^2(\theta)\cos^2(\psi) * \beta_{bca}$$

According to the above equations, the hyperpolarizability quantities β_{abc}, β_{acb} and β_{bca} can be used for orientation analysis and can be calculated from the Raman tensors and IR transition dipoles found in sections 3.2 and 3.3.

$$\beta_{abc} = 8.68 * (-1.20) = -10.42$$

$$\beta_{acb} = -7.56 * 3.80 = -28.73 \quad \textbf{(5.22)}$$

$$\beta_{bca} = -20.48 * 0.52 = -10.65$$

SFG vibrational spectroscopy is a technique in which signal intensity is dependent on the orientation of the oscillators and is intrinsically sensitive to asymmetric systems (or systems with no inversion symmetry). It was questioned previously whether SFG can be used to study β-sheet structure due to its semi-symmetric structure. We successfully detected both chiral and achiral SFG amide I signals from interfacial β-sheet structures,

even though such signals are weak.[81, 84] In principle, all three SFG active modes, which are related to the molecular hyperpolarizability components β_{abc}, β_{acb} and β_{bca} (equations 5.19, 5.20, 5.21), can be observed using SFG. However, given that β_{abc} is roughly 3 times higher than the next strongest vibrational mode (9 folds stronger in intensity), we will focus on the detection of achiral and chiral signals of the B_2 vibrational mode for the orientation analysis of the anti-parallel β-sheet, if the B_2 mode is observed experimentally.

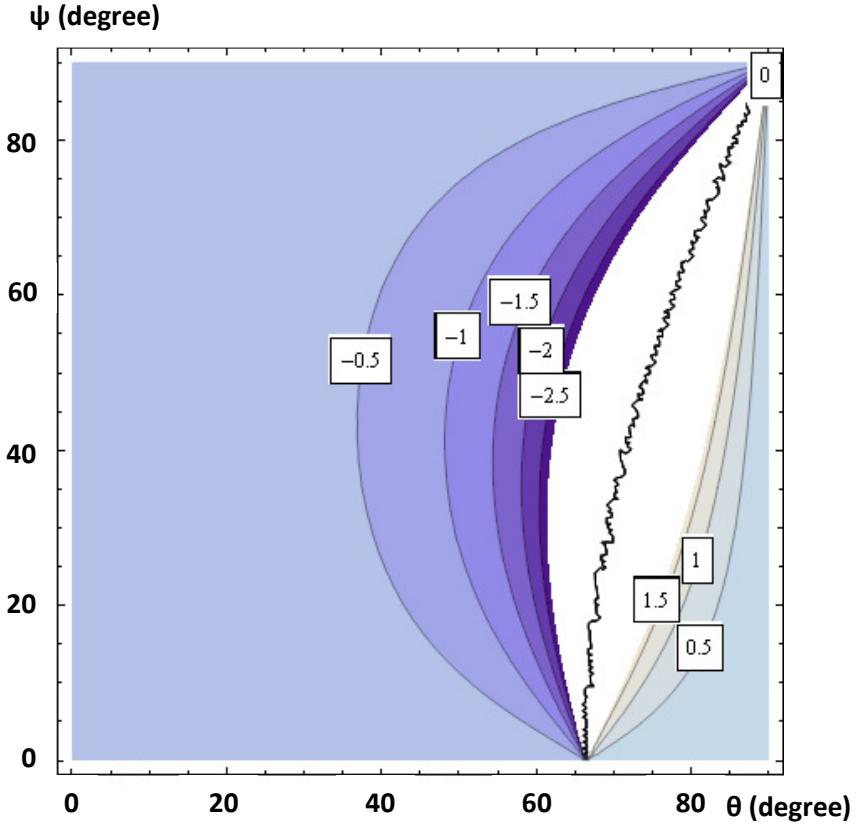

Figure 5.4: The relationship between the SFG susceptibility ratio $\frac{\chi^{(2)}_{sspB2}}{\chi^{(2)}_{sppB2}}$ and the tilt (θ) and twist angle (ψ) of the β-sheet

We will also demonstrate the feasibility of applying the interference enhancement method to enhance the chiral signal in situations in which none of the chiral signals is observed directly, as in the case of tachyplesin I adsorbed onto DPPG/dDPPG lipid bilayers. The spp spectrum was deduced by using interference between ssp and spp, where the visible polarization was tuned ±20° away from the p polarization.[81]

$$I(\pm 20) = K|\chi_{ssp}^{(2)} \sin(\pm 20) + \chi_{spp}^{(2)} \cos(\pm 20) e^{-i\Delta\varphi}|^2 \qquad \textbf{(5.23)}$$

where K is a constant and $\Delta\varphi$ is the phase difference between $\chi_{ssp}^{(2)}$ and $\chi_{spp}^{(2)}$. The relationship between the SFG susceptibility ratio $\frac{\chi_{sspB2}^{(2)}}{\chi_{sppB2}^{(2)}}$ and the two orientation angles θ and ψ is shown in Figure 5.4, illustrating the ability to determine the two orientation angles based on observed SFG signal. Figure 5.5 shows the relationship between the SFG susceptibility component $\chi_{spp}^{(2)}$ of the B_1 mode and the tilt (θ) and twist angle (ψ) of the β-sheet. The same relationship for the B_2 mode is displayed in Figure 5.6.

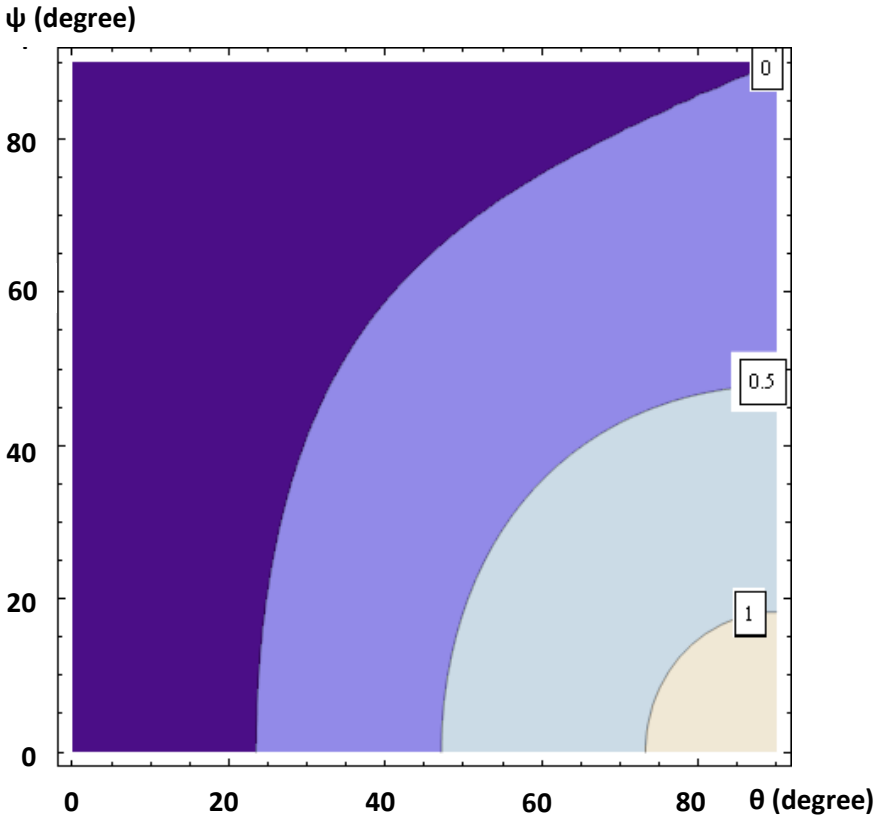

Figure 5.5: The relationship between the SFG susceptibility component $\chi^{(2)}_{spp}$ of the B_1 mode and the tilt (θ) and twist angle (ψ) of the β-sheet

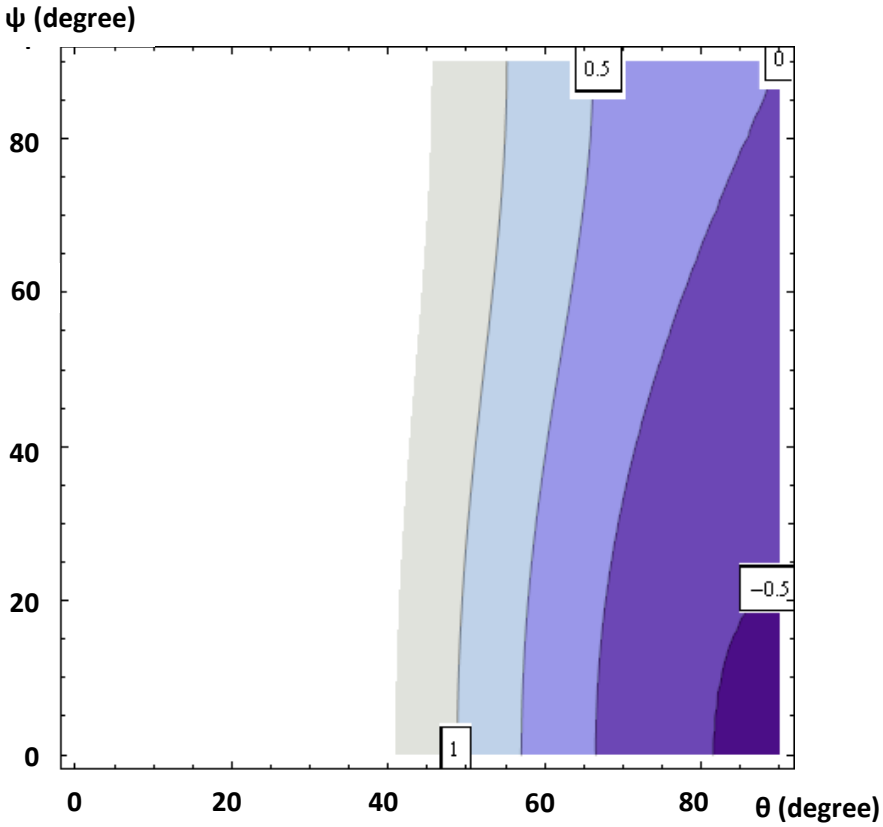

Figure 5.6: The relationship between the SFG susceptibility component $\chi^{(2)}_{spp}$ of the B_2 mode and the tilt (θ) and twist angle (ψ) of the β-sheet

5.4. Experimental results and discussion

5.4.1. The interaction between tachyplesin I and PS polymer surface.

SFG spectra were collected from the PS/tachyplesin I solution (700 nM) using different polarization combinations such as ssp (Figure 5.7) and spp (Figure 5.8). As we discussed in our previous publication[81], ssp polarization combination can be used to probe achiral signal, while spp polarization probes the chiral signal of the molecule. The ssp signal (Figure 5.7) has several contributions which are centered at 1635 cm^{-1}, 1642 cm^{-1}, 1665 cm^{-1}, 1685 cm^{-1} and 1730 cm^{-1}, dominated by the 1635 cm^{-1} and 1730 cm^{-1}

peaks. These signals correspond to the B_2 mode, unordered structure, β-turns/unordered structures, B_1/inter-β-strand and B_3/side chains, respectively.[20, 81, 93] The spp spectrum (Figure 5.8) is dominated by a peak centered at 1635 cm^{-1}, belonging to the B_2 mode. A very weak peak centered at 1685 cm^{-1} from the B_1 mode, along with two weak bands at 1615 cm^{-1} and 1710 cm^{-1}, are also observed. The peak at 1710 cm^{-1} is likely to arise from the B_3 mode, which has been predicted to appear around 1720 cm^{-1}. From the spectral fitting outcomes, the intensity of this peak matches closely with the calculated result. If this is true, we once more demonstrate the superb sensitivity of SFG over ATR-FTIR and Raman, which have been unable to see this vibrational mode of this particular D_2 point group. As we discussed above in section 5.3.4, we can obtain some orientation information of the anti-parallel β-sheet structure of tachyplesin I using the signal strength measured in these two polarization combinations (ssp and spp). Due to the D_2 symmetry point group of the β-sheet structure, orientation information of this structure includes both the tilt angle (θ) and the twist angle (ψ). Because the SFG measurements in ppp and ssp polarization combination for the D_2 symmetry point group are not independent to each other; their intensity ratio stays constant (about 2.0), regardless of the β-sheet orientation. We collected ssp and ppp spectra and found that the strength ratio is indeed around 2. Even though such a combination of measurements does not provide information on orientation determination, it verifies the accuracy of our polarizer settings and the data analysis model.

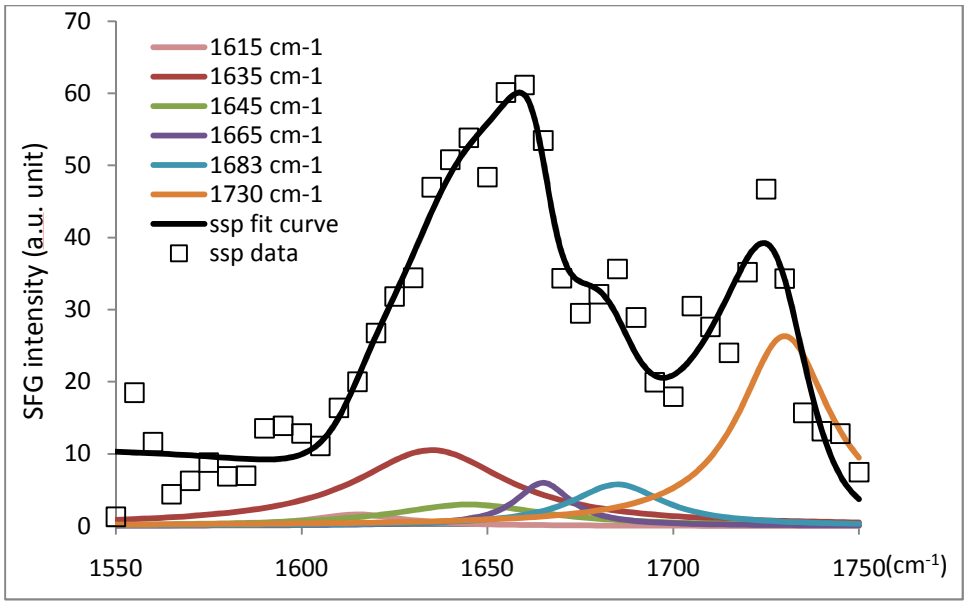

Figure 5.7: SFG amide I spectrum of tachyplesin I (700 nM) adsorbed onto PS surface in ssp polarization combination.

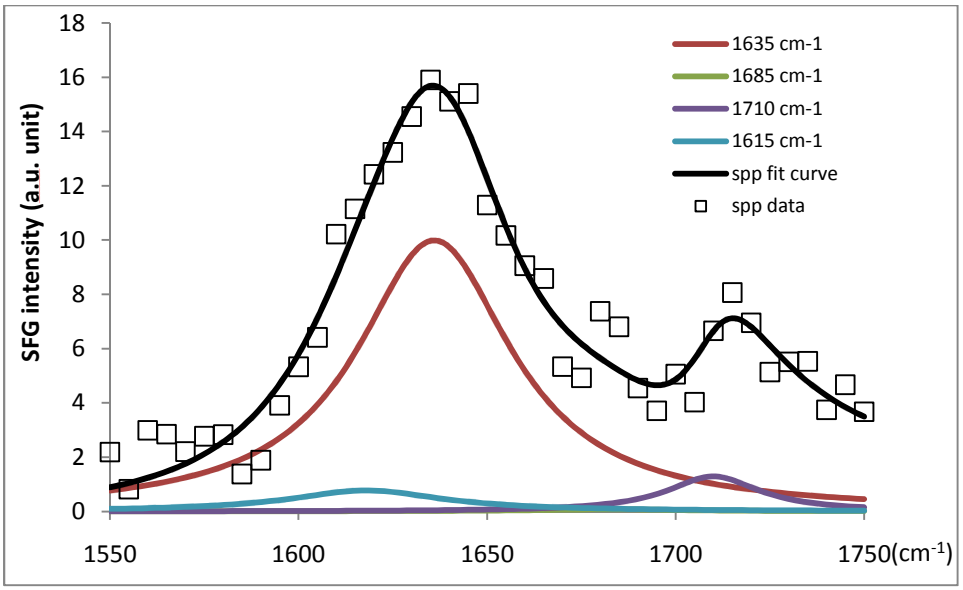

Figure 5.8: SFG amide I spectrum of tachyplesin I (700 nM) adsorbed onto PS surface in spp polarization combination.

In this chapter, the average orientation of tachyplesin I on a PS surface was determined by combining the results from ATR-FTIR and SFG measurements. Polarized ATR-FTIR spectra collected from the PS/tachyplesin I solution interface are presented in Figure 5.9. The orientation determination methodology using ATR-FTIR of the anti-parallel β-sheet has been previously reported by Marsh.[93] Assuming the staggering of the hydrogen bond between the adjacent strands is by one peptide unit, the strand tilt angle with the sheet was calculated to be 35° (or 60° if the staggering is caused by two peptide units).[111] The tilt angle, θ, of the β-sheet structure can be written as

$$R^{ATR}(amide\ I) = \frac{E_x^2}{E_y^2} + \frac{2\langle cos^2\theta\rangle}{3-\langle cos^2\theta\rangle}\frac{E_z^2}{E_y^2} \qquad \textbf{(5.24)}$$

where E_x, E_y and E_z are the components of the electric field vector.

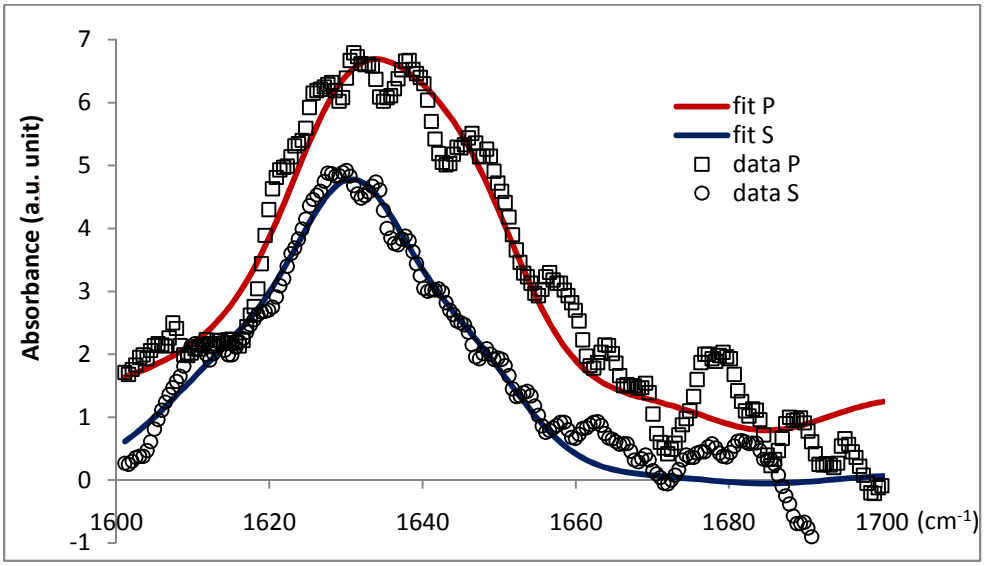

Figure 5.9: ATR-FTIR spectra of tachyplesin I (600 nM) adsorbed onto PS surface in s and p polarizations.

Combining ATR-FTIR with the SFG measurements, the following equations can be used to determine the complete orientation of the β-sheet.

$$\begin{cases} R^{ATR}(amide\ I) = \frac{E_x^2}{E_y^2} + \frac{2\langle cos^2\theta\rangle}{3-\langle cos^2\theta\rangle}\frac{E_z^2}{E_y^2} \\ \chi_{ssp}^{(2)} = L_{yyz}\chi_{yyz}^{(2)} = \frac{1}{2}L_{yyz}\mathrm{N_s}(\langle\cos(\theta)\rangle\langle\cos(\psi)\rangle\langle\sin(\psi)\rangle - \langle\cos^3(\theta)\rangle\langle\cos(\psi)\rangle\langle\sin(\psi)\rangle) * \beta_{\mathrm{acb}} \\ \chi_{spp}^{(2)} = L_{yxz}\chi_{yxz}^{(2)} + L_{yzx}\chi_{yzx}^{(2)} = \frac{1}{2}L_{yxz}\mathrm{N_s}\langle\sin^2(\theta)\rangle\langle\cos^2(\psi)\rangle * \beta_{\mathrm{acb}} - \frac{1}{2}L_{yzx}\mathrm{N_s}\langle\cos^2(\theta)\rangle * \beta_{\mathrm{acb}} \end{cases}$$

(5.25)

From experimental measurements the ratio $\frac{\chi_{ssp}^{(2)}}{\chi_{spp}^{(2)}}$ was found to be 1.04 (Figures 5.7 and 5.8), and the R^{ATR} was determined to be 0.95 (Figure 5.9). After inputting the appropriate radiation electric field vectors (E_x, E_y, E_z), we obtained two sets of solutions ($\theta = 76^o$, $\psi = 82^o$) and ($\theta = 76^o$, $\psi = 16^o$) for equations (5.25). However, according to the spectral fitting results of the chiral signal observed with spp polarization combination (Figure 5.8), there was no discernible B_1 mode, which excludes the solution set with $\psi = 16^o$ which would give relatively strong signal in B_1 mode (Figure 5.5). Therefore the tilt and twist angles for tachyplesin I at the PS/tachyplesin I solution are 76^o and 82^o, respectively. This result agrees with our recent molecular dynamics simulation outcomes, which will be presented in an upcoming report.

In addition to the PS, we also applied a similar method to study molecular interactions between tachyplesin I and sulfonated polystyrene. Similarly, both SFG chiral and achiral amide I signals were observed. To ensure that the observed SFG signal is indeed from the β-sheet structure, dithiothreitol (DTT) was added to the interaction medium before the additions of the peptide, which can denature the native structure of tachyplesin I by breaking the disulfide bonds. With the presence of DTT in the interaction medium, after the addition of the peptide, no chiral signal was observed from the s-PS/tachyplesin I solution interface in spp polarization combination (Figure 5.10) and the ssp spectrum underwent a significant blue shift (Figure 5.11). The blue shift seen

in the ssp spectrum corresponds to the loss of β-sheet signal centered at 1635 cm^{-1}. The disappearance of the chiral signal and the spectral change in the achiral signal after the addition of DTT indicates the original chiral signal and the 1635 cm^{-1} peak in the ssp spectrum are contributed by the β-sheet structure. The detailed data analysis suggests a slightly different orientation of tachyplesin I at the sulfonated PS/tachyplesin I solution interface, which will be reported in the future.

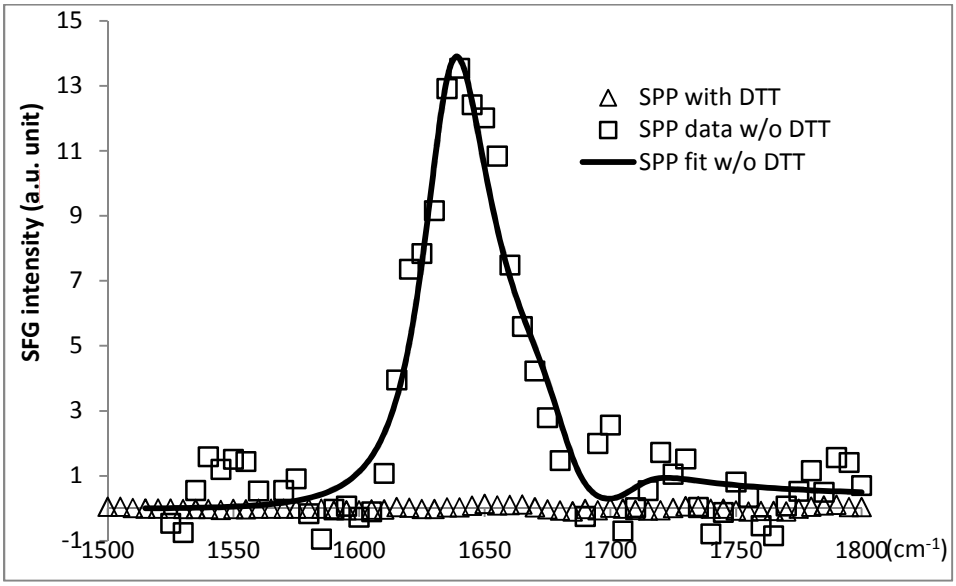

Figure 5.10: The chirality of tachyplesin I was broken upon the addition of DTT, observed in spp polarization combination, on sPS surface.

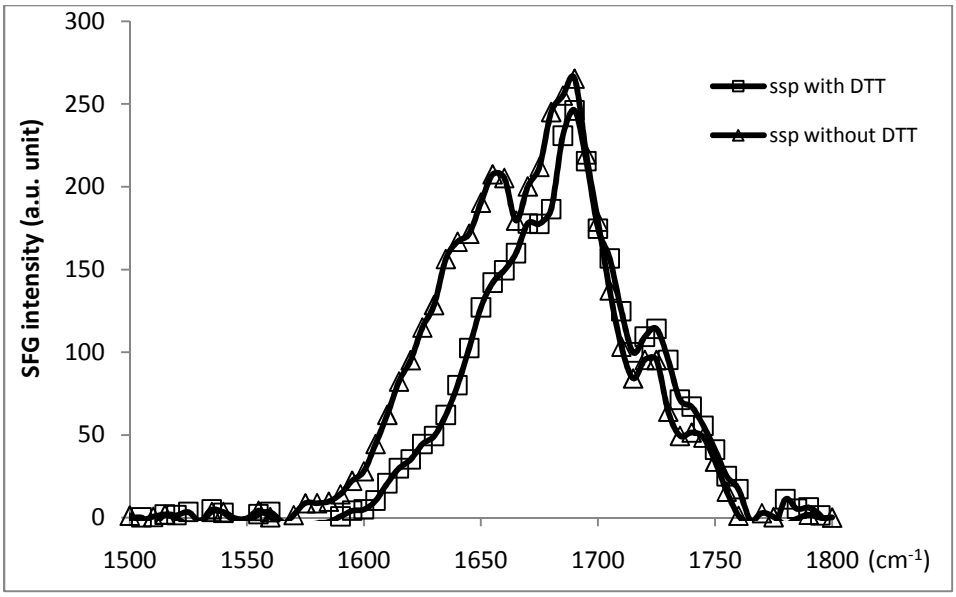

Figure 5.11: SFG ssp amide I spectra of tachyplesin I adsorbed to sPS surface with and without addition of DTT.

5.4.2. The interaction between tachyplesin I and DPPG/dDPPG lipid bilayer.

Tachyplesin I is an effective antimicrobial peptide that interacts with bacterial and mammalian cell membranes differently.[112, 113] Using SFG, we successfully probed different interactions and orientations of tachyplesin I in both model mammalian and bacterial cell membranes. In brief, tachyplesin I does not bind effectively onto zwitterionic lipids such as 1-Palmitoyl-2-Oleoyl-sn-Glycero-3-Phosphocholine (POPC) or 1,2-Dimyristoyl-sn-Glycero-3-Phosphocholine (DMPC), which are similar to the major components of mammalian cell membranes. On the other hand, it binds quickly to the negatively charged lipid such as 1-Palmitoyl-2-Oleoyl-sn-Glycero-3-[Phospho-rac-(1-glycerol)] (POPG) and DPPG (similar to the major components of bacterial cell

membranes) by the aid of the electrostatic attraction. We also obtained the SFG amide I achiral and chiral signal of membrane bound tachyplesin I (Figures 5.12 and 5.13). The achiral signal from the peptide is relatively strong; however, the chiral signal could not be observed directly using the spp polarization combination. The interference enhancement method, which was discussed in our previous publication[81], was implemented to deduce the weak chiral signal. A chiral spp spectrum was deduced, dominated by a clear peak centered at around 1685 cm^{-1}, featuring the B_1 vibrational mode (Figure 5.13). By combining the signal strengths of the B_1 and B_2 modes, the orientation angles of tachyplesin I on the DPPG/dDPPG lipid bilayer can be estimated (Figures 5.5 and 5.6): the tilt angle (θ) has a range of 70-80 degrees and the twist angle (ψ) has a range of 0-15 degrees. Tachyplesin I evidently adopts quite a different twist angle on DPPG/dDPPG lipid bilayer than it does on PS or sPS polymer surfaces. The different twist angles must be caused by the different molecular interactions between tachyplesin I and polymer surfaces and between tachyplesin I and negatively charged lipids. We believe that this is the first time the orientation information (θ, ψ) of antimicrobial peptides with β-sheet structure in cell membranes is determined using vibrational spectroscopies. Such information is important in understanding molecular mechanisms of interactions between β-sheet peptides and cell membranes, aiding in the design and development of improved anti-microbial peptides with β-sheet structures.

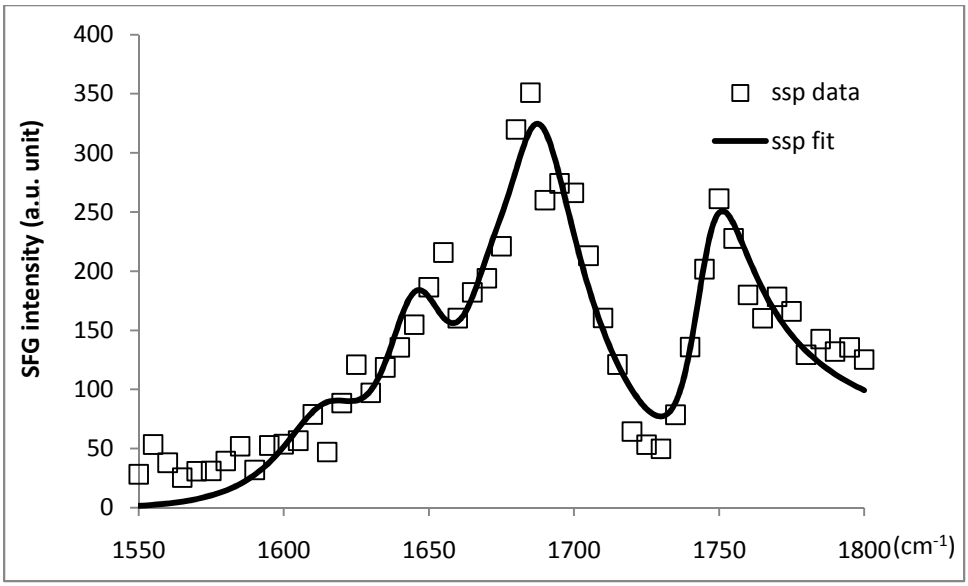

Figure 5.12: SFG spectrum of tachyplesin I (~700 nM) adsorbed onto DPPG/dDPPG lipid bilayer in ssp polarization combination.

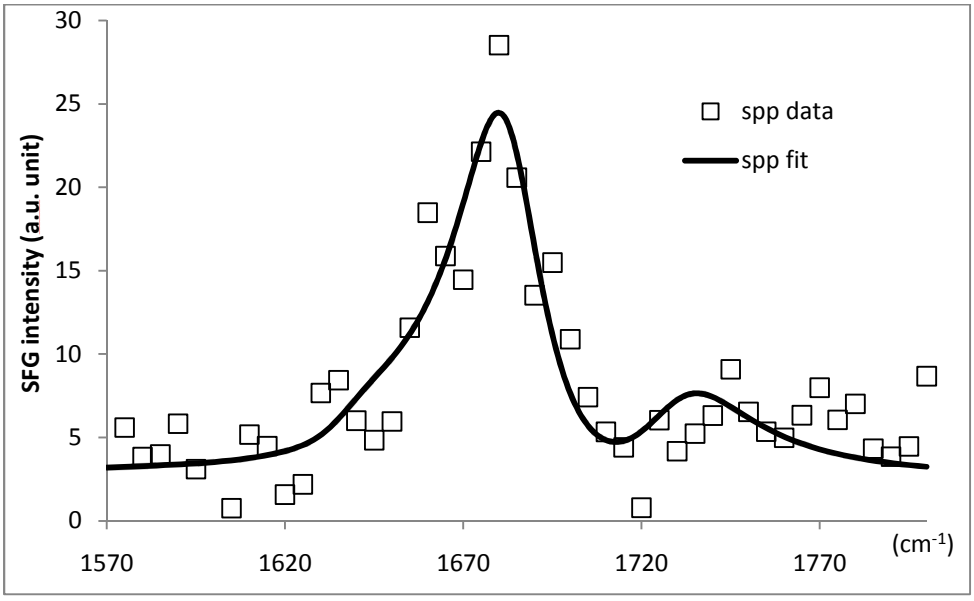

Figure 5.13: SFG spectrum of tachyplesin I (~700 nM) adsorbed onto DPPG/dDPPG lipid bilayer in ssp polarization combination.

In addition to tachyplesin I, other peptides with β-sheet structure, such as subtilosin A, have also been studied using SFG. Details on such results will be reported in the future.

5.5. Conclusion

In this chapter, for the first time, a systematic method for determining β-sheet orientation on surfaces using SFG vibrational spectroscopy together with ATR-FTIR was presented. Using the bond additivity model, the IR transition dipole and the Raman polarizability tensor were calculated for the β-sheet structure. From the calculated IR dipole and Raman polarizability, the molecular hyperpolarizability was found, which was used to determine the tilt angle (θ) and the twist angle (ψ) of the β-sheet at different interfaces. Using SFG, the chiral and achiral components of the B_2 vibrational mode were selectively probed and were ultimately used to deduce the orientation of tachyplesin I adsorbed to a PS surface. The relative SFG signal intensities of B_1 and B_2 modes were then used to estimate the orientation angles of tachyplesin I in DPPG/dDPPG lipid bilayers. This methodology can be applied to the study of β-sheets and β-sheet containing proteins/peptides on surfaces such as polymer surfaces or cell membranes *in situ*, with the capability of performing real time studies on conformational changes that occur in many interfacial proteins. In the future, various signal enhanced methods will be developed to directly probe modes other than B_2 to provide additional measured parameters. If all the vibrational modes B_1, B_2 and B_3 can be probed, more complicated orientations or orientation distributions that protein/peptide molecules adopt can be determined. Coupled with previously reported orientation analysis of α-helices[1], this

method lends itself to the study of larger and more complex interfacial proteins that have α-helix and/or β-sheet components.

5.6 References

(1) Nguyen, K. T.; Le Clair, S. V.; Ye, S.; Chen, Z. *J. Phys. Chem. B* **2009,** *113,* 12169-12180.

(2) Chen, X.; Wang, J.; Boughton, A. P.; Kristalyn, C. B.; Chen, Z. *J. Am. Chem. Soc.* **2007,** *129,* 1420-1427.

(3) Wang, J.; Lee, S. H.; Chen, Z. *J. Phys. Chem. B* **2008,** *112,* 2281-2290.

(4) Pauling, L.; Corey, R. B.; Brandon, H. R. *Proc. Nat. Acad. Sci. U.S.A.* **1951,** 205-211.

(5) Nabedryk, E.; Garavito, R. M.; Breton, J. *Biophys. J.* **1988,** *53,* 671-676.

(6) Sugiyama, Y.; Inoue, Y.; Muneyuki, E.; Haneda, H.; Fujimoto, M. *J. Electron. Micros.* **2006,** *55,* 143-149.

(7) Cerf, E.; Sarroukh, R.; Tamamizu-Kato, S; Breydo, L.; Derclaye, S; Dufrene, Y. F.; Narayanaswami, V; Goormaghtigh, E.; Ruysschaert, J.; Raussens, V. *Biophys. J.* **2009,** *421,* 415-423.

(8) Axelsen, P. H.; Kaufman, B. K.; McElhaney, R. N.; Lewis, R. N. *Biophys. J.* **1995,** *69,* 2770-2781.

(9) Axelsen, P. H.; Citra, M. J. *Prog. Biophys. Molec. Biol.* **1996,** *66,* 227-253.

(10) Bechinger, B.; Ruysschaert, J. M.; Goormaghtigh, E. *Biophys. J.* **1999,** *76,* 552-563.

(11) Bradbury, E. M.; Brown, L.; Downie, A. R.; Elliot, A.; Fraser, R. D. B.; Hanby, W. E. *J. Mol. Biol.* **1962,** *5,* 230-247.

(12) Fraser, R. D. B. *J. Chem. Phys.* **1953,** *21,* 1511-1515.

(13) Higgs, P. W. *Proc. R. Soc. Lond. A* **1953,** *220,* 472-485.

(14) Lee, S. H.; Krimm, S. *Biopolymers* **1998,** *46,* 283-317.

(15) Marsh, D.; Müller, M.; Schmitt, F. J. *Biophys. J.* **2000,** *78,* 2499-2510.

(16) Marsh, D. *Methods Enzymol.* **1999,** *294,* 59-92.

(17) Marsh, D. *Biophys. J.* **1998,** *75,* 354-358.

(18) Miyazawa, T.; Blout, E. R. *J. Am. Chem. Soc.* **1961,** *83,* 712-719.

(19) Reisdorf, W. Jr.; Krimm, S. *Biophys. J.* **1995,** *69,* 271-273.

(20) Tamm, L. K.; Tatulian, S. A. *Q. Rev. Biophys.* **1997,** *30,* 365-429.

(21) Tsuboi, M. *J. Polymer Sci.* **1962,** *59,* 139-153.

(22) Chen, L. X.; Strauss, H. L.; Snyder, R. G. *Biophys. J.* **1993,** *64,* 1533-1541.

(23) Dwivedi, A. M.; Krimm, S. *Biopolymers* **1984,** *23,* 2025-2065.

(24) Fanconi, B.; Tomlinson, B.; Nafie, L. A.; Small, W.; Peticolas, W. L. *J. Chem. Phys.* **1969,** *51,* 3993-4005.

(25) Fanconi, B. *Biopolymers* **1973,** *12,* 2759-2776.

(26) Koenig, J. L.; Sutton, P. L. *Biopolymers* **1969,** *8,* 167-171.

(27) Lee, S. -H.; Krimm, S. *J. Raman Spectrosc.* **1998,** *29,* 73-80.

(28) Overman, S. A.; Tsuboi, M.; Thomas G. J. Jr. *J. Mol. Biol.* **1996,** *259,* 331-336.

(29) Tsuboi, M.; Benevides, J. M.; Bondre, P.; Thomas, G. J. Jr. *Biochemistry* **2005,** *44,* 3091-3100.

(30) Tsuboi, M.; Ikeda, T.; Ueda, T. *J. of Raman Spectrosc.* **1991,** *22,* 619-626.

(31) Wilser, W. T.; Fitchen, D. B. *J. Chem. Phys.* **1975,** *62,* 720-724.

(32) Andronesi, O. C.; Becker, S.; Seidel, K.; Heise, H.; Young, H. S.; Baldus, M. *J. Am. Chem. Soc.* **2005,** *127,* 12965-12974.

(33) Bechinger, B. *Biochim. Biophys. Atca* **1999,** *1462,* 157-183.

(34) Bechinger, B.; Aisenbrey, C.; Bertani, P. *Biochim. Biophys. Atca* **2004,** *1666,* 190-204.

(35) Durr, U. H. N.; Yamamoto, K.; Ramamoorthy, A. *J. Am. Chem. Soc.* **2007,** *129,* 6670-6671.

(36) Dvinskikh, S. V.; Durr, U. H. N.; Yamamoto, K.; Ramamoorthy, A. *J. Am. Chem. Soc.* **2007,** *129,* 794-802.

(37) Fernandez, C.; Adeishvili, K.; Wuthrich, K. *Proc. Nat. Acad. Sci. U.S.A.* **98,** *98,* 2358-2363.

(38) Lee, D.; Walter, K. F. A.; Bruckner, A. K.; Hilty, C.; Becker, S.; Griesinger, C. *J. Am. Chem. Soc.* **2008,** *130,* 13822-13823.

(39) Lindblom, G.; Grobner, G. *Curr. Opin. Colloid Interface Sci.* **2006,** *11,* 24-29.

(40) Naito, A.; Kawamura, I. *Biochim. Biophys. Atca* **2007,** *1768,* 1900-1912.

(41) Shen, Y. R.; Ostroverkhov, V. *Chem. Rev.* **2006,** *106,* 1140-1154.

(42) Shultz, M. J.; Baldelli, S.; Schnitzer, C.; Simonelli, D. *J. Phys. Chem. B* **2002,** *106,* 5313-5324.

(43) Stiopkin, I. V.; Jayathilake, H. D.; Bordenyuk, A. N.; Benderskii, A. V. *J. Am. Chem. Soc.* **2008,** *130,* 2271-2275.

(44) Voges, A. B.; Stokes, G. Y.; Gibbs-Davis, J. M.; Lettan, R. B.; Bertin, P. A.; Pike, R. C.; Nguyen, S. T.; Scheidt, K. A.; Geiger, F. M. *J. Phys. Chem. C* **2007,** *111,* 1567-1578.

(45) Li, Q., Hua, R., Cheah, I. J., Chou, K. C. *J. Phys. Chem. B* **2008,** *112,* 694-697.

(46) Ye, S. J.; McClelland, A.; Majumdar, P.; Stafslien, S.; Daniels, J.; Chisholm, B.; Chen, Z. *Langmuir* **2008,** *24,* 9686-9694.

(47) Anglin, T. C.; Conboy, J. C. *Biophys. J.* **2008,** *95,* 186-193.

(48) Baldelli, S. *Acc. Chem. Res.* **2008,** *41,* 421-431.

(49) Belkin, M. A.; Shen, Y. R. *Int. Rev. Phys. Chem.* **2005,** *24,* 257-299.

(50) Dreesen, L.; Sartenaer, Y.; Humbert, C.; Mani, A. A.; Methivier, C.; Pradier, C. M.; Thiry, P. A.; Peremans, A. *Chem. Phys. Chem.* **2004,** *5,* 1719-1725.

(51) Dreesen, L.; Humbert, C.; Sartenaer, Y.; Caudano, Y.; Volcke, C.; Mani, A. A.; Peremans, A.; Thiry, P. A.; Hanique, S.; Frere, J. M. *Langmuir* **2004,** *20,* 7201-7207.

(52) Fourkas, J. T.; Walker, R. A.; Can, S. Z.; Gershgoren, E. *J. Phys. Chem. C* **2007,** *111,* 8902-8915.

(53) Gautam, K. S.; Dhinojwala, A. *Phys. Rev. Lett.* **2002,** *88,* 145501.

(54) Gopalakrishnan, S.; Liu, D. F.; Allen, H. C.; Kuo, M.; Shultz, M. J. *Chem. Rev.* **2006,** *106,* 1155-1175.

(55) Gracias, D. H.; Chen, Z.; Shen, Y. R.; Somorjai, G. A. *Acc. Chem. Res.* **1999,** *32,* 930-940.

(56) Holman, J.; Ye, S.; Neivandt, D. J.; Davies, P. B. *J. Am. Chem. Soc.* **2004,** *126,* 14322-14323.

(57) Hopkins, A. J.; McFearin, C. L.; Richmond, G. L. *Curr. Opin. Solid State Mater. Sci.* **2005,** *9,* 19-27.

(58) Iwahashi, T.; Miyamae, T.; Kanai, K.; Seki, K.; Kim, D.; Ouchi, Y. *J. Phys. Chem. B* **2008,** *112,* 11936-11941.

(59) Kim, C.; Gurau, M. C.; Cremer, P. S.; Yu, H. *Langmuir* **2008,** *24,* 10155-10160.

(60) Ma, G.; Allen, H. C. *Langmuir* **2007,** *23,* 589-597.

(61) Moore, F. G.; Richmond, G. L. *Acc. Chem. Res.* **2008,** *41,* 739-748.

(62) Opdahl, A.; Koffas, T. S.; Amitay-Sadovsky, E.; Kim, J.; Somorjai, G. A. *J. Phys. Condens. Matter.* **2004,** *16,* R659-R677.

(63) Richmond, G. L. *Chem. Rev.* **2002,** *102,* 2693-2724.

(64) Rupprechter, G.; Weilach, C. *J. Phys. Condens. Matter* **2008,** *20,* 184019.

(65) Bain, C. D. *J. Chem. Soc. Faraday Trans.* **1995,** 1281-1296.

(66) Chen, X.; Chen, Z. *Biochim. Biophys. Acta* **2006,** *1758,* 1257-1273.

(67) Chen, X.; Clarke, M. L.; Wang, J.; Chen, Z. *Int. J. Mod. Phys. B.* **2005,** *19,* 691-713.

(68) Clarke, M. L.; Wang, J.; Chen, Z. *J. Phys. Chem. B* **2005,** *109,* 22027-22035.

(69) Evans-Nguyen, K. M.; Fuierer, R. R.; Fitchett, B. D.; Tolles, L. R.; Conboy, J. C.; Schoenfisch, M. H. *Langmuir* **2006,** *22,* 5115-5121.

(70) Kim, J.; Cremer, P. S. *Chem. Phys. Chem.* **2001,** *2,* 543-546.

(71) Kim, J.; Somorjai, G. A. *J. Am. Chem. Soc.* **2003,** *125,* 3150-3158.

(72) Kim, G.; Gurua, M. C.; Lim, S. M.; Cremer, P. S. *J. Phys. Chem. B* **2003,** *107,* 1403-1409.

(73) Kim, G.; Gurau, M. C.; Kim, J.; Cremer, P. S. *Langmuir* **2002,** *18,* 2807-2811.

(74) Knoesen, A.; Pakalnis, S.; Wang, M.; Wise, W. D.; Lee, N.; Frank, C. W. *IEEE J. Sel. Top. Quantum Electron.* **2004,** *10,* 1154-1163.

(75) Mermut, O.; Phillips, D. C.; York, R. L.; McCrea, K. R.; Ward, R. S.; Somorjia, G. A. *J. Am. Chem. Soc.* **2006,** *128,* 3598-3607.

(76) Rocha-Mendoza, I.; Yankelevich, D. R.; Wang, M.; Reiser, K. M.; Frank, C. W.; Knoesen, A. *Biophys. J.* **2007,** *93,* 4433-4444.

(77) Weidner, T.; Breen, N. F.; Drobny, G. P.; Castner, D. G. *J. Phys. Chem. B*, **2009**, *113*, 15423–15426.

(78) Wang, J.; Even, M. A.; Chen, X.; Schmaier, A. H.; Waite, J. H.; Chen, Z. *J. Am. Chem. Soc.* **2003,** *125,* 9914-9915.

(79) Wang, J.; Buck, S. M.; Chen, Z. *Analyst* **2003,** *128,* 773-778.

(80) Wang, J.; Clarke, M. L.; Zhang, Y. B.; Chen, X.; Chen, Z. *Langmuir* **2003,** *19,* 7862-7866.

(81) Wang, J.; Chen, X.; Clarke, M. L.; Chen, Z. *Proc. Nat. Acad. Sci. U.S.A.* **2005,** *102,* 4978-4983.

(82) Wang, J.; Chen, X.; Clarke, M. L.; Chen, Z. *J. Phys. Chem. B* **2006,** *110,* 5017-5024.

(83) York, R. L.; Holinga, G. J.; Guyer, D. R.; McCrea, K. R.; Ward, R. S.; Somorjai, G. A. *Appl. Spectrosc.* **2008,** *62,* 937-1047.

(84) Chen, X.; Wang, J.; Sniadecki, J. J.; Even, M. A.; Chen, Z. *Langmuir* **2005,** *21,* 2262-2264.

(85) Chen, X.; Boughton, A. P.; Tesmer, J. J. G.; Chen, Z. *J. Am. Chem. Soc.* **2007,** *129,* 12658-12659.

(86) Chen, X.; Wang, J.; Paszti, Z.; Wang, F.; Schrauben, J. N.; Tarabara, V. V.; Schmaier, A. H.; Chen, Z. *Anal. Bioanal.Chem.* **2007,** *388,* 65-72.

(87) Wang, J.; Chen, C.; Buck, S. M.; Chen, Z. *J. Phys. Chem. B*, **2001**, *105*, 12118-12125.

(88) Chen, X.; Wang, J.; Kristalyn, C. B.; Chen, Z. *Biophys. J.* **2007,** *93,* 866-875.

(89) Moad A. J.; Simpson, G. J. *J. Phys. Chem. A.* **2005,** *109,* 1316-1323.

(90) Moad, A. J.; Simpson, G. J. *J. Phys. Chem. B.* **2004,** *108,* 3548-3562.

(91) Suzuki, E. *Spectrochim. Acta. A.* **1967,** *23,* 2303-2308.

(92) Fraser, R. D. B.; Suzuki, E. *Spectrochim. Acta. A.* **1970,** *26,* 423-426.

(93) Marsh, D. *Biophys. J.* **1997,** *72,* 2710-2716.

(94) Miyazawa, T. *J. Chem. Phys.* **1960,** *32,* 1647-1652.

(95) Tsuboi, M.; Kaneuchi, F.; Ikeda, T.; Akahane, F. *Can. J. Chem.* **1991,** *69,* 1752-1757.

(96) Tsuboi, M.; Kubo, Y.; Akahane, K.; Benevides, J. M.; Thomas, G. J. Jr. *J.Raman Spectrosc.* **2006,** *37,* 240-247.

(97) Krimm, S.; Abe, Y. *Proc. Nat. Acad. Sci. USA* **1972,** *69,* 2788-2792.

(98) Rousseau, M. E.; Lefevre, T.; Beaulieu, L.; Asakura, T.; Pezolet, M. *Biomacromolecules* **2004,** *5,* 2247-2257.

(99) Chirgadze, Y. N.; Nevskaya, N. A. *Biopolymers* **1976,** *15,* 607-625.

(100) Choi, J. -H.; Hahn, S.; Cho, M. *Biopolymers* **2006,** *83,* 519-536.

(101) Belkin, M. A.; Shen, Y. R. *Phys. Rev. Lett.* **2003,** *91,* 213907(1)-213907(4).

(102) Haupert, L. M.; Simpson, G. J. *Annu. Rev. Phys. Chem.* **2009,** *60,* 345-365.

(103) Oh-e, M.; Yokoyama, H.; Yorozuya, S.; Akagi, K.; Belkin, M. A.; Shen, Y. R. *Phys. Rev. Lett.* **2004,** *93,* 267402(1)-267402(4).

(104) Simpson, G. J. *ChemPhysChem* **2004,** *5,* 1301-1310.

(105) Belkin, M. A.; Kulakov, T. A.; Ernst, K. -H.; Yan, L.; Shen, Y. R. *Phys. Rev. Lett.* **2000,** *85,* 4474-4477.

(106) Heinz, T. F.; Tom, H. W. K.; Shen, Y. R. *Phys. Rev. A* **1983,** *28,* 1883-1885.

(107) Heinz, T. F. *In Nonlinear Surface Electromagnetic Phenomena;* North-Holland: New York,1991; 29,352.

(108) Mazely, T. L.; Hetherington,W. M. III. *J. Chem. Phys.* **1987,** *86,* 3640-3647.

(109) Simpson, G. J.; Perry, J. M.; Ashmore-Good, C. L. *Phys. Rev. B* **2002,** *66,* 65437(1)-65437(10).

(110) Shen, Y. R. *The Principles of Nonlinear Optics;* John Wiley & Sons: New York, 1984.

(111) Manella, C. A.; Forte, M.; Columbini, M. *VDAC. J. Bioenerg. Biomembr.* **1992,** *24,* 7-19.

(112) Kawano, K.; Yoneya, T.; Miyata, T. *J. Biol. Chem.* **1990,** *265,* 15365-15367.

(113) Nakamura, T.; Furunaka, H.; Miyata, T. *J. Biol. Chem.* **1988,** *263,* 16709-16713.

CHAPTER 6

CONCLUSION

Even though it has been only twenty years after the first SFG spectrum was published, SFG has been developed rapidly into a powerful and versatile technique to study many important topics in surface science. SFG has been applied to investigate a wide range of systems from different materials (semi-conductors, adhesives, anti-biofouling coatings, etc.) and biosensors (for homeland security applications as well as uses for medical diagnostics) to biological molecules such as proteins, peptides, and lipids. I have been fortunate to have the opportunity to apply SFG to investigate interfacial structures of biomolecules. In spite of the fact that the learning curve of SFG (both in the theoretical and experimental aspects) is definitely not on the flat side, I am glad that all the efforts and hassles I have gone through were worthwhile. The more I get involved in working with this technique, the more suitable and unique I realize SFG is for studying complex topics in surface chemistry. The difficulties and hassles one may encounter in learning the SFG technique are rewarded by substantive structural information of interfacial molecules which no other optical vibrational techniques can provide.

Some analytical techniques can be interface/surface sensitive because their penetration depth is small. Structural studies of interfacial biomolecules require the right

"penetration depth" which should closely match the effective thickness of the interfacial biomolecules under investigation. However, each biological system has its own properties; therefore, having a fixed penetration depth will eliminate the versatility of the spectroscopic technique being used. Luckily, in most cases, the concept of "penetration depth" does not exist in SFG vibrational spectroscopy. Due to its selection rules, SFG is intrinsically surface sensitive and is blind to the bulk, which makes SFG an excellent surface specific tool among all the other conventional spectroscopic techniques.

Having tremendous potential in surface chemistry research, SFG requires interpretation or data analysis to translate the language in spectroscopy to "a picture" or "a story" that makes sense to somebody who is not a spectroscopist. During the past twenty years, many mathematical models have been proposed and applied in the interpretation of SFG signals. This dissertation focuses on applying the bond additivity model and group theory in the orientation analysis methods for various secondary structures in proteins or peptides. In chapter 2, we applied these two primary means in solving the tilt angle of α- and 3-10 helical structures using SFG. The bond additivity model and group theory have been used by our group previously in the tilt angle calculation of an ideal α-helix (which is comprised of integer multiples of 18 amino acid residues). My work in chapter 2 refines that methodology, which allows for the orientation determination of interfacial α- and 3-10 helical structures of any length. Chapter 3 is an application of the method developed in chapter 2. The interactions between an antimicrobial α-helical peptide, magainin 2, and two types of lipid bilayers were studied in chapter 3. Magainin 2 was found to be non-disruptive to a zwitterionic lipid bilayer (POPC/POPC bilayer) and formed pores in a negatively charged lipid bilayer

(POPG/POPG bilayer). The helical tilt angles of the peptide were also determined quantitatively when it interacted with these two lipid bilayers. The outcome of this project was correlated well with the results available in the literature.

Chapter 4 of this dissertation focuses on the SFG study of *Cyt b5*. In this study, the tilt angle of the protein's α-helical membrane anchoring tail was determined. In addition, we performed experiments to investigate the mechanism of the anchoring process. It was found that the binding was assisted by the linker region connecting the protein's anchoring tail and the water soluble domain. Without the linker or with a linker of shorter length (less than 6 amino acid residues), the anchoring process doesn't happen. Interestingly, we also found that the temperature plays a role in the insertion of the membrane anchoring domain.

Chapter 5 is the other major part of my thesis research work in the Zhan Chen laboratory. In this work, an orientation determination methodology using SFG was established for the anti-parallel β-sheet structure. We probed SFG signals in different polarization combinations to obtain the normal (achiral) and chiral signals of the structure. When combining SFG with polarized ATR-FTIR we were able to determine the two orientation angles (the tilt and the twist angles) of this particular secondary structure. In addition to the proposed methodology, we determined the orientation of tachyplesin I (an antimicrobial peptide that has β-sheet structure) on a polystyrene film and in a dDPPG/dDPPG lipid bilayer. The presented orientation analysis method established for the anti-parallel β-sheet structure opens up the possibility of investigating the β-sheet components of complex proteins. This independent set of information would

greatly assist the protein structural analysis based on the helical segments which has been done so far.

In this thesis research, my focus is the SFG data analysis methodology development for determining interfacial protein and secondary structure orientation and applying such methods to deduce interfacial secondary structures' orientation experimentally using SFG as well as other vibrational spectroscopic methods. Previous works of the extraordinary individuals in my research group prior to my arrival at Michigan are able to show the potential of some of the more complex and powerful data analysis approaches. Among these, the maximum entropy approach clearly shows its tremendous potential in verifying our calculations. In the instrumental aspect, the two dimensional spectroscopic technique, double resonance SFG, promises great potential in studies of secondary structures especially structures with chirality. Additionally, using double resonance SFG, we can also investigate the coupling between the molecular vibrational modes and electronic transitions of the interfacial chemical groups. More advanced data analysis methods and SFG techniques should further develop surface chemistry studies, especially the structural determination of interfacial biomolecules. Broadband SFG, which uses femosecond lasers, has recently been developed to studies biological systems. However, picoseconds lasers are still excellent systems for vibrational spectroscopy due to the matching bandwidth of the vibrational modes and the laser pulses. Although having lower resolution than narrowband SFG, broadband SFG has the potential in studies of surface dynamics and the capability for multiplexing.